A Modular Design Architecture for Application to Community-Scale Photovoltaic-Powered Reverse Osmosis Systems

by

Amy M. Bilton

Bachelor of Applied Science, Engineering Science,
University of Toronto, 2004
Master of Science, Aeronautics and Astronautics,
Massachusetts Institute of Technology, 2006

Submitted to the Department of Aeronautics and Astronautics
in Partial Fulfillment of the Requirements for the Degree of

Doctor of Philosophy in Aeronautics and Astronautics

at the

MASSACHUSETTS INSTITUTE OF TECHNOLOGY

February 2013

Signature of Author: .....
Department of Aeronautics and Astronautics
October 16, 2012

Certified by: .....
Steven Dubowsky
Professor of Aeronautics and Astronautics & Mechanical Engineering
Thesis Supervisor

Certified by: .....
John H. Lienhard V
Samuel C. Collins Professor of Mechanical Engineering

Certified by: .....
Karen Willcox
Professor of Aeronautics and Astronautics

Accepted by: .....
Eytan Modiano
Professor of Aeronautics and Astronautics
Chairman, Graduate Program Committee

A Modular Design Architecture for Application to Community-Scale Photovoltaic Reverse Osmosis Systems

by

Amy M. Bilton

Submitted to the Department of Aeronautics and Astronautics
on October 16, 2012 in Partial Fulfillment of the
Requirements for the Degree of Doctor of Philosophy in
Aeronautics and Astronautics

ABSTRACT

Access to safe, clean drinking water is a major challenge for many communities. These communities are often near seawater and/or brackish groundwater sources, making desalination a possible solution. Unfortunately, desalination is energy intensive and a reliable, inexpensive power supply is also challenging for remote locations. Photovoltaic reverse osmosis systems (PVRO) can be used to provide water for underserved communities. A feasibility study which demonstrates the economic viability of such systems is discussed here.

PVRO systems are assembled from mass-produced modular components. This approach reduces manufacturing costs. However, designing a system optimized for a specific location is difficult. For even a small inventory of components, the number of design choices is enormous. A designer with significant expertise is required to tailor a PVRO system for a given location, putting this technology out of reach of many communities.

This thesis develops a modular design architecture which can be implemented in a computer program to enable non-experts to configure systems from inventories of modular components. This architecture is not limited to PVRO systems, but can also be used to design other systems composed of modular components such as cars, electronics, and computers. The method uses a hierarchy of filters to limit the design space based on design principles and calculations. The system is then configured from the reduced design space using optimization methods and detailed system models.

In this thesis, the modular design architecture is implemented for PVRO systems. A set of detailed physics-based system models are developed to enable this process. A novel method of representing a PVRO system using a graph is developed to enable rapid evaluation of different system configurations. This modeling technique is validated using the MIT Experimental PVRO system constructed as part of this research.

A series of case studies are conducted to validate the modular design approach for PVRO systems. The first set of case studies considers a deterministic solar input and water demand. The design goal is to determine the lowest cost system that meets the water demand requirements. It is shown that the method is able to tailor systems for a wide range of locations and water demands from a large system inventory. The validity of these solutions is demonstrated by simulating a custom designed system in the wrong location. Another case study shows that the approach can be used to determine market potential of new components.

The second set of case studies considers variations in the solar radiation and water demand. The design goal is to determine the lowest cost PVRO system that meets the water demand profile with a specified probability. Two methods that use historical solar insolation and water demand to account for variations are presented. The first method characterizes the historical data and develops models to synthetically generate solar insolation and water demand profiles, and then simulates the system performance over 100 years to calculate the loss-of-water probability. In the second method, distributions of solar radiation and water demand are calculated from historical data and used to directly calculate the probability of running out of water in the worst month of the year. Both methods are implemented and shown to produce feasible system configurations. The direct calculation method is shown to reduce the required computation time and is suitable for different systems with variable inputs.

Thesis Supervisor: Steven Dubowsky
Title: Professor of Aeronautics and Astronautics & Mechanical Engineering

ACKNOWLEDGEMENTS

Writing a Ph.D. dissertation is a long process that many graduate students dread, myself included. Over the course of the past couple of months while preparing this thesis, I've had a chance to reflect on my past four years at MIT and the people who've helped me out along the way. As I slogged through those chapters, I've looked forward to writing this tribute to all these sources of support.

I'd like to thank the sponsors of this research. Thanks to the Cyprus Institute for the fellowship which supported the first 3 years of this research. The feedback received during our meetings aided in the development of this work. Thanks also to the MIT-KFUPM Center for Clean Energy and Water for the financial support of the experimental equipment and the financial support of this research.

I'd like to thank the members of my Ph.D. committee. Professor Dubowsky, thank you for giving me the fantastic opportunity of working in the FSRL. I've learned about both life and research from you during the course of my M.S. and Ph.D. You've been a great research advisor, mentor and friend. I'd also like to thank my committee members Professor Willcox and Professor Lienhard for their helpful discussions and critiques of my work over the past few years.

Research is something that you can't do on your own and there is no way I would have been able to complete this work without the assistance of my fellow lab members. Thanks to Roman Geykhman and Davide Del Pozzo for their assistance with the construction of the experimental system. I also want to thank Francesco Mazzini and Elizabeth Reed for their useful feedback on my work and keeping the lab spirits high. I especially thank Leah Kelley for providing feedback on my ideas, helping with experiments, reading this thesis, supporting me during tough times and just being a great friend.

I'd also like to thank my support outside the lab. These past four years, I've been so fortunate to become part of an enormous family at Sidney-Pacific. Thanks so much to Professor Roger Mark and Dottie Mark for inviting me into their home so many times and making sure that I'm always well fed. I've learned so much from both of you. I've made so many great friends at SP (way more than I can list here) and it's been fantastic to live with all of you these past few years. SP has taught me to always think big and that anything is possible as long as you have a great team.

I also want to thank my friends and family. Been Kim, thanks for being a great source of support throughout my degree. I know my qualifying exam experience would have been much different without you (the study sessions would not have been nearly as fun). Mom and Dad, thanks for always believing in me and supporting my endeavors no matter how crazy they may seem.

Last, I want to thank my biggest source of support. Andreas, thanks for always being there, even though you are on the other side of the globe. Thanks for being a sounding board for

my ideas, lifting my spirits, and for encouraging me when things seem out of reach. You've always been my biggest fan and there's no way this thesis would have been completed without your love and support.

CONTENTS

FIGURES

TABLES

CHAPTER

1

INTRODUCTION

1.1 Motivation

Access to safe, clean drinking water is a major concern for many communities. Currently, over 880 million people don't have access to an adequate fresh water source [1]. Many of these people live in coastal areas with an abundance of seawater. Additionally, many inland areas have access to brackish groundwater. Desalination is a natural solution for these locations.

For densely populated areas, large-scale desalination plants are practical. Desalination requires tremendous amounts of energy, and system efficiency is a driving factor that determines the operating costs and practicality of these systems. Large-scale plants are advantageous because they have lower capital costs due to economies of scale and tend to be more energy efficient than small-scale systems. The economics of these large systems justify one-of-a-kind optimized designs.

As shown in Table 1.1, there are a broad range of potential desalination solutions for these large communities [2-6]. These processes can be divided into two groups: thermal processes and membrane processes. Membrane processes include reverse osmosis, where water is forced through a membrane using a pressure higher than the osmotic pressure, leaving behind concentrated brine. In thermal processes, a phase change is used to make fresh water. Table 1.1 shows the energy requirements for the different processes which are separated into thermal energy used to heat the seawater and electrical energy used to drive pumps, compressors and auxiliary equipment. For seawater desalination, reverse osmosis requires the least amount of overall energy. However, if thermal energy is inexpensive, a thermal desalination process like multi-effect distillation can be practical.

Table 1.1: Energy consumption of common desalination processes [6].

Desalination Process	Thermal Energy (kJ/kg)	Electrical Energy (kWh/m^3)
Seawater		
Multi-Stage Flash (MSF)	190-290	4-6
Multi-Effect Distillation (MED)	150-290	2.5-3
Vapor Compression (VC)	-	8-12
Reverse Osmosis (RO) without Energy Recovery	-	7-10
Reverse Osmosis (RO) with Energy Recovery	-	3-5
Brackish Water		
Reverse Osmosis (RO) with Energy Recovery	-	1-3
Reverse Osmosis (RO) without Energy Recovery	-	1.5-4
Electrodialysis	-	1.5-4

For small, remote communities, custom designs are not a viable solution. These areas are often off major electrical grids and rely on transported water or small-scale desalination plants. Diesel generators are commonly used to meet desalination energy requirements. However, diesel generators pollute the environment and their fuel cost makes them expensive to operate. Fortunately, these arid areas also typically have an abundance of sunshine. This is shown in Figure 1.1. Areas which are shown on the left as water scarce coincide with areas which have high solar insolation on the right. This shows that using clean, renewable solar energy to produce clean water would be ideal for these communities.

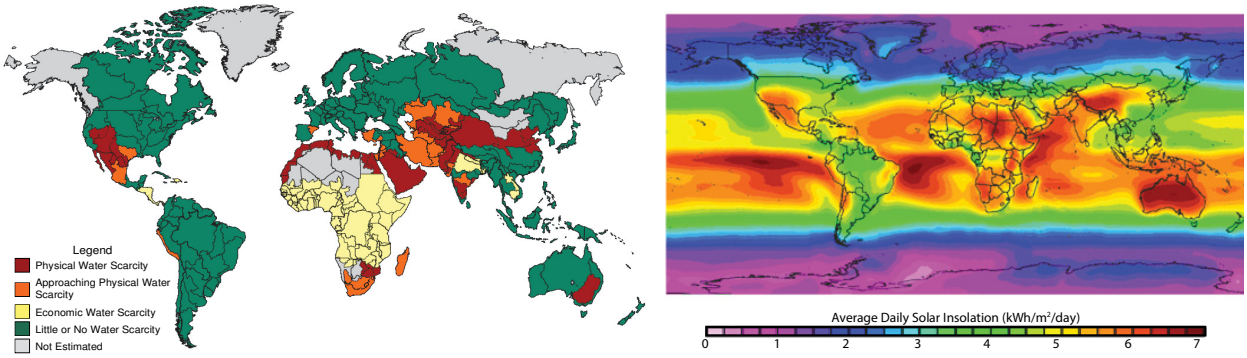

Figure 1.1: Water scarcity [7] (left) and average solar insolation, data from [8].

For large communities, with tens of thousands of people, solar thermal desalination systems can be economical [4, 9]. However, this technology is not easily scaled for small communities with lower water demands. For smaller communities, photovoltaic reverse osmosis (PVRO) systems assembled from mass-produced, modular components are a potential solution. PVRO has minimal environmental impact, and can be configured for different demand profiles using modular components. PVRO systems can also be easily maintained and repaired by non-

expert technicians. However, to be most efficient, such systems should be custom configured for the water demand, solar insolation and water characteristics of a specific location. Making these systems accessible to small communities is the motivation of the modular design algorithms developed in this research.

1.2 Modular Design

System manufacturing costs are often a dominant factor that determines the success of a product. A common method to reduce manufacturing costs in many applications, such as automobiles, electronics, and robotics, is to develop products composed of mass-produced modular components. The advantages include ease of construction, repair and recycling of system components.

Systems composed of modular components still require a custom design for a particular application. Designing a custom system configured from an inventory of potential modular components is not a simple task. For a given modular inventory, a large number of possible system configurations exist. A designer with significant expertise is required to select the correct components and configuration. This process is expensive and time consuming. For individuals without these skills, selecting the best components and system architecture is nearly impossible.

This thesis presents design methods to configure custom systems from inventories of modular components. These methods apply simple engineering principles to first reduce the size of the design space. Optimization methods are then be employed to determine the modular system configuration. The methods are formulated to be robust to uncertainties in system requirements and operating conditions. The modular design methods developed in this research enable non-experts to configure tailored systems for their particular application, opening technologies to previously unreachable areas.

1.3 Problem Statement

This thesis considers the problem of designing complex systems assembled from inventories of available modular components. It is assumed that there is an inventory of well-characterized components that can be included in the system. It is also assumed that the behavior of the assembled system is a complex function of the components. In these problems, the

performance of a system is highly coupled to the design choices, unlike the effect paint color choice has on car performance. In addition, the operating environment of the system is variable and has a direct impact on the system performance. This research develops design algorithms to enable custom design of modular systems given these assumptions.

The design of a PVRO desalination system for a remote community is the motivating problem of this research. The basic structure of this problem is shown in Figure 1.2. Here, it is assumed that the designer has access to an inventory consisting of different photovoltaic (PV) panels, pumps, reverse osmosis (RO) membranes, pressure vessels, energy recovery devices and control electronics. Also, it is assumed that the designer has access to the system specifications which define the location and water demand for the community. Using this information, the algorithms developed in this research can be used to configure a custom system for the community.

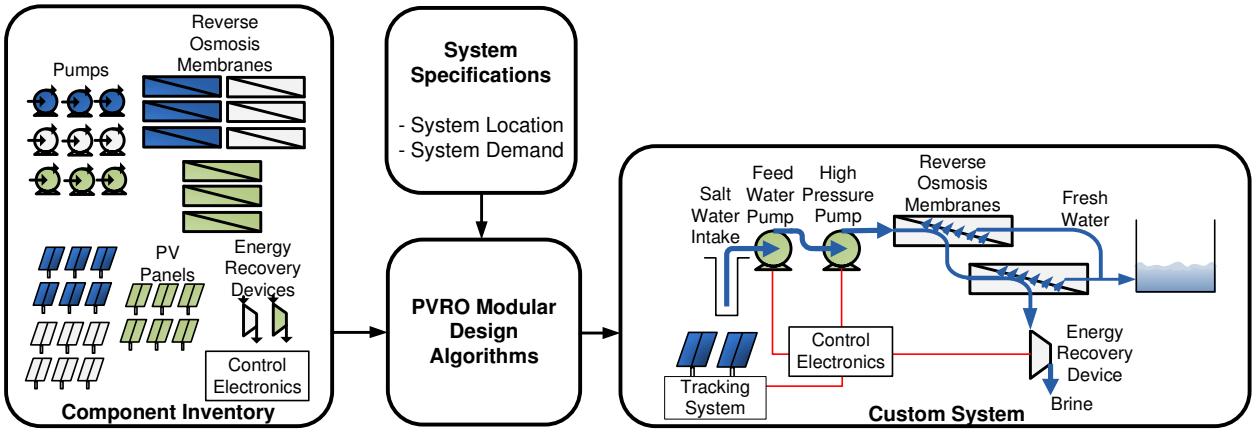

Figure 1.2: PVRO modular design problem.

One challenge of designing a system composed of modular components is, for a given inventory, a very large number of possible system configurations exist. Any algorithms that are developed must be able to efficiently deal with this large design space to find the best configuration. Another challenge is that there is often uncertainty in many parameters that determine the system performance. For example, in the PVRO system, the amount of input solar energy and water demand is variable. The final challenge is that component age and degradation will affect system performance. These factors need to be considered in an effective modular design algorithm.

1.4 Thesis Contributions

This research develops a new design approach to tailor a modular system from an inventory of potential components. The application of interest considered here is the design of a PVRO system. The contributions of this thesis can be separated into three main parts: a method to study the feasibility of photovoltaic reverse osmosis systems, the development of a general modular design approach, and the application of the design approach to photovoltaic reverse osmosis systems while considering the stochastic nature of the environment.

The primary contribution of this work is the development of a new design method to tailor systems composed of modular components for individual applications. The challenge is that even with a small modular inventory, there are a very large number of possible system configurations. This method employs engineering principles to first limit the size of the design space and make the design problem tractable. Optimization methods are then used over the reduced design space to determine a customized system for an individual application. This method has many different potential uses. The obvious use is to easily determine a tailored system configuration for an individual application. Another use of this approach is to determine if new components would make an impact on the market. Both of these uses are demonstrated for the application of interest, the design of PVRO systems.

This thesis also presents a new method to analyze the feasibility of PVRO systems as water supplies for remote communities. This method determines the lifetime water cost based on local solar insolation and water salinity data. This cost is compared with the lifetime costs of other water sources such as diesel-powered desalination systems. The analysis shows that there are a wide range of locations where PVRO systems are economically feasible.

The application of the modular design approach to PVRO systems results in new system analysis techniques. First, to implement the approach, a new graph-based model representation is developed to facilitate the analysis of any potential PVRO system configuration. In this formulation, a PVRO system can be simply represented by a series of integer and binary variables. Secondly, since the analysis of the system performance is complex due to the variations in the power source and demand, this thesis presents two methods to incorporate these temporal variations into the design of the system to ensure it is able to meet the requirements with a specified probability. The first new method analyzes the historical solar data and simulates the system performance over a long time horizon. The second new method uses a

statistical approach to analyze the PVRO system performance during the critical period of the year. These two methods are compared to deterministic design cases and are shown to develop robust system topologies.

1.5 Thesis Organization

This thesis has eight chapters. This chapter presents motivation and the problem being addressed in this thesis. Chapter 2 provides a detailed technical discussion of the system of interest, photovoltaic reverse osmosis systems and a review of the background literature. Chapter 3 presents a method to evaluate the feasibility of using PVRO systems to provide water for small communities. Chapter 4 presents the modular design approach developed in this thesis and design space studies used to demonstrate the power of the approach. Chapter 5 presents system models which were developed for the application of interest, PVRO systems, and the experimental validation of those models. Chapters 6 and 7 present the application of the modular design approach to PVRO systems for deterministic and uncertain environmental conditions. Chapter 8 summarizes the thesis and suggests avenues for future research.

CHAPTER

2

BACKGROUND AND LITERATURE REVIEW

2.1 Photovoltaic Reverse Osmosis Systems

2.1.1 PVRO Overview

There are many ways to configure a PVRO system. One simple configuration is shown in Figure 2.1. As shown, the photovoltaic panels power a feed pump and a high-pressure pump to pressurize the source water. The water is then driven through the reverse osmosis membrane array by the high pressure, producing clean, drinkable water. Due to energy considerations, the membranes are configured as crossflow separators and only a portion of the water is desalinated, leaving high salt concentration brine. The high-pressure brine passes through an energy recovery device, such as a pressure exchanger or turbine, to recover the useful energy in the brine before it exits the system.

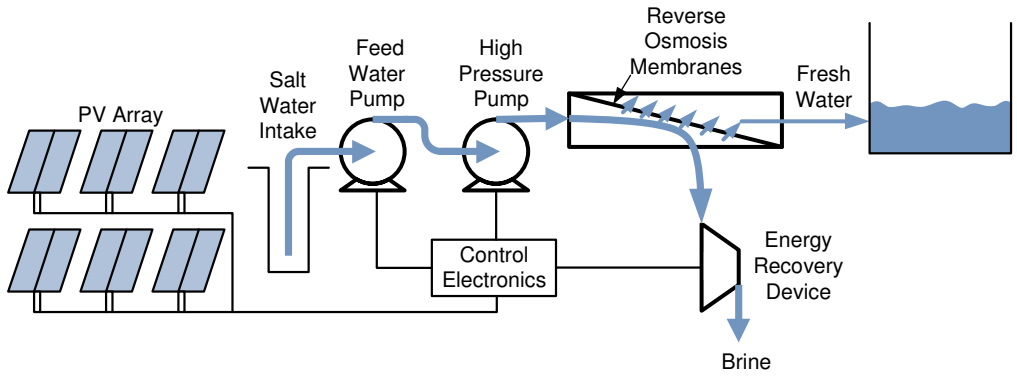

Figure 2.1: Simple PVRO system.

PVRO systems have been a topic of much research. Accurately modeling the reverse osmosis system has been a topic of interest [10-17]. One focus of these models has been to evaluate system suitability for individual locations such as Jordan [10, 11], Greece [12, 13], or Eritrea [14, 15]. Studies between different system components, such as energy recovery devices [16], and different system configurations have been performed [14, 15]. Finally, system models

are used in control development for particular systems [14, 15, 17]. These models are fixed for a specific system configuration and are not suitable for implementation in a modular design approach, where multiple configurations must be considered.

Many PVRO systems have been built and field tested [11, 14, 15, 18-30]. All of these systems are community scale, producing between 100 L and 10 m^3 of water per day. These systems can be divided into two main categories: brackish water systems and seawater systems.

Brackish water PVRO systems have been designed and tested in a wide range of locations [18-21, 29, 30]. Many of these systems are simple and do not incorporate an energy recovery device due to the small scale and reduced pressure requirements. Examples include small systems designed and tested in Brazil [20], the Southwestern United States [19], Jordan [29], and Portugal [21]. There are also small brackish water PVRO systems that incorporate energy recovery devices. The most notable of these systems is SolarFlow, which has been tested in the Australian Outback [18].

Seawater PVRO systems have also been developed [13-15, 22-28, 31]. Many of the early systems were simply a photovoltaic array and battery bank used to power an existing reverse osmosis system. Such systems were found to be inefficient, so recent research has focused on increasing system efficiency, with some success. The Canary Islands Technological Institute has developed a small battery-based system [22, 23]. Battery-based systems have also been commercialized by Spectra Watermakers [28]. Hybrid solar/wind reverse osmosis systems have been developed [25-27]. Research has also led to the development of more cost-effective seawater PVRO systems without batteries [13-15, 31].

2.1.2 PVRO System Design and Control

Despite the large body of work in designing and field testing PVRO systems, very little research has been done to determine the most effective way to operate such systems. Control techniques in systems containing batteries focus on maximizing the power transferred to the batteries and then running the system at a fixed operating point. Some simple batteryless systems operate using only one pump and maximize the power transfer. For example, Carvalho optimizes system performance by controlling the operating point of the reverse osmosis pump to maximize the PV panel power output [32]. More complex systems have multiple pumps and other actuators to control the system operation. For these cases, researchers have treated system operation as a

power management problem and distribute the power to maximize the overall water produced [14, 15, 17, 31, 33].

Although these strategies have been shown to maximize water production for a given system in the short-term, none of these strategies consider the degradation effects of different components. A common concern with variable operation of PVRO systems is the fouling of the reverse osmosis membranes [5, 14, 15, 25]. Studies have shown that this is not a major concern over the course of days [33], but no studies have yet quantified the long term effects. Long term degradation effects need to be quantified for an effective system design.

Methods for designing PVRO systems have also been developed. Mohamed presents a method to design a hybrid PV and wind powered RO system using a spreadsheet model and average solar and wind data to size the individual system components [13]. Voivontas describes a design program to aid in the design of a renewable energy powered desalination system [34]. The software tool uses the user inputs to size the energy system and perform a financial analysis, and allows users to analyze different options. Bourouni, et al., developed a method to optimize a renewable energy powered RO system that considers photovoltaics and wind energy as possible power sources [35]. Their software sizes the components and simulates the system operations over a typical year to determine if the configurations are feasible. Though similar to the modular design problem proposed, none of these approaches include different types of components, system topology optimization, uncertainty in power available, variations in system demand and the effects of component degradation.

2.1.3 RO System Design and Control

Researchers have developed different system operation and cost models to guide the design of reverse osmosis systems. Aspects of these models can be used to develop modular design algorithms for PVRO systems. The models range from cost models based on empirical relationships to technical models based on first principles. Wilf develops basic models that can be used for evaluating the cost of RO systems, and how these costs vary by water type [36, 37]. Malek determined empirical cost relationships for components in a reverse osmosis system [38]. Gambier developed a model of the reverse osmosis system based on first principles for use in control system design [39].

Design methods for reverse osmosis desalination systems have been developed. El-Halwagi was the first to formulate the optimization of reverse osmosis networks as a mixed integer non-linear programming (MINLP) problem [40]. El-Halwagi used a general superstructure to represent any two-stage reverse osmosis network and used a resolution method to minimize the system capital cost. Voros simplified El-Halwagi's approach and formulated the problem as a non-linear program (NLP) [41]. Marcovecchio used an iterative solution method to solve the same problem [42]. Saif used the same general superstructure and solved the problem using a branch and bound approach [43]. Recently, Lu used the general superstructure to optimize reverse osmosis systems with different membrane types and also considered membrane degradation [44, 45]. Vince extended the problem using the set structure to a multi-objective optimization to determine a system that minimizes the cost and environmental impact [46]. Although these methods are useful, their ability to determine the most effective reverse osmosis system configuration is limited, as they were restricted to two stage problems. In addition, they are not appropriate for a modular design approach considered in this research, since only a few types of membranes are considered and no inventory is considered for other system components.

Another representation of reverse osmosis systems for design optimization has been developed by Maskan that uses an alternate representation of the reverse osmosis system based on graph theory [47]. Despite having a framework to evaluate many different configurations, Maskan only considered eight standard system configurations in design. Additionally, only one type of each component is considered.

The operation of reverse osmosis systems has also been topic of some research. Typically, the operating point of a reverse osmosis system is determined during the design stage and the control problem becomes a regulator problem. Approaches considered include model predictive control [48, 49], fault tolerant control [50] and optimal control methods [51]. The setpoint optimization for a given reverse osmosis system has been considered. Bartman developed a method to minimize the specific energy consumption for a system without energy recovery [52]. Poullikkas developed a method to evaluate the economics of different operational schemes for reverse osmosis desalination systems [53]. Guria used genetic algorithms to determine optimum pressure setpoints for reverse osmosis systems [54]. These methods, while useful for reverse osmosis systems without power limitations, are not directly applicable to PVRO systems. A

PVRO system must be able to accommodate power fluctuations to maximize system production while considering system component degradation.

2.2 Modular Design

There are many different systems composed of modular components. Automatic modular design methods have been developed for applications such as robotic systems, electronics, and chemical processing plants. These developments are briefly reviewed in this section.

2.2.1 Modular Design of Robotic Systems

The robotics community has looked to modular systems to reduce system cost and fabrication times [55-60]. As a result, modular design methods have been developed for robotic systems. Rutman developed a method to configure a field robot from an inventory of modular components using a series of design filters to reduce the number of possible configurations and then searched the design space for the best option [58]. Farritor further refined this design approach and used a genetic algorithm to determine the best robot configurations [57]. Hornby developed another method to configure modular robots, in which the robots are defined as a serial chain and evolutionary algorithms are used to design both the robots and the control commands to accomplish a given task [59]. Another notable work in the area of modular robotics was Leger's software package Darwin2K, which synthesizes robotic designs from modular components [60]. Leger developed a graph approach to represent the robot structure and coupled this to a set of evolutionary algorithms to determine the best modular robot design.

2.2.2 Modular Design of Electronic Circuits

Modular design has been widely used in the field of electronics, especially in the areas of automated analog and digital circuit design. The vast majority of work in analog circuit design uses evolutionary algorithms to optimize a circuit [61-64]. Koza developed a method to design filters using genetic programming [61, 62]. Similarly, Lohn developed a method using genetic algorithms to automatically design filters and transistor based amplifier circuits [63]. They configured the optimization algorithm to operate in parallel and used the circuit simulation tool SPICE to evaluate different configurations. Other optimization algorithms such as simulated

annealing [64] have also been used in automated analog circuit design problems with somewhat limited success.

The majority of the methods used for automated digital circuit design also employ genetic algorithms to configure the circuits. One example is Miller, who used genetic algorithms to configure circuits to perform arithmetic operations [65]. Miller's method was somewhat limited as it requires the total number of components to be input as a parameter. Another example of digital circuit design is Sentovich, who focused on synthesizing VLSI circuits using evolutionary algorithms [66].

2.2.3 Modular Design of Computer Programs

Another area where modular design optimization algorithms have been employed is the automated generation of computer programs. This field, called Genetic Programming, was pioneered by Koza [67, 68]. In this application, a desired program output is specified and the evolutionary algorithm generates program trees that are optimized using the algorithm to have the specified behavior. Genetic programming uses a population of potential designs like genetic algorithms, but uses special operators to perform the mating and mutation tasks.

2.2.4 Synthesis of Chemical Networks

Design algorithms have been employed for heat exchangers, mass exchangers and chemical processing networks. These problems are commonly solved using genetic algorithms [69-71]. An example of the mass exchange problem that can be used with a genetic algorithm was formulated by Garrard [69], but requires the user to specify the overall system size. Lewin formulated a heat exchanger network problem as a mixed integer linear program which was solved in two parts [70]. First, a genetic algorithm was used to determine the heat exchanger network configuration. Second, a linear program was used to solve for the system parameters. In this approach, the overall system size was also a user input parameter. These methods provide insight for the modular design problem, but are not directly applicable. Another approach, considered by Cantoni, used genetic algorithms to optimize a plant configuration while considering downtime of components for maintenance [72]. This approach only considered simple processes such as transporting and crushing materials. All of these approaches have

limited system topology optimization, and do not incorporate variations in available power or variations in system demand.

2.3 Design with Uncertain Inputs

PVRO desalination system design should incorporate knowledge about the statistical nature of the environment. This topic has not been directly addressed in literature, but the design of similar systems, such as PV power systems and renewable energy systems have been discussed. An overview of methods developed to accommodate this uncertainty using design rules, simulation, and statistical design methods is presented in this section.

2.3.1 General Design Rules

Uncertainty is commonly accommodated by applying general design rules, such as historical averaging and safety factors. For example, PV-battery systems are often sized using historical average values to determine the required array size and the number of consecutive cloudy days to determine the sizing of the components. Safety factors are incorporated to ensure that the system load is met with a defined level of confidence. Mack developed a method to size stand-alone PV-battery systems for remote telecommunication systems [73]. This method used general rules of thumb to size the individual components. Mack's method was simplified by Chapman, who used average data from the worst month to determine the PV array and battery capacities that would provide a power supply with a desired reliability [74]. Another method, developed by Sidrach-de-Cardona, uses relationships derived from detailed numerical studies of individual locations to determine system configurations using data found in any solar radiation atlas [75]. Although these methods provide useful guidelines, they are unable to guarantee a system reliability level and often result in oversized or undersized PV-battery systems. In addition, they do not consider variations in system load, which are critical for the design of PVRO systems.

2.3.2 Robust Design Methods

Robust optimization has been studied extensively in many fields including operations research. The robust optimization methods outlined in literature can be differentiated into two

main classes [76]. In the first class, the robustness metrics can be directly calculated using numerical techniques and the resulting optimization problem can be solved deterministically. In the second class, the uncertainties are treated directly by optimizing noisy functions and constraints through Monte Carlo techniques. Both classes of methods have been employed in the design of PV systems.

Methods of the first class make simplifications to the statistical properties of the solar radiation to achieve a closed form expression for the probability of meeting a given power demand. Researchers developed methods to determine the loss of load probability for different system configurations. Bucciarelli developed a random walk method to determine probability that a PV system with storage is able to meet demand [77]. This method used two states – increasing or decreasing capacity – to determine if a system would meet demand and resulted in a closed-form solution to the loss of power probability. Bucciarelli then expanded this approach to consider correlations between consecutive days to improve the overall accuracy [78]. Bagul expanded the method to include three states when analyzing the reliability of a PV-battery system [79]. Gordon also used a random-walk method to determine the loss-of-load probability [80]. McComber assumed daily insolation is an uncorrelated normal random variable with known mean and variance to estimate the loss of load probability for different PV-battery systems[81]. These methods have not been implemented in an optimization framework to determine the system configuration, but the analytical insight they provide is directly transferrable to the PVRO design problem.

Other approaches for designing renewable energy systems have used time-series data to determine which systems are able to meet demand. In an approach developed by Koutroulis, a measured solar radiation profile and wind profile is used over a 20-year time period to determine which PV-Wind-battery systems are able to meet demand [82]. Different combinations of components are selected and then sized using a genetic algorithm to determine the best system configuration. Other researchers have also used recorded data to simulate the performance of renewable energy systems and determine the lowest cost option to satisfy a given demand [83-85]. Since time-series analysis requires significant computation time, other researchers have limited the time-series analysis to reduce it. Markvart extracted critical times from the year to determine the sizing curve for a PV-battery system with a given reliability [86]. The use of time-series data is convenient, but due to the limited number of years of data available (~20 years),

it's impossible to guarantee a loss of load probability less than 1% [87]. In addition, time-series data is not available for all locations, making its use for design limited. Some researchers have developed methods which use simulated time-series data that matches the statistical parameters of the locations to circumvent these issues [88].

Sampling methods have also been used to accommodate the variations in solar radiation in the design of renewable energy systems. Gainnakoudis developed a method to optimize the design of a renewable energy system using Monte Carlo sampling [89]. In the optimization, the renewable energy system was evaluated for an average year where the random input was a percentage deviation from the normal year. Arun used a similar method to consider variations on the solar radiation [90]. Dominguez-Munoz developed a method to analyze the reliability of a solar thermal system using Monte Carlo methods [91]. Roy used a similar technique to analyze the reliability of stand-alone wind-battery energy systems [92]. While the work done in designing stand-alone renewable energy systems provides insight, there are additional factors that should be considered when designing PVRO systems. None of these methods incorporate variation in the load into the design, something that is critical for PVRO systems.

2.4 Summary

This section provided an overview of related work to the modular design problem applied to the photovoltaic reverse osmosis systems. Modular design approaches for different applications such as robotics, circuit design, and computer programs were overviewed. Methods for designing PV and RO systems were also reviewed. The methods developed provide insight into the problem, but none are directly applicable to the PVRO modular design problem. The challenges of dealing with a large inventory, complex system physics, and variations in the system environment make this problem challenging and unique.

CHAPTER

3

PVRO SYSTEM FEASIBILITY

3.1 Introduction

In this section, a method for determining the engineering feasibility of community-scale PVRO systems is developed. A PVRO system is engineering feasible if it is both technically and economically feasible. Technical feasibility of community-scale PVRO systems has been established [11, 14, 15, 18-30]. Economic feasibility for the PVRO system is established based on a cost comparison with equivalent water supply methods for remote locations. Several examples illustrating application to both remote and populated areas are presented.

Studies have been conducted to evaluate the economic feasibility of community-scale photovoltaic reverse osmosis systems for remote locations. A cost analysis was performed for a photovoltaic reverse osmosis system in Oman [24]. The economic feasibility of a reverse osmosis system powered by wind turbines and photovoltaics in Greece has also been analyzed [12]. Photovoltaic and diesel powered reverse osmosis systems in the United Arab Emirates have been compared [93]. These studies have shown that engineering feasibility of these systems is critically dependent on location. Typically, the focus is on the cost of the photovoltaic panels and reverse osmosis membranes, which are generally very expensive. To date, no generalized methods to evaluate the feasibility of these systems including the effects of location have been developed.

3.2 Approach

In this section, a generalized method to determine the engineering feasibility of community-scale, photovoltaic-powered seawater and brackish water reverse osmosis systems is presented. As discussed above, PVRO has been shown to be technically feasible. However, to be practical for implementation, PVRO systems must also be economically feasible. Economic

feasibility is heavily dependent on local political and social considerations [94, 95]. Here, economic feasibility is determined by comparing the PVRO water cost with water provided by conventional methods. The main means to provide fresh water to remote, water scarce regions is by transporting water or by using diesel powered water desalination. Here, the feasible regions are considered to be water scarce areas that satisfy the following two criteria. First, the cost of water produced by the photovoltaic reverse osmosis system is less than the cost of transported water. The second criterion is that the photovoltaic reverse osmosis system must be less expensive than an equivalent diesel-powered reverse osmosis system. Grid-based systems are not evaluated.

In this approach, the lifecycle costs (capital, operation, and maintenance costs) of photovoltaic-powered and diesel-powered reverse osmosis systems are analyzed. The lifecycle cost for both systems is broken into two main components, the system capital costs and the operating costs. These costs are based on the water demands, local solar energy resource, and water characteristics. Due to the energy intensive nature of reverse osmosis, a detailed energy analysis is used to determine the solar array size, diesel generator size and the diesel fuel consumption. Then, local political factors such as carbon taxes and renewable energy incentives are added. The resulting water cost for the PVRO system is compared with the cost of water produced by a diesel generator system and transported water to determine the most cost effective option.

To demonstrate the method, seawater reverse osmosis case studies were completed for representative locations. Clearly, solar energy and water type vary by location. To account for these variations, global Geographic Information Systems (GIS) data was obtained for solar energy and water characteristics [8, 96]. The lifecycles for diesel and photovoltaic-powered 10 m^3 water per day reverse osmosis systems were analyzed to determine the overall water cost. A 10 m^3 system provides 100 people with 100 liters of water per day, more than enough to meet basic household needs [97]. These two costs were then compared to determine where the photovoltaic-powered systems are less expensive. Areas which have lower costs for the photovoltaic-powered system and an overall water cost less than \$10.00 per m^3 (approximate cost of water transportation in the Greek Islands [98]) are considered feasible. Individual sites were then chosen for a detailed cost breakdown.

Brackish water reverse osmosis case studies are also presented. The feasibility of photovoltaic-powered brackish water reverse osmosis is also location dependent. Unfortunately, global GIS data for groundwater conditions is not available, so only a site-specific analysis could be conducted. For these sites, the analysis was conducted in the same manner as the seawater systems. The energy requirements for each site were determined based on water salinity and water depth. The required solar energy and diesel power systems were configured. A full life cycle cost analysis was performed for both systems to determine where photovoltaic-powered reverse osmosis systems would be economically feasible.

3.3 Analysis

3.3.1 Assumptions

For this analysis, it is assumed that the solar-powered reverse osmosis systems do not incorporate any energy storage and will only operate when the solar power is available. In addition, average yearly values for solar insolation, water salinity, and water temperature are used. Also, this analysis considers only the energy required to perform the reverse osmosis. It does not include the energy requirements for pretreatment, post-treatment, water transportation and brine disposal. The energy required for these tasks is relatively small compared to the energy for the reverse osmosis process. Finally, it is assumed that water is incompressible and is taken from the nearest possible seawater or brackish water source.

3.3.2 Energy Requirements

3.3.2.1 Photovoltaic Reverse Osmosis System Sizing

For the photovoltaic-powered system, it is assumed that the reverse osmosis system will operate intermittently when solar power is available, eliminating the cost and complications of batteries. As a result, the plant capacity as well as feed and product flows need to be scaled according to the number of hours that the system operates. For the photovoltaic-powered system, the average product flow in m^3/hour during daylight operation, $Q_{p,s}$, is given by:

$$Q_{p,s} = \frac{V_{cap}}{t_{sun}} \tag{3.1}$$

where V_{cap} is the daily system production capacity in m^3/day and t_{sun} is the number of daylight hours at the location. The size of the reverse osmosis system is scaled to produce the required amount of water in the daylight hours and this value varies by location due to the variation in daily sunshine hours. In the analysis presented below, an availability factor is used to account for daylight hours when the photovoltaic reverse osmosis plant is not operational due to limited sunlight or maintenance.

3.3.2.2 Diesel Reverse Osmosis System Sizing

The diesel-powered system is assumed to operate 24 hours a day and the corresponding flow of desalinated water for the diesel system in m^3/hour is computed as:

$$Q_{p,d} = \frac{V_{cap}}{24} \tag{3.2}$$

In this analysis, the capacity of the system and the diesel system product flow rate are the same for all locations. The product flow rate for the solar-powered system will be greater than that of the diesel-powered system.

3.3.2.3 Reverse Osmosis Power Requirements

A simple schematic of the photovoltaic reverse osmosis system considered is shown in Figure 2.1. The diesel generator system differs only in the power source, otherwise the schematic is identical. In this system, the energy source powers a feed pump and a high-pressure pump to pressurize the incoming water. The water is then driven through the reverse osmosis membrane array by the high pressure produced by the pumps, leaving high salt concentration brine on one side and low salt concentration water on the other side. The high-pressure brine stream passes through a turbine to recover its energy before exiting the system.

The power required by the reverse osmosis system can be expressed as:

$$P_{RO} = P_{HP} - P_{ER} \tag{3.3}$$

where P_{HP} is the power required by all pumps and P_{ER} is the power recovered from the exiting bring by the energy recovery device. All power units are in kW.

The power required to pressurize the high pressure stream is determined by:

$$P_{HP} = 27.78 \frac{p_f Q_f}{\eta_{HP}} \tag{3.4}$$

where p_f is the reverse osmosis membrane feed pressure in bar, Q_f is the reverse osmosis unit feed flow rate in m^3/hour, the constant is the unit conversion factor, and η_{HP} is the efficiency of the motor and pump.

The brine exits the reverse osmosis unit at a high pressure. It is important to recapture this energy to reduce the power consumption of the reverse osmosis process and hence the cost. The power recovered by an energy recovery device is given by:

$$P_{ER} = 27.78 p_b Q_b \eta_{ER} \tag{3.5}$$

where p_b is the reverse osmosis membrane brine exit pressure in bar, Q_b is the reverse osmosis membrane brine flow rate in m^3/hour, the constant is a unit conversion factor, and η_{ER} is the efficiency of the energy recovery system.

The pressures and flow rates for the reverse osmosis system are found using equations (3.6)-(3.10) given below. Water is nearly incompressible under pressures considered here. Hence, the volume of the water is conserved and the system flow rates are related by:

$$Q_f = Q_b + Q_p \tag{3.6}$$

where Q_f is the feed flow rate, Q_b is the brine flow rate and Q_p is the product flow rate in m^3/hour. The flow of the product water through the reverse osmosis membrane is related to the feed pressure by [99]:

$$Q_p = K_p K_{TCF} A_{mem} p_{nd} \tag{3.7}$$

where K_p is the permeability of the membrane to water in m/bar-hour, K_{TCF} is the membrane permeability temperature correction factor, A_{mem} is the membrane area in m^2, and p_{nd} is the net driving pressure in bar as given by:

$$p_{nd} = \Delta\overline{p} - \Delta\overline{\pi} \tag{3.8}$$

where $\Delta\overline{p}$ is the average differential pressure across the membrane in bar, and $\Delta\overline{\pi}$ is the average difference in osmotic pressure across the membrane in bar. The osmotic pressure differential can be determined using the method outlined in [99]. The pressure of the brine is determined using the following empirical relation [99]:

$$p_b = p_f - 0.054\left(\frac{Q_f + Q_b}{2}\right)^2 \tag{3.9}$$

As the feed water temperature increases, the membrane permeability also increases. This is incorporated into the reverse osmosis model through the membrane permeability temperature correction factor, empirically found to be [99]:

$$C_{TCF} = \begin{cases} exp\left(2640\left(\frac{1}{298} - \frac{1}{273+T}\right)\right) & T \geq 25 \\ exp\left(3020\left(\frac{1}{298} - \frac{1}{273+T}\right)\right) & T < 25 \end{cases} \tag{3.10}$$

where T is the feed water temperature in ^{o}C.

The system recovery ratio is an important design variable of a reverse osmosis system, which is given by:

$$R = \frac{Q_p}{Q_f} \tag{3.11}$$

3.3.2.4 Water Transportation Energy Requirements

It is assumed that the reverse osmosis unit is located close to the sea or a brackish well and that transporting the water over long distances is not necessary. However, the reverse osmosis unit will be located some distance above the water line. The power required to raise the water in kW is given by:

$$P_{FP} = \frac{Q_f \rho g h}{3.6\times10^6 \eta_{FP}} \tag{3.12}$$

where ρ is the water density in kg/m^3, g is the acceleration due to gravity in m/s^2, h is the change in the water height in m, and η_{FP} is the feed pump efficiency. For the seawater analysis, h is given by the site elevation above sea level. For the brackish water analysis, h is the depth of the water source.

3.3.3 Energy Source

3.3.3.1 Solar Array Requirements

For the photovoltaic powered reverse osmosis system, the total energy required in kWh is given by:

$$E_{PV} = (P_{FP} + P_{RO}) t_{sun} \tag{3.13}$$

Assuming that the desired water production is averaged over many years, the solar array area necessary to provide this power can be written as:

$$A_{PV} = \frac{E_{PV}}{\eta_{PV} H} \tag{3.14}$$

where H is the solar insolation at the location in kWh/m^2-day and η_{PV} is the efficiency of the array.

The photovoltaic array power rating in kW can then be found from the array area using:

$$W_p = \eta_{PV} A_{PV} G_r \tag{3.15}$$

where G_r is the radiation that is used for the solar array peak power rating in kW/m^2. The standard value used by most solar panel manufacturers is 1 kW/m^2.

3.3.3.2 Diesel Generator Requirements

If a diesel generator is providing the energy required for the reverse osmosis system, it can run continuously. The power rating of the generator required, in kW, can be written as:

$$P_{GEN} = \frac{P_{FP} + P_{RO}}{LF} \tag{3.16}$$

where LF is the generator load factor. For this rate of power generation, the rate of diesel fuel used in kg/s is given by:

$$\dot{m}_{fuel} = \frac{P_{FP} + P_{RO}}{\eta_{GEN} \Delta H^0_{comb}} \tag{3.17}$$

where η_{GEN} is the diesel-powered generator overall efficiency, and ΔH^0_{comb} is the net calorific value of diesel fuel, which equals 42.8 MJ/kg at 25^{o}C [100].

3.3.4 System Cost

This section outlines the financial analysis of reverse osmosis systems. The method utilized was the annualized life cycle cost method outlined by Ettouney [94]. The costs are separated into capital system costs and operating costs. The cost elements are presented in this section.

3.3.4.1 Assumptions

It is assumed that system costs, including capital costs and costs of consumables such as diesel, are a function of location. Accounting for these local political and social considerations on a global scale is beyond the scope of this analysis. Here, average values for system capital costs and consumable costs are used as an example. These values can be modified for a particular location and demand.

3.3.4.2 Overall Cost of Desalinated Water

The total equivalent annual cost for the solar-powered and the diesel-powered reverse osmosis systems can be expressed as:

$$A_{Total,PV} = A_{CC,PV} + A_{Op,RO} + A_{Op,PV} \tag{3.18}$$

$$A_{Total,GEN} = A_{CC,GEN} + A_{Op,RO} + A_{Op,GEN} \tag{3.19}$$

where $A_{CC,PV}$ is the annual capital cost of the photovoltaic reverse osmosis system in USD, $A_{CC,GEN}$ is the annual capital cost of the diesel reverse osmosis system in USD, and $A_{Op,RO}$ represents the annual subsystem operating costs.

From the total equivalent annual cost for both systems, the cost per m^3 of water can be found using:

$$C_w = \frac{A_{Total}}{365nfV_{cap}} \tag{3.20}$$

where n is the system lifetime in years, f is the reverse osmosis plant availability, and V_{cap} is the system water production capability in m^3/day.

3.3.4.3 Capital Costs

Capital costs consist of the cost of the reverse osmosis system and the cost of the energy production system. The capital costs are converted into equivalent annual costs using [94]:

$$A_{cc} = \frac{i(1+i)^n}{(1+i)^n - 1} DC \tag{3.21}$$

where i is the interest rate, and DC is the full system direct capital cost of the photovoltaic or diesel reverse osmosis system.

3.3.4.4 Reverse Osmosis System

The costs for a reverse osmosis system vary with system size. The total cost of the reverse osmosis system including water intake, pretreatment, post-treatment and installation is given by:

$$C_{RO} = 24 Q_p U_{RO} \tag{3.22}$$

where U_{RO} is the specific cost of the reverse osmosis system in \$/m^3/day. For the community-scale seawater systems considered here, the total capital costs of \$2400 and \$1200 per m^3 of daily capacity are assumed for seawater and brackish water systems respectively [94, 101]. The breakdown of the reverse osmosis system components is shown in Table 3.1.

Table 3.1: Reverse osmosis components cost breakdown [102].

System Component	Contribution to Capital Costs
Intake Cost	25% of System Capital Costs
Pretreatment System	10% of System Capital Costs
Reverse Osmosis Components	25% of System Capital Costs
Post-Treatment & Brine Disposal	5% of System Capital Costs
Installation & Infrastructure	30% of System Capital Costs
Professional Costs	5% of System Capital Costs

3.3.4.5 Photovoltaic Power System

The capital cost of the entire photovoltaic power system, including the costs of the control electronics, wiring, supporting structures and installation can determined using:

$$C_{PV} = W_p U_{PV} \tag{3.23}$$

where W_p is the peak power rating of the array in Watts and U_{PV} is the unit cost in \$/Watt. Government incentives can substantially change these costs. For this analysis, a historical price \$9.00 per watt peak was chosen for the installed cost of the solar energy systems [103].

3.3.4.6 Diesel Generator System

For comparison with the solar energy system, the capital cost of the diesel generator system should be included. Here, the cost of the diesel generator system is estimated from manufacturer cost data [104]. An installation cost of 10% is assumed in addition to the generator price, so the total cost of the diesel generator system is given by:

$$C_{GEN} = 1.1U_{GEN} \tag{3.24}$$

where U_{GEN} is the cost of the generator set in $.

3.4 Operating Costs

3.4.1 Reverse Osmosis

The total annual operational cost for the reverse osmosis system is given by:

$$A_{Op,RO} = A_l + A_{chem} + A_{r,RO} \tag{3.25}$$

where A_l is the annual labor cost, A_{chem} is the annual chemical cost, and $A_{r,RO}$ is the annual cost of component replacement in $.

The annual cost of the labor is expressed as:

$$A_l = 365\gamma f V_{cap} \tag{3.26}$$

where γ is the specific operating labor cost in $/m^3-day, f is the fraction of time the reverse osmosis system is operating (the plant availability factor), and V_{cap} is the plant capacity in m^3/day. In this analysis, the nominal labor cost was chosen as $3.00/m^3-day [93].

The chemical costs are also location specific as the pre-treatment chemicals are dependent on local water conditions. The total annual cost of treatment chemicals is given by:

$$A_{chem} = 365kfV_{cap} \tag{3.27}$$

where k is the average cost of chemicals $/m^3. In this analysis, the treatment chemical cost per m^3 is assumed to be $0.033 [94].

Throughout its lifetime, certain components of the reverse osmosis system will require replacement. The major components that will require regular replacement are the reverse osmosis membranes. Although it's never been shown, researchers have speculated that membrane life in PVRO systems would be reduced due to the cycles associated with system operation. To address this issue, it is assumed that the membranes in the PVRO system will be replaced twice as often. Less frequently, the motors and pumps may also require replacement. The components and their replacement rates for a typical system are given in Table 3.2.

Table 3.2: Replacement rates for reverse osmosis components [93].

Component	Cost	Annual Replacement Rate – Diesel-RO System	Annual Replacement Rate – PVRO System
Membranes	40% of RO Components	20%	40%
Pumps	15% of RO Components	10%	10%
Motors	15% of RO Components	10%	10%
Energy Recovery Devices	15% of RO Components	10%	10%

Using the data in Table 3.2 and the component costs found in Table 3.1, the annual cost for component replacement can written as:

$$A_{r,RO} = C_{mem}RR_{mem} + C_pRR_p + C_{motor}RR_{motor} + C_{er}RR_{er} \tag{3.28}$$

where C represents the component costs and RR is the component replacement rate.

3.4.2 Photovoltaic Power System

The annual costs for the photovoltaic-power system are low since the energy for this system comes directly from the sun. The photovoltaic panels will not require replacement during the system lifetime since their expected life is 25 years. Other portions of the photovoltaic-power system will require maintenance and replacement over the system operational life. The system electronics are the major component that will require replacement; the replacement rate for the electronics is taken to be 10% annually and the cost is given by:

$$C_{PV,E} = 0.72W_p \tag{3.29}$$

where W_p is the peak power rating of the photovoltaic array in W, and the average cost of electronics is \$0.72/W [105]. The equivalent annual operating cost for the photovoltaic power system is given by:

$$A_{r,PV} = C_{PV,E}RR_{PV,E} \tag{3.30}$$

where $RR_{PV,E}$ is the replacement rate for the photovoltaic system components.

3.4.3 Diesel Generator System

The total annual cost for the generator is given by:

$$A_{Op,GEN} = A_{f,GEN} + A_{O\&M,GEN} + A_{r,GEN} + A_{Ctax,GEN} \tag{3.31}$$

where $A_{f,GEN}$ is the annual fuel cost, $A_{O\&M,GEN}$ is the annual operation and maintenance cost, $A_{r,GEN}$ is the annual replacement cost for the generator system, and $A_{Ctax,GEN}$ is the annual carbon tax on the generator emissions.

Fuel costs are sensitive to location and vary from season to season. The price of diesel fuel fluctuates, but in general its price has increased over time. An average diesel fuel escalation rate of 12% was found through analysis of data from the Energy Information Administration of the US Government data [106]. Using this escalation rate, the annual diesel fuel costs can be calculated using [107]:

$$A_{f,GEN} = PV_{fuel}\frac{i(1+i)^n}{(1+i)^n-1} = 365\,fC_{fuel}V_{fuel}\left[\frac{1-(1+j)^n(1+i)^{-n}}{i-j}\right]\frac{i(1+i)^n}{(1+i)^n-1} \tag{3.32}$$

where f is the reverse osmosis plant availability, C_{fuel} is the diesel cost in \$/L during year 1, V_{fuel} is the volume of fuel used per day in Liters, and j is the fuel cost escalation rate.

The operating and maintenance costs of the diesel generator in \$/hour are estimated using [104]:

$$C_{O\&M,GEN} = \frac{(0.242+0.3505P_{GEN})18+143.1}{600} \tag{3.33}$$

where P_{GEN} is the power rating of the generator in kW. The constants in the equation above are derived from empirical data [104].

Using the above hourly operational cost, the annual operating and maintenance cost for the generator is given by:

$$A_{O\&M,GEN} = 365(24)\,fC_{O\&M,GEN} \tag{3.34}$$

The diesel generator will also require replacement during the lifetime of the system. The generator lifetime will depend on the generator model. Here, an average lifetime of 21000 operating hours for a diesel generator is assumed [104]. This corresponds to an average rate of replacement of 40%. This annual replacement cost of the diesel generator is given by:

$$A_{r,GEN} = C_{GEN}RR_{GEN} \tag{3.35}$$

where C_{GEN} is the diesel generator cost in \$ and RR_{GEN} is the annual replacement rate for the generator system.

Many countries around the world have imposed economic penalties on the production of $C0_2$. This impact can also be factored into the analysis. The annual cost due to $C0_2$ emissions can be found using:

$$A_{Ctax,Gen} = C_{CO_2}m_{CO_2} \tag{3.36}$$

where C_{CO_2} is the carbon tax in \$/kg, and m_{CO_2} is the mass of CO_2 produced per year in kg which can be found using equation (3.37). Carbon taxes are due to the local political conditions: for example, in France, the current carbon tax is \$0.25/kg [108].

The rate of carbon dioxide production by the generator can be calculated using the relationship [93]:

$$\dot{m}_{CO_2} = \dot{m}_C \frac{M_{CO_2}}{M_C} = \dot{m}_{fuel} w_C \frac{M_{CO_2}}{M_C} \tag{3.37}$$

where $M_{CO_2}$is the molar mass of carbon dioxide, M_C is the molar mass of carbon, and w_c is the mass fraction of carbon in the diesel fuel.

3.5 Case Studies

3.5.1 Seawater Systems

3.5.1.1 Analysis for Any Location

The feasibility of community-scale seawater reverse osmosis systems is analyzed for all locations using Geographic Information Systems (GIS) data. GIS data on a 1° by 1° grid was collected for annual average solar insolation for latitude tilt [8], water salinity and water temperature [96]. This data was then analyzed using the method outlined in equations (3.1)-(3.37). The constants used in the analysis are given in Table 3.3.

Table 3.3: Input parameters for seawater reverse osmosis analysis.

Parameter	Value
Plant Capacity, V_{cap}	10 m^3
Plant Lifetime, n	25 years
Interest Rate, i	5%
Plant Availability Factor, f	90%
Recovery Ratio, R	40%
Reverse Osmosis Membrane Permeability, K_p [99]	3.5 x 10^{-10} m/bar-s
Reverse Osmosis Motor & Pump Efficiency, η_{HP} & η_{FP} [93]	70%
Energy Recovery System Efficiency, η_{ER} [93]	80%
Array System Efficiency, η_{PV}	15%
Generator Efficiency, η_{GEN} [104]	30%
Generator Load Factor, LF [104]	80%
Reverse Osmosis System Cost, U_{RO} [94]	\$2400 / m^3
Installed Array System Cost, U_{PV} [103]	\$9.00 / W_p
Initial Diesel Fuel Cost, C_{fuel} [106]	\$0.66 / L (\$2.50 / Gallon)
Diesel Fuel Annual Inflation Rate, j [106]	12%

The Middle East is a large market for desalination since the majority of the region does not have access to an adequate freshwater resource. Hence, a more detailed analysis was carried out

for this region. GIS data was obtained for a denser grid of 0.25° by 0.25° to provide a more detailed picture of this region.

The solar array area required for the 10 m^3 per day reverse osmosis system discussed above is shown in Figure 3.1. It is evident from this figure that array area requirements are lower for equatorial regions that have high solar insolation. Also, the majority of areas in the Middle East require less than 40 m^2 of solar array area to power a small reverse osmosis system. The area requirements for systems in equatorial regions are reasonable.

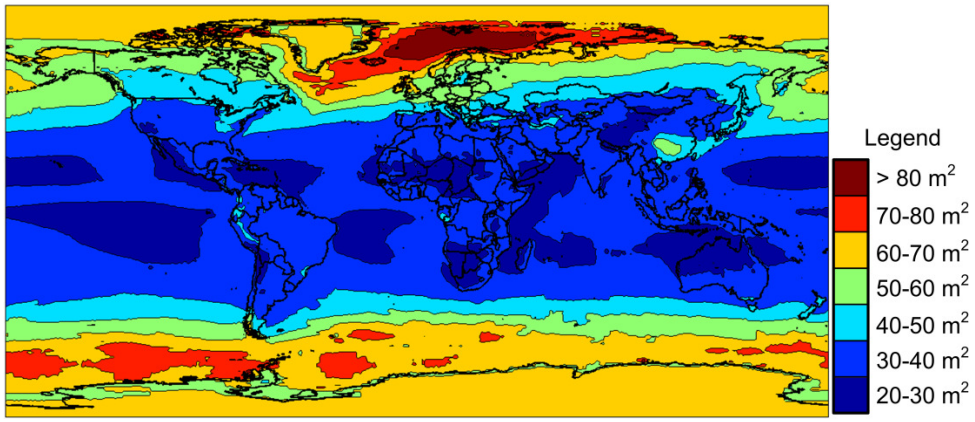

Figure 3.1: Array area required for 10m^3 system.

The cost of water produced by the photovoltaic powered reverse osmosis system is presented in Figure 3.2 and Figure 3.3. Figure 3.2 shows that the majority of equatorial regions are able to produce fresh water for less than $6.00 per m^3. Based on published water transportation cost data of $10.00 per m^3 [109], PVRO is a feasible alternative to transported water supplies.

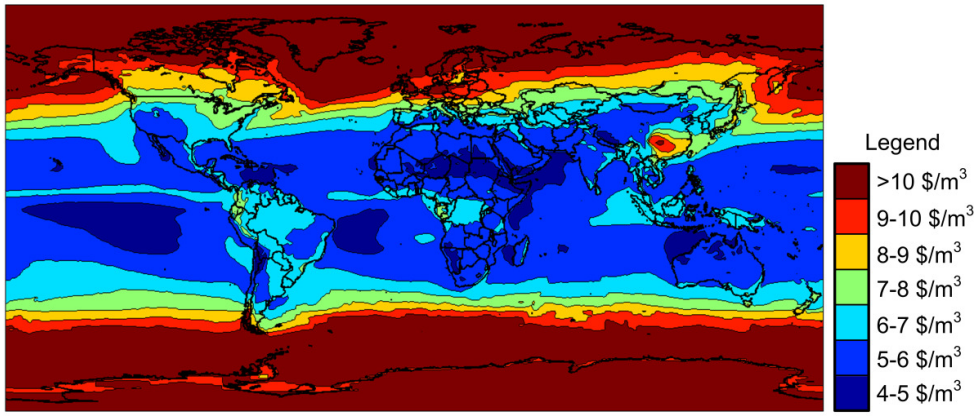

Figure 3.2: Water cost for 10m^3 system.

Figure 3.3 shows water prices for the photovoltaic reverse osmosis system in the Middle East. Many coastal areas in this region are able to produce clean water using photovoltaics for less than $5.00 per m^3. As expected, water prices increase for Northern areas that receive less sunshine. Water prices also increase in areas that have higher salinity feed water, such as the Persian Gulf and the Mediterranean Sea.

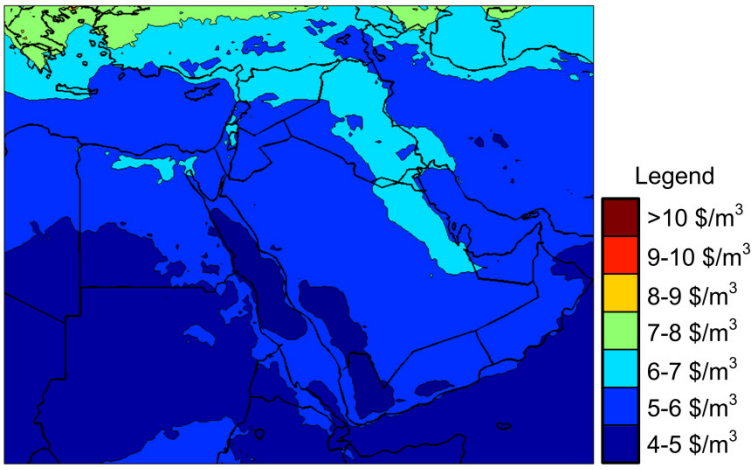

Figure 3.3: Water cost for a $10m^3$ system in the Middle East.

In order for the photovoltaic-powered reverse osmosis system to be cost competitive, the cost of the water produced should be less than the cost of water produced by an equivalent diesel-powered system. Figure 3.4 and Figure 3.5 show regions where a solar-powered reverse osmosis system would be more cost effective than using diesel-powered reverse osmosis. Photovoltaic-powered reverse osmosis systems are economically feasible throughout large areas of water scarce regions. The coastal regions of Northern Africa, the Middle East, South Africa, Mexico and the Caribbean are all examples of water stressed areas where a solar-powered seawater reverse osmosis system could feasibly deliver clean water to small communities at a lower cost than a diesel powered reverse osmosis system.

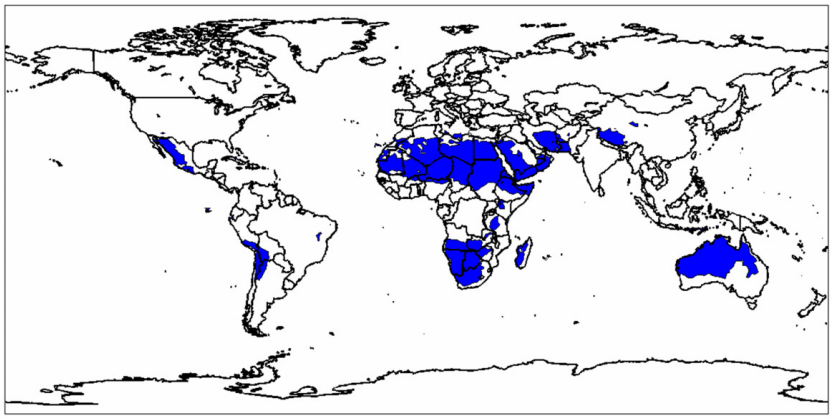

Figure 3.4: Areas where PVRO systems are feasible.

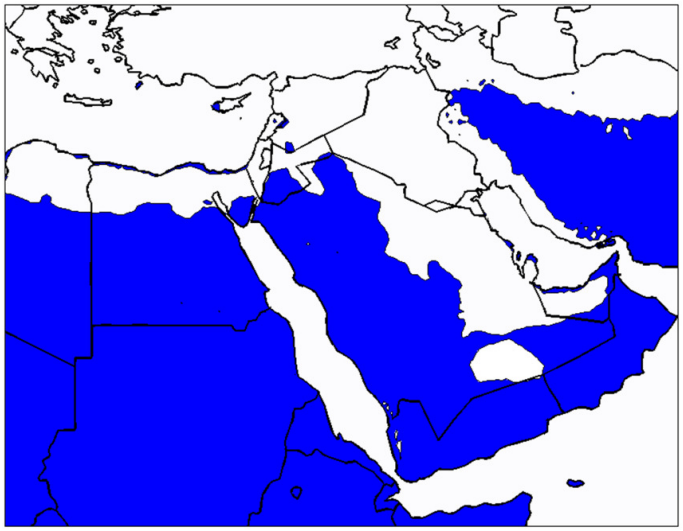

Figure 3.5: Areas in Middle East where PVRO systems are feasible.

3.5.1.2 Site Analysis

Table 3.4 gives detailed results for six sites. As expected, the areas with higher water salinity require more energy to perform reverse osmosis. Also, as expected, the areas listed with low solar insolation are not favorable for the solar powered systems. For the price assumptions made, the photovoltaic-powered systems are less expensive for sites in Cyprus, Haiti and Saudi Arabia. PVRO is feasible in areas with a good solar resource.

Table 3.4: Site-specific analysis results – seawater without incentives and carbon tax.

Location	Boston, USA	Los Angeles, USA	Limassol, Cyprus	Aqaba, Jordan	Cap-Haïtien, Haiti	Jeddah, Saudi Arabia
Latitude	42.35 N	34.05 N	34.67 N	29.52 N	19.76 N	16.89 N
Longitude	71.06 W	118.24 W	33.03 E	35.07 E	72.2 W	42.55 E
Average Latitude Tilt Solar Insolation (kWh/m^2-day)	4.4	5.6	6.1	5.9	6.0	6.6
Daylight Hours (hours)	9.08	9.88	9.87	10.25	10.93	11.13
Water Salinity (ppm)	32664	33505	39182	41160	36275	38340
Energy Required per day (kWh)	29.2	30.1	34.1	35.7	31.9	33.4
Solar Array Area (m^2)	44.2	35.8	37.3	40.3	34.8	33.7
Total Solar RO System Capital Cost ($)	149,830	123,349	120049	125,696	118,296	111,748
Solar RO System Equivalent Annual Cost ($)	23,042	18,553	17,494	18,225	17,457	16,311
Total Diesel System Capital Cost ($)	46,718	46,644	46,362	46,279	46,497	46,445
Diesel System Equivalent Annual Cost ($)	17,147	17,295	17,983	18,231	17,626	17,758
Cost of Water Solar ($/m^3)	7.01	5.64	5.32	5.55	5.31	4.96
Cost of Water Diesel ($/m^3)	5.21	5.25	5.47	5.54	5.36	5.41

3.5.2 Brackish Water Systems

Brackish groundwater is present in many water stressed locations. For these areas, brackish water RO desalination could be a major potential solution to fresh water shortage. These areas also typically have an abundance of sunshine, so photovoltaics can be coupled with RO systems to provide the required energy. Due to a lack of global data sets for groundwater salinity and depth, only a site specific analysis was performed to demonstrate the methodology for brackish water desalination. The input parameters for this analysis are given in Table 3.5.

Table 3.5: Input parameters for brackish water reverse osmosis analysis.

Parameter	Value
Plant Capacity, V_{cap}	10 m^3
Plant Lifetime, n	25 years
Interest Rate, i	5%
Plant Capacity Factor, f	90%
Recovery Ratio, R	40%
Reverse Osmosis Membrane Permeability, K_p [99]	7.5 x 10^{-10} m/bar-s
Reverse Osmosis Motor & Pump Efficiency, η_{HP} & η_{FP} [93]	70%
Energy Recovery System Efficiency, η_{ER} [93]	80%
Array System Efficiency, η_{PV}	15%
Generator Efficiency, η_{GEN} [104]	30%
Generator Load Factor, LF [104]	80%
Reverse Osmosis System Cost, U_{RO} [94]	$1200 / m^3
Installed Array System Cost, U_{PV} [103]	$9.00 / W$_p$
Initial Diesel Fuel Cost, C_{fuel} [106]	$0.66 / L ($2.50 / Gallon)
Diesel Fuel Annual Inflation Rate, j [106]	12%

Table 3.6 gives the details for all four sites analyzed. As expected, the energy requirements are higher for the areas with higher salinity water. Also, there is an energy penalty associated with raising the water from the source. Additionally, the high cost of diesel fuel results in a lower unit price for the solar powered reverse osmosis systems in all four cases. Photovoltaic reverse osmosis systems are economically feasible for brackish water desalination.

Table 3.6: Site-specific analysis results – brackish water without incentives and carbon tax.

Location	Alamogordo, NM, USA [110]	Jurf El-Darwish, Jordan [111]	Broken Hill Australia [112]	Djebeniana, Tunisia [113]
Latitude	32.88 N	30.700 N	31.95 S	35.05 N
Longitude	105.95 W	35.867 E	141.43 E	10.9 E
Average Solar Insolation (kWh/m^2-day)	5.8	5.7	5.7	5.2
Daylight Hours (hours)	9.98	10.15	10.07	9.80
Water Salinity (ppm)	3000	2421	6000	3500
Water Depth (m)	120	100	15	20
Energy Required (kWh)	20.8	19.9	18.4	16.0
Solar Array Area (m^2)	23.9	23.3	21.5	20.5
Total Solar RO System Capital Cost ($)	71,189	68,263	58,227	59,509
Solar RO System Equivalent Annual Cost ($)	7,944	7,775	7,148	7,512
Total Diesel System Capital Cost ($)	32,154	30,274	21,977	22,882
Diesel System Equivalent Annual Cost ($)	12,652	12,306	11,438	10,987
Cost of Water Solar ($/m^3)	2.41	2.36	2.17	2.28
Cost of Diesel Water($/m^3)	3.85	3.75	3.48	3.34

3.5.3 Comparison with Other PVRO Studies

Other researchers have also investigated PVRO systems and estimated the overall cost of water produced. A summary of these systems are listed in Table 3.7. The estimated water costs vary greatly due to variable system efficiency and assumptions that are made during the cost analysis. It should be noted that the calculated costs of between \$4.96/m^3 and \$7.00/m^3 for seawater photovoltaic reverse osmosis systems and between \$3.34/m^3 and \$3.85/m^3 for brackish water systems lie within the established range.

Table 3.7: Summary of estimated water costs for PVRO systems.

Location	Water Salinity (mg/L)	Water Production (m^3/day)	PV Power Rating (kW$_p$)	Batteries (kWh)	Energy Recovery	Water Cost ($US/m^3)	Year
Cituis, Indonesia[114]	3500*	12.0	25.7	132	No	\$3.68	1983
Coité–Pedreiras, Brazil [115]	1200*	0.55	1.1	9.6	No	\$12.76	2004
Hammam Lif, Tunisia [116]	2800*	0.05	0.59	No	No	\$8.00	2005
Heelat Ar Rakah, Oman [24, 117]	1010*	5.0	3.4	9.6	No	\$6.52	1998
Mesquite, Nevada [19]	3910*	1.5	0.54	No	No	\$3.46	2003
Athens, Greece[13]	40000	0.35	0.85	No	Yes	\$11.45	2008
Canary Islands, Spain [22, 23]	35500	3.0	4.8	60	Yes	\$9.60	1998
Massawa, Eritia[14, 15]	32800	3.0	2.4	No	Yes	\$3.00	2001

*brackish water

3.6 Conclusions

This chapter presented a method for determining the engineering feasibility of community-scale photovoltaic reverse osmosis systems as a function of location and water demand. This method compares the cost of water produced using photovoltaic reverse osmosis to water produced using diesel-powered reverse osmosis. This method uses physics-based models to size the system and determine the system energy requirements. The energy requirements are then

used to determine the water cost for each system. A PVRO system is considered feasible if it is more cost effective than an equivalent diesel-based system or transported water.

Case studies presented in this chapter clearly show the location dependence of the feasibility of photovoltaic-powered reverse osmosis. This dependency is due to the differences in terrain characteristics, the solar resources and water characteristics. For the conditions analyzed, the photovoltaic reverse osmosis is feasible for many water stressed regions. The high fuel costs for the diesel-powered systems results in higher water costs for most locations. When the system is configured for a region without a good solar resource, the high capital costs for community-scale seawater photovoltaic reverse osmosis systems are not recovered during the system lifetime. With modular design methodologies and intelligent system control of the photovoltaic-powered reverse osmosis systems, it is possible that the system costs could be further reduced, and the PVRO systems could become affordable for larger geographic regions.

CHAPTER

4

MODULAR DESIGN APPROACH

This section provides an overview of the modular design approach developed in this thesis. This approach can be used to custom tailor modular systems from inventories of potential components. This section also demonstrates the power of the developed approach for the application of interest, the design of PVRO systems, as well as the design of a hybrid automobile.

4.1 Modular Design

A common method to reduce manufacturing costs in many applications, such as automobiles, electronics, and robotics, is to develop products composed of mass-produced modular components. As stated in Chapter 1, this approach has many advantages, but designing a custom system configured from an inventory of potential modular components is not a simple task. For a given modular inventory, a large number of possible system configurations exist. A designer with significant expertise is required to select the correct components and configuration.

The problem considered in this thesis is the design of a system from an inventory of mass-produced, modular components. Here, it is assumed that the design algorithms have access to an inventory of potential components with known characteristics and a design objective. It is also assumed that the performance of a system is highly coupled to the design choices.

For the PVRO problem, this inventory consists of different PV panels, motors, pumps, reverse osmosis membranes, pressure vessels, energy recovery devices and control electronics. For the cases considered, the systems are designed to operate variably to eliminate the need for energy storage in the form of batteries, instead storing the energy in the form of clean water and reducing overall system cost. Also, the design algorithms have access to the system specifications which define the location and water demand of the community. The algorithm developed should enable a non-expert to configure a custom system for the community from

modular components. The design goal of the modular design of the PVRO system is to determine the most cost-effective option in terms of lowest lifetime cost that meets the water production and quality requirements.

4.2 Design Approach

The design framework developed to configure a custom system from a library of potential modular components can be seen in Figure 4.1. In this framework, a series of different filters are used to systematically reduce the size of the design space. The preliminary filters are based on computationally efficient, simple tests to eliminate inappropriate modules and subassemblies quickly. The smaller design space is further refined by a topology filter using simple, low-fidelity models and tests. Finally, a high-fidelity model is used on the fully reduced design space to optimize the system and determine the final system configuration. This approach greatly reduces the size of the design space and dramatically speeds the optimization, as is shown in examples in sections 4.3 and 4.4.

Different optimization techniques can be used on the reduced design space to determine a final system configuration. For the design of a PVRO system, a genetic algorithm is used to optimize the final system configuration [118]. This method is used because the PVRO system configuration is represented by a series of binary, integer and continuous design variables. In addition, the equations which describe the system performance are non-linear. Genetic algorithms can easily encode discrete variables and can handle non-linear equations by evaluating a large population of potential configurations. Genetic algorithms are often the preferred choice for topology optimization problems and are well-matched for the design of other modular systems [47, 57, 59, 60, 63, 69, 71].

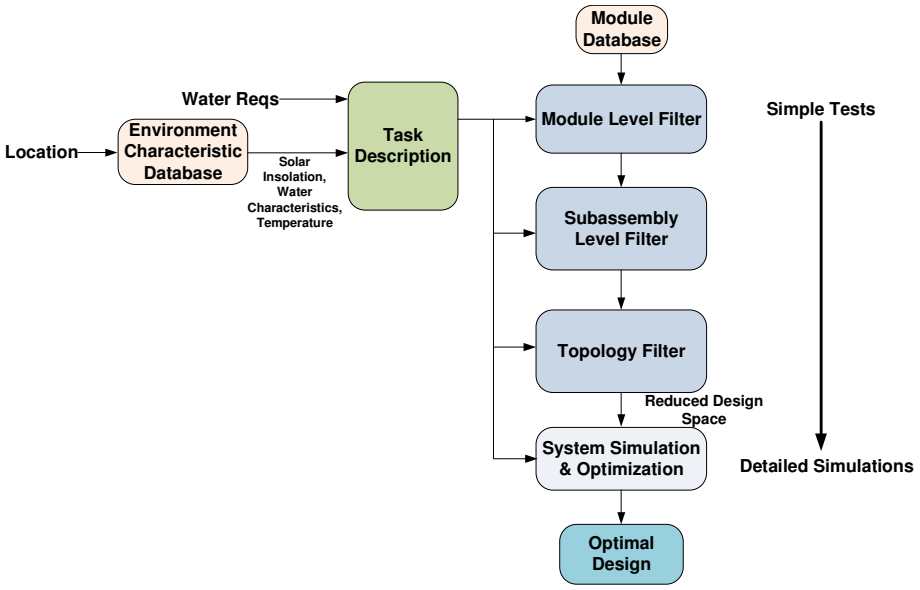

Figure 4.1: Modular design approach.

4.3 PVRO System Design Space Study

4.3.1 Overview

To show the effectiveness of this approach for a PVRO system, a design space study for a modular inventory was performed. In this study, the total number of system combinations is enumerated through each of the steps outlined in the modular design approach. The inventory considered in the design space study is shown in Figure 4.2 and the component details are given in Table 4.1. In this example, this simple inventory will be used to design a small, 1 m^3/day water production, brackish water system for Haiti.

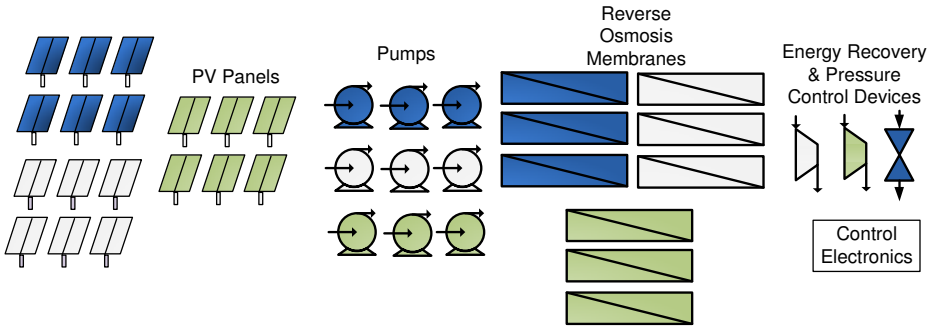

Figure 4.2: Inventory used in design space study.

Table 4.1: Sample inventory used for design space study.

Component	Details				
PV Panels	**Quantity**	**Power Rating**	**Efficiency**		**Cost**
PV Model 1	6	250 W	15%		$500
PV Model 2	6	200 W	13%		$300
PV Model 3	6	300 W	18%		$450
RO Membranes	**Quantity**	**Water Type**	**Area**	**Rated Water Production**	**Cost**
RO Membrane Model 1	3	Brackish Water	2.8 m^2	3.2 m^3/day	$120
RO Membrane Model 2	3	Brackish Water	7.5 m^2	9.1 m^3/day	$220
RO Membrane Model 3	3	Seawater	2.8 m^2	2.6 m^3/day	$150
Motor + Pump Units	**Quantity**	**Maximum Pressure**	**Maximum Power**	**Efficiency**	**Cost**
Pump Model 1	3	25 bar	200 W	65%	$300
Pump Model 2	3	80 bar	400 W	82%	$800
Pump Model 3	3	80 bar	800 W	80%	$1500
Energy Recovery + Pressure Control Valves	**Quantity**	**Maximum Pressure**	**Maximum Flow Rate**	**Efficiency**	**Cost**
Energy Recovery Model 1	1	80 bar	0.5 L/s	85%	$3500
Energy Recovery Model 2	1	80 bar	0.3 L/s	90%	$3000
Pressure Control Valve 1	1	80 bar	1 L/s	0%	$200

4.3.2 Enumerating Full Design Space

To determine the initial design space, it is assumed that each system must contain at least one PV panel, one pump and motor, one RO membrane, and one energy recovery device or pressure control valve. It is also assumed that the required pressure vessels, connecting components and power control electronics are readily available. The system is being configured for a location with one water intake, one brine disposal, and one potable water storage facility in place. It is also assumed that not all the components need to be used.

The PVRO system has two main subsystems, the reverse osmosis system and the photovoltaic power system which are coupled via the control electronics. The total number of system configurations is given by

$$N_{PVRO} = N_{RO} \times N_{PV} \tag{4.1}$$

where N_{RO} is the number of different RO system configurations and N_{PV} is the number of PV system configurations.

Each reverse osmosis system is formed by selecting and connecting components from the modular inventory. This results in a large number of possibilities for a given inventory, which can be expressed as:

$$N_{RO} = \sum_{n_{p,1}=0}^{N_{p,1}} \cdots \sum_{n_{p,N_p}=N_{p,base}}^{N_{p,N_p}} \sum_{n_{ro,1}=0}^{N_{ro,1}} \cdots \sum_{n_{ro,N_{ro}}=N_{ro,base}}^{N_{ro,N_{ro}}} \sum_{n_{er,1}=0}^{N_{er,1}} \cdots \sum_{n_{er,N_{er}}=N_{er,base}}^{N_{er,N_{er}}} \frac{1}{\prod_{i=1}^{N_p} n_{p,i}! \prod_{i=1}^{N_{ro}} n_{ro,i}! \prod_{i=1}^{N_{er}} n_{er,i}!}$$

$$\times \left[2^{(n_{outputs})(n_{inputs})} + \sum_{l=1}^{n_{outputs}} \sum_{m=1}^{n_{inputs}} \left[\binom{n_{outputs}}{l} \binom{n_{inputs}}{m} 2^{(n_{outputs}-l)(n_{inputs}-m)} (-1)^{(l+m)} \right.\right. \tag{4.2}$$

$$\left.\left. + \binom{n_{outputs}}{l} 2^{(n_{outputs}-l)(n_{inputs}-m)} (-1)^{l} + \binom{n_{inputs}}{m} 2^{(n_{outputs}-l)(n_{inputs}-m)} (-1)^{m} \right] \right]$$

where $N_{p,i}$ is the number pumps of type i in the inventory, $N_{ro,i}$ is the number of reverse osmosis membranes of type i in the inventory, $N_{er,i}$ is the number of energy recovery devices and pressure control valves of type i in the inventory, n_{inputs} is the number of component inputs for a configuration as given by:

$$n_{outputs} = \sum_{i=1}^{N_p} n_{p,i} + 2\sum_{i=1}^{N_{ro}} n_{ro,i} + \sum_{i=1}^{N_{er}} n_{er,i} + 1 \tag{4.3}$$

and $n_{outputs}$ is the number of components outputs for the configuration as given by:

$$n_{inputs} = \sum_{i=1}^{N_p} n_{p,i} + \sum_{i=1}^{N_{ro}} n_{ro,i} + \sum_{i=1}^{N_{er}} n_{er,i} + 2 \tag{4.4}$$

$N_{p,base}$, $N_{ro,base}$, and $N_{er,base}$ are indices that ensure each configuration has at least one pump, one reverse osmosis membrane, and one energy recovery or pressure control valve and are expressed as:

$$N_{p,base} = \max\left(1 - \sum_{i=1}^{N_p - 1} n_{p,i}, 0\right) \tag{4.5}$$

$$N_{ro,base} = \max\left(1 - \sum_{i=1}^{N_{ro} - 1} n_{ro,i}, 0\right) \tag{4.6}$$

$$N_{er,base} = \max\left(1 - \sum_{i=1}^{N_{er} - 1} n_{er,i}, 0\right) \tag{4.7}$$

The derivation of equations (4.2) - (4.7) are presented in Appendix A.

There are many ways to configure a PV system from an inventory of PV panels. Provided the PV array voltage and current output is compatible with the control electronics, the configuration of the PV array does not greatly impact the overall power production. Therefore,

the number of distinct configurations can be determined by the number of ways to select groups of PV panels from the inventory as given by:

$$N_{PV} = \prod_{i=1}^{N_{pv,type}} \left(n_{pv,i} + 1\right) - 1 \tag{4.8}$$

where $N_{pv,type}$ is the number of different types of PV panels in the inventory, $n_{pv,i}$ is the number of PV panels of type i in the inventory. The derivation of equation (4.8) is presented in Appendix A.

Using equations (4.1)-(4.8), the total number of configurations for the inventory presented in Figure 4.2 can be computed. The resulting number of system configurations is 1.9 x 10^{173}. This number far exceeds the approximate number of atoms in the observable universe, which is estimated to be 9.4 x 10^{79} [119]. Optimizing a system with a design space this large is infeasible.

4.3.3 Module Level Filters

Using the modular design approach outlined in Figure 4.1, the size of the design space is reduced. In the initial step, module level filters are applied to the motor/pump units, reverse osmosis membranes, energy recovery devices and PV panels to remove inappropriate elements from the inventory. The filters applied for PVRO systems are detailed here.

For the PVRO system, the design goal is to minimize the lifetime system cost. The filters presented here assume that the expected life of all components of the same type is identical. As a result, the applied value metrics only consider capital costs. If lifetimes of components are different and known, the value metrics should be adjusted to account for such differences.

4.3.3.1 Motor/Pump Filters

For the motors and pumps, the following filters are applied to reduce the size of the design space:

1. Motor/pump combinations that are designed for pressures that are inappropriate for the given system are eliminated from the inventory. Since the salt concentration varies for different source waters, the typical operating pressures also vary. For brackish desalination, the typical operating pressure is 30 bar, while for seawater desalination, the operating pressures go up to 80 bar.

2. Motors and pumps with inappropriate power ratings are eliminated from the inventory. Based on the energy requirements, shown in Table 1.1, the average power requirement of the system can be calculated as follows:

$$P = \frac{\text{Average Energy Requirements}}{\text{Number of Operating Hours}} = \frac{\text{Average Energy Requirements}}{\text{Number of Peak Sun Hours}} \tag{4.9}$$

   Using the solar data at the site, the power requirement can be estimated. Pumps that are rated for more than two times the average power requirement are oversized and are removed from the inventory.
3. Value metrics are applied to pumps/motor units. The cost per percent efficiency is used to compare possibilities. Since different system scales require different types of pumps, these metrics are evaluated by power rating. Pump/motor units that do not rank in the top 50% for one of these metrics are removed from the design problem.

When applied in the context of designing a brackish water PVRO system capable of producing 1 m^3 of clean water per day in Haiti, these filters remove Pump/Motor 3 from the inventory since it is oversized for the system energy requirements.

4.3.3.2 Reverse Osmosis Membrane Filters

For the reverse osmosis membranes, the following filters are applied to reduce the size of the design space:

1. Membranes are removed that are for the incorrect water type. For example, when designing a system for brackish water desalination, the seawater filters are removed from the design space.
2. Value metrics are applied to membranes. The cost per water permeability and cost per salt permeability are calculated for each type of component. Since different system scales require different membrane areas, these metrics are compared by membrane size. Membranes that do not rank in the top 50% of their category for one of these metrics are removed from the design problem.

For the sample Haiti PVRO system design problem, the filters remove Reverse Osmosis Membrane 3 from the inventory.

4.3.3.3 Energy Recovery Device and Pressure Control Valve Filters

The following filters are applied to the energy recovery/pressure control devices to reduce the size of the design space:

1. Components that have inappropriate pressure and flow ratings for the application are eliminated from the design space. Expected operating pressures for the brackish water systems are 30 bar and for seawater systems the expected operating pressure is between 60-80 bar. Devices that have pressure ratings too low are removed from the inventory.

   The expected flowrate through the energy recovery system is calculated as follows:

   $$Q_{ERD} = \frac{Q_{Sys}}{R} \qquad (4.10)$$

   where Q_{sys} is the rated system flowrate and R is the expected recovery ratio. For the small systems considered here, the recovery ratio will range between 10% and 30%. Using these numbers, the range of required flowrates is calculated. Energy recovery devices with maximum flowrates below the expected range will be eliminated from the inventory.
2. Value metrics are applied to energy recovery devices. The cost per percentage efficiency is calculated for each ERD. ERDs that do not rank in the top 50% for one of these metrics are removed from the inventory.

When applied to the brackish water system design problem for Haiti, these filters remove Energy Recovery Model 1 from the inventory based on the component value metric.

4.3.3.4 PV Panel Filters

For the PV panels, the following filters are applied to reduce the size of the design space:

1. Value metrics are applied to the PV panels. The cost per percentage efficiency and cost per power rating is calculated for each PV panel. Since the possible power ratings of the PV array are discrete, the inventory should contain PV panels with lower power ratings to ensure that PV array is not oversized. As a result, value metrics are compared for PV panels with power ratings less than or equal to 200 Watts or greater than 200 W. Panels that do not rank in the top 50% in their category for one of these metrics are removed from the inventory.

The filters remove PV Model 2 from the inventory based on the value metric when applied to the Haiti brackish system design problem.

After eliminating these components from the inventory, the total number of possible system configurations has decreased to 7.5 x 10^{88}. The design space at this stage is still much too large to configure a system design using optimization methods. Further design space reduction is required to make the problem tractable.

4.3.4 Subassembly Filters

In the next algorithm step, subassembly level filters are applied to limit the design space. This step configures subassemblies that can be used in the full system. For the small-scale PVRO system design problem, subassemblies such as the PV array and reverse osmosis membrane array are sized. In addition, the total numbers of pumps and energy recovery devices to be considered during the design are determined.

The PV array is sized based on simple energy calculations. For the brackish water case, the range of energy consumption is assumed to range from 1 kWh/m^3 to 5 kWh/m^3. These numbers can be used with the solar insolation at the site to set the limits on the PV array power ratings as follows:

$$P_{\max/\min} = \frac{E_{\max/\min} V_{cap} G_{rate}}{H} \tag{4.11}$$

where $P_{max/min}$ is the maximum or minimum array rating required in kW, $E_{max/min}$ is the maximum or minimum specific energy requirement for the water desalination in kWh/m^3 as given in Table 1.1, V_{cap} is the desired system capacity, G_{rate} is the solar radiation that the panels are tested at (typically 1 kW/m^2) and H is the average annual solar insolation in kWh/m^2 at the site. For the Haiti system with an average insolation of 6.05 kWh/m^2 [8], the maximum array power rating is 661 W and the minimum requirements are 165 W. Using these max and minimum values, limits are placed on the number of panels required. Panels in a PVRO system configuration are limited to a single model unless the calculated limits exceed what is available for a single model in the inventory.

Similarly, the maximum and minimum size for the reverse osmosis array can be determined. For given water production, the average clean water flow rate can be determined by:

$$Q_{p,ave} = \frac{V_p}{n_{sun}} \tag{4.12}$$

where n_{sun} is the number of hours of peak sunshine. For the 1 m^3/day Haiti system being considered, the average flowrate would be 165 L/hour. Using this flowrate, the number of each membrane type required can be determined. A 50% safety factor is incorporated to ensure that resulting subsystems result in feasible system designs.

For the system pumps and energy recovery devices, rules of thumb are used to limit the total number of pumps that can be included. For the community-scale systems considered here, conventional systems are used as a guide. For small systems with a daily capacity less than $2m^3$, typical systems contain two pumps or fewer. To allow for innovative designs, an upper bound on the number of pumps in the system is placed at 3. For larger systems with daily production capacities above $2m^3$, the number of pumps allowed in the system is placed at 5 to allow for innovative configurations.

For small-scale PVRO systems, energy recovery devices are typically expensive and dominate the system cost. As the devices are scaled up for larger flowrates, they tend to be more cost effective. As a result, the total number of energy recovery devices that can be placed in the system is limited to one. In addition, one pressure control valve will be allowed in the final RO system.

After these subassembly level filters are applied, the size of the design space for the Haiti system design problem is reduced to 9.8×10^{49}. This design space is still very large for direct application of an optimization algorithm.

4.3.5 Topology Filters

The next step in the modular design algorithm is the topology filter. This limits the number of configurations which can be assembled from the subsystems by applying simple calculations and design rules. For the PVRO system design problem, unreasonable system topologies are eliminated. The filters applied here can be broken into two categories: RO system topology filters and PVRO system filters.

The topology filters for the RO system eliminate the following cases:

1. Configurations with permeate stream and brine stream mixing which negates the purpose of the reverse osmosis process. Mixing of the permeate stream and the feed is

allowed for brackish water systems. Given the low water salinity and the discrete nature of the system configurations, diluting desalinated water with feed water may be the most cost effective option and is used in practice [120].

2. Configurations where not all components are connected or a path does not exist from the reverse osmosis water input and the brine and permeate outputs.
3. Configurations where input water is not pressurized before entering the reverse osmosis membranes. In these cases, there would not be the driving force necessary for desalination.
4. Configurations containing loops without pumps or energy recovery devices in the reverse osmosis setup. These cases are infeasible.
5. Configurations where pumps are directly connected to energy recovery exhaust streams. In these cases, energy is being put into the water by the pumps and then being removed by the energy recovery unit without any product water being produced. Since these processes are not 100% efficient, this results in wasted energy.
6. Configurations where high pressure pumps are directly connected to permeate or brine outputs. Any pump connected to these outlets would waste energy. In addition any configuration where the exiting brine stream doesn't pass through a pressure control valve or energy recovery device is eliminated. These components are required to produce the pressure for reverse osmosis.

Examples of these cases are depicted in Figure 4.3 below.

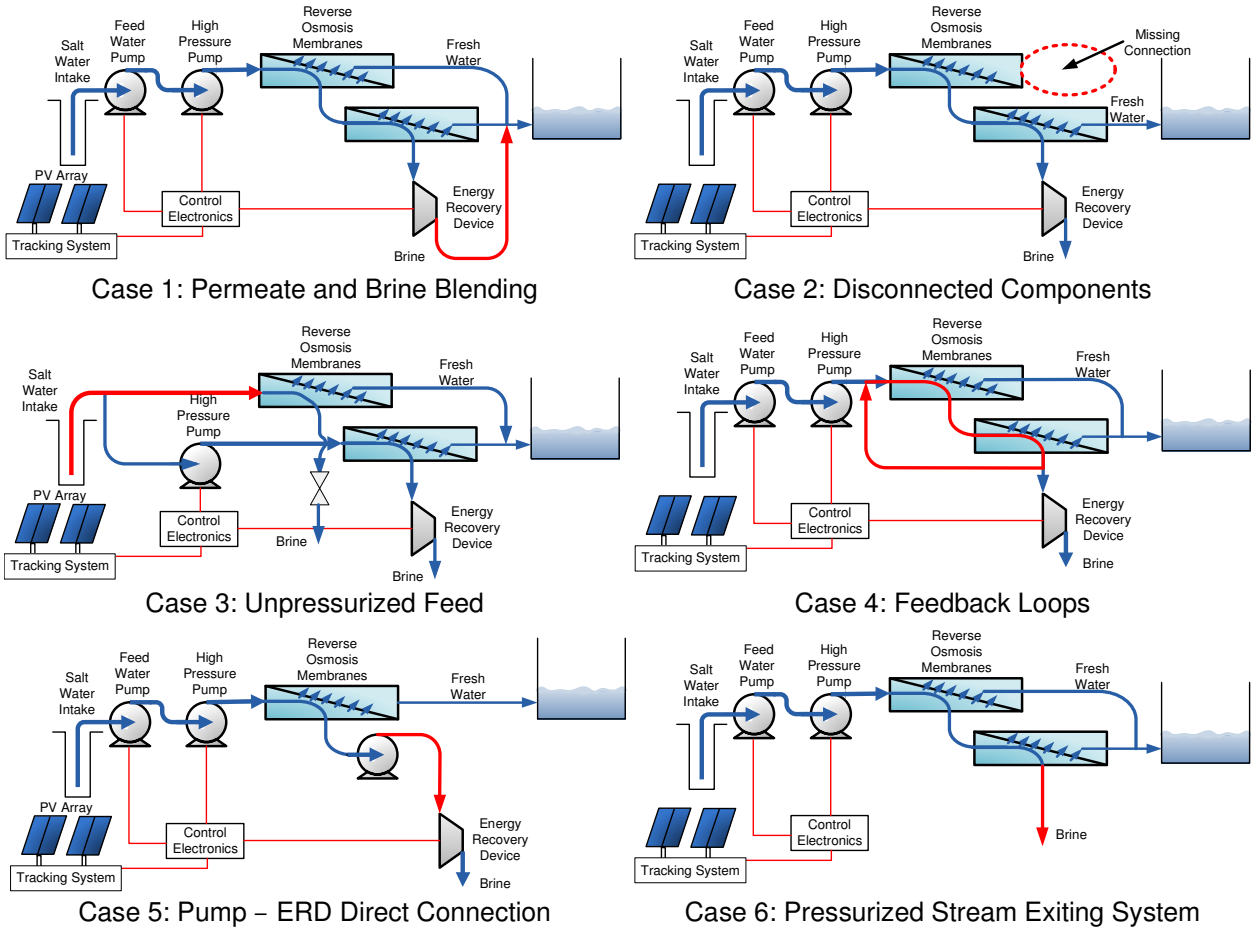

Figure 4.3: Examples of RO system configurations eliminated by the topology filter.

The remaining assembly filters match the size of the PV array with the RO system designs. The amount of energy required for the desalination will vary greatly depending on the use of energy recovery devices, as shown in Table 1.1. The allowable power ratings for each PV array for systems with/without energy recovery devices are determined using the expected energy requirements and equation (4.11).

After applying assembly level filters, the design space is greatly reduced to 3.4 x 10^7 different configurations. This size of design space is a much more reasonable size for optimization. The modular design algorithm has made this problem more tractable. A summary of the results of the design space study are shown in Table 4.2.

Table 4.2: Summary of PVRO modular design study.

Filter Level	Design Space Size
Component Library	1.9 x 10^{173}
Module Filter	7.5 x 10^{88}
Subassembly Filter	9.8 x 10^{49}
Topology Filter	3.4 x 10^7

4.4 Parallel Example – Hybrid Car Powertrain

There are many different modular systems that can be configured using the approach developed in this thesis. This section details a simplified design example for a hybrid electric car. Here, the design problem is to determine the vehicle configuration with the minimum fuel consumption while maintaining the following objectives:

1. 0-100 kph time less than 12 seconds
2. Minimum all electric range of 25 km.
3. Range of 600 km.

For this design space study, the module inventory detailed in Table 4.3 is used. This inventory has a selection of vehicle platforms, combustion engines, electric motors, generators, batteries, and gas tank sizes.

Table 4.3: Modules considered in hybrid car design study.

Batteries	Chemistry	Number of Cells in Inventory	Cell Voltage	Cell Capacity	Cell Weight	Charge/Discharge Efficiency
Battery 1	Li-ion	150	3.3 V	4.2 Ah	205g	97%
Battery 2	Li-ion	150	3.7 V	21 Ah	313g	95%
Battery 3	Li-ion	150	3.6 V	52 Ah	1000g	97%
Battery 4	NiMH	150	1.2V	6.5 Ah	170g	70%
Battery 5	NiMH	150	1.2V	30 Ah	760g	67%

Motors	Type	Maximum Power Output	Max Torque Output	Weight	Max Efficiency
Motor 1	AC	91.0 kW	166.8 Nm	162 kg	89.2%
Motor 2	AC	50.0 kW	151.8 Nm	115 kg	89.3%
Motor 3	DC	21.5 kW	94.9 Nm	70.8 kg	89.1%
Motor 4	DC	27.7 kW	183.0 Nm	104 kg	91.4%
Motor 5	DC	22.1 kW	162.7 Nm	167 kg	86.4%

Engines	Engine Size	Max Power Output	Max Torque Output	Weight	Max Efficiency
Engine 1	1 L	48.5 kW	118.0 Nm	97.5 kg	32%
Engine 2	1.4 L	62.7 kW	131.5 Nm	99.8 kg	29%
Engine 3	1.6L	110.4 kW	229.1 Nm	101.6 kg	30%
Engine 4	2.0L	149.2 kW	299.6 Nm	133.8 kg	33%
Engine 5	2.4L	167.9 kW	348.5 Nm	164.7 kg	29%

Generators	Max Power Output	Weight	Efficiency
Generator 1	54 kW	74 kg	92%
Generator 2	44 kW	82 kg	90%
Generator 3	34 kW	35 kg	85%
Generator 4	22 kW	55 kg	89%
Generator 5	8 kW	10 kg	80%

Platforms	Type	Average Drag Area (C_dA)	Average Weight
Platform 1	Subcompact	0.7 m^2	2000 lbs
Platform 2	Compact	0.65 m^2	2500 lbs
Platform 3	Midsize	0.58 m^2	3000 lbs
Platform 4	SUV	1.08 m^2	3500 lbs

Tank	Volume
Tank 1	37.8 L
Tank 2	45.4 L
Tank 3	56.8 L
Tank 4	68.1 L

For hybrid cars, there are two main system configurations. In one configuration, the electric motor and fuel powered engine are in parallel, in the other the motor and engine are connected in series. These two configurations can be seen in Figure 4.4. It is assumed for this study that the transmission and electronics are readily available and selected independent of the other components.

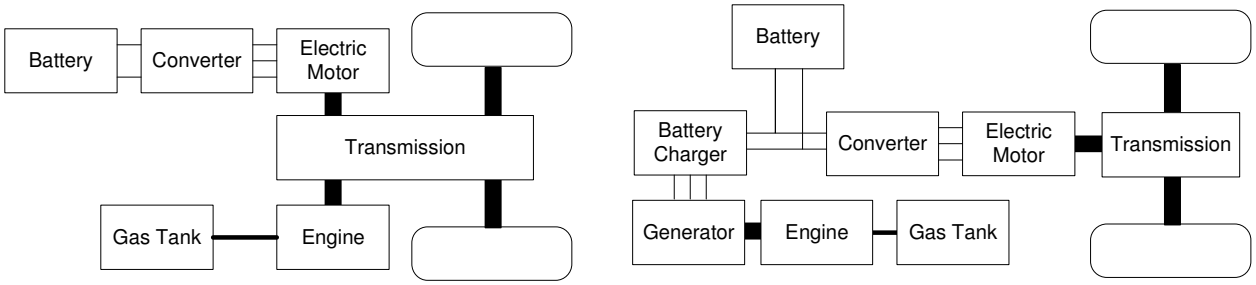

Figure 4.4: Parallel hybrid car (left) and series hybrid car (right) configurations.

The total number of system configurations can be determined as follows:

$$N_{hybrid} = N_{para} + N_{series} \tag{4.13}$$

where N_{para} is the number of parallel configurations and N_{series} is the number of series system configurations. The number of parallel system configurations is determined by the product rule:

$$N_{para} = N_{Plat} N_{Bat} N_{Eng} N_{Motor} N_{Gas} \tag{4.14}$$

where N_{Plat} is the number of vehicle platforms, N_{Bat} is the number of different battery system configurations, N_{Eng} is the number of engines in the inventory, N_{motor} is the number of motors in the inventory, and N_{Gas} is the number of gas tanks in the inventory. The number of series system configurations is determined by the product rule:

$$N_{series} = N_{Plat} N_{Bat} N_{Eng} N_{Gen} N_{Motor} N_{Gas} \tag{4.15}$$

where N_{Gen} is the number of generators in the inventory.

Assuming that all batteries in the vehicle pack are the same and the arrangement of batteries in series and parallel can be accommodated by the electronics, the number of battery configurations is given by:

$$N_{Bat} = \prod_{i=1}^{N_{Bat,type}} \left(n_{Bat,i} + 1\right) - 1 \tag{4.16}$$

where $n_{Bat,i}$ is the number of batteries of type i in the inventory, and $N_{Bat,type}$ is the total number of battery types.

Using equations (4.13) to (4.16), the full design space can be enumerated. For the inventory specified, the total number of system configurations is 2.4 x 10^{14}. This number of configurations here is much smaller than the PVRO system since there are a limited number of system topologies.

The design space is reduced by applying the module level filters. Since the design goal here is to maximize the fuel economy while maintaining performance, efficiency and power metrics are applied. For the platform, the different configurations are ranked based on weight and drag. The platforms that didn't rank in the top 50% in either category were eliminated. For the example, the SUV design is eliminated due to high mass and drag characteristics.

The engine configurations are filtered based on weight, power, and efficiency. Engines are ranked according to maximum power output per unit weight and efficiency. Engines that don't rank in the top 50% are eliminated. Engine 5 is eliminated due to low efficiency and power output.

The generators are used to convert mechanical energy from the gasoline engine into electrical energy to store in the batteries and must be sized appropriately. For the inventory selected, the minimum power input to the generator would be 48 kW. Generators with maximum power ratings below this value are undersized for the application. As a result, Generator 4 and 5 are eliminated from the inventory.

The batteries are filtered based on energy density, power density and charge/discharge efficiency. Again, batteries are ranked for each of the above categories and the components that do not rank in the top 50% for any of the criteria are eliminated. For the batteries, the NiMH configurations are eliminated due to their high weight and low efficiency.

The filtering of the electric motors is broken into two categories. If the vehicle has the series configuration, the motor must provide all the power to the wheels. In the parallel configuration, the electric motor assists the gasoline engine. Motors which are able to provide high power (above 100 kWh) are evaluated separately from the smaller motors. The motors are ranked in terms of overall efficiency and maximum power output per unit weight. The motors that do not rank in the top 50% are eliminated. As a result, Motor 5 is eliminated from the inventory.

The number of tanks in the inventory is limited using simple mileage calculations. A reasonable hybrid car achieves at least 12.75 km/L in the city. Therefore to guarantee a 600 km

range, a tank volume of 47 L is required. As a result, the 68.1 L tank is removed from the inventory.

Based on the filters specified above, the total number of system configurations drops to 9.9 x 10^8. This is a large reduction from the initial design space size, but with additional filters, this number can further decreased.

In the next step of the modular design approach, subassembly level filters are applied to reduce the size of the design space. In this step, engines and generators are matched based on torque and speed characteristics. In addition, battery packs are configured from battery modules. Maximum and minimum numbers of batteries are determined based on energy calculations. The average power usage of current hybrid vehicles is 22 kWh per 100 km [121]. The minimum capacity on each battery pack is set at 4 kWh, which provides enough energy to drive the minimum range considering a 25% increase in system efficiency. Using these filters, the size of the design space is reduced to 2.8 x 10^6.

In the final step, full system assemblies are considered. Since there is limited topology optimization for the hybrid car case, only a few filters are applied. In the series configuration, all the power is applied to the wheels using the electric motor, and only the higher power configurations (Motor 1 and Motor 2) are considered. For the parallel configuration, the electric motors share the power with the gasoline engine and the smaller motors (Motor 3 and Motor 4) are considered. The total number of system configurations is 1.4 x 10^6. Detailed analysis can then be used on these configurations to determine the system configuration using optimization methods.

The reduction of the design space size of the hybrid car problem using the modular design approach is detailed in Table 4.4. This section provides an example of how this approach can be used for other modular design problems. It does not provide an exhaustive list of potential filters for the design of a hybrid car drivetrain. This example only considers the fuel economy objective, but other objectives involving cost can also be incorporated into the design approach.

Table 4.4: Modules considered in hybrid car design study.

Filter Level	Design Space Size
Component Library	2.4 x 10^{14}
Module Filter	9.9 x 10^8
Subassembly Filter	2.8 x 10^6
Topology Filter	1.4 x 10^6

4.5 Summary

This section presented the modular design approach. The approach uses a series of tests based on engineering principles to reduce the size of the discrete design space and make the problem tractable for optimization algorithms. The power of the approach is demonstrated through two sample design space studies, the design of a photovoltaic reverse osmosis system and the design of a hybrid car. In both cases, the approach is shown to greatly reduce the size of the design space.

The final step in the modular design algorithm is to optimize the system over the reduced design space using a detailed system model. The optimization problem is challenging as the cost function and constraints are non-linear, resulting in a mixed integer nonlinear program (MINLP). The detailed system model is described in Chapter 5 and the optimization setup is described in Chapter 6.

CHAPTER

5

PVRO SYSTEM MODEL

This section describes the models used for the modular design of PVRO systems. The components overviewed below are: the environment, PV system, control electronics, motors, pumps, reverse osmosis membranes, and energy recovery devices. These models account for all the main physical characteristics and losses. However, these models neglect the fast system dynamics and assume the system can quickly adapt to changing levels of solar insolation.

5.1 Environment Models

5.1.1 Solar Energy Model

Solar radiation varies greatly from location to location. For any given location, the radiation varies greatly over the course of the day and year. The solar energy model used for the design of modular PVRO systems accounts for these variations by using site specific solar radiation data provided by the NASA Solar Radiation Database [8]. This database provides daily solar insolation values for any location derived from satellite imagery.

This solar radiation data is used differently for each of the case studies presented in chapters 6 and 7. In all of the cases presented, the daily solar insolation is used to generate daily radiation profiles to analyze the system performance. The hourly data is generated from the daily insolation as follows. First, the sun position for each hour is calculated using:

$$\cos\theta_{zs} = \sin\delta\sin\phi + \cos\delta\cos\phi\cos\omega = \sin\gamma_s \tag{5.1}$$

$$\cos\psi_s = \frac{\left(\sin\gamma_s\sin\phi - \sin\delta\right)}{\cos\gamma_s\cos\phi}\left[sign\left(\phi\right)\right] \tag{5.2}$$

where θ_{zs} is the solar zenith angle (angle between vertical and the sunlight direction), ψ_s is the solar azimuth (angle between the meridian and the sun), γ_s is the solar elevation (angle between

the sun and the horizon), ω is the true solar time, ϕ is the latitude of the location, δ is the solar declination as given by:

$$\delta = 23.45^{o} \sin\left(\frac{360(d_n + 284)}{365}\right) \tag{5.3}$$

where d_n is the day number. All angles are expressed in degrees.

The true solar time is the angular difference between solar noon and current time as given by:

$$\omega = 15^{o}\left(T - \Delta_{GMT} + \frac{4\varsigma + 9.87\sin(2\delta) - 7.53\cos\delta - 1.5\sin\delta}{60} - 12\right) \tag{5.4}$$

where T is the local time in hours, Δ_{GMT} the time difference between Greenwich Mean Time in hours, and ς the longitude of the site.

Using equation (5.1), the sunrise angle, ω_s can be found. At sunrise, the solar elevation (γ_s) is 0, and therefore:

$$\omega_s = -\arccos(-\tan\delta\tan\phi) \tag{5.5}$$

Outside the earth's atmosphere, the radiation from the sun can be easily determined. The radiation on a flat surface outside the atmosphere, in W/m^2, is given by:

$$B_0(T) = B_0\varepsilon_0\cos\theta_{ZS} \tag{5.6}$$

where B_0 is the solar constant outside the earth's atmosphere which equals 1367 W/m^2 and ε_0 is eccentricity of the earth's orbit which is given by:

$$\varepsilon_0 = 1 + 0.033\cos\left(\frac{360 d_n}{365}\right) \tag{5.7}$$

The extraterrestrial radiation integrated over the course of the day gives:

$$B_{0d} = \frac{24}{\pi} B_0\varepsilon_0\left[-\frac{\pi}{180}\omega_s\sin\delta\sin\phi - \cos\delta\cos\phi\sin\omega_s\right] \tag{5.8}$$

The ratio between the extraterrestrial radiation at a given instant and the daily irradiation can be used to determine the radiation at the earth's surface as follows [122]:

$$G(t) = \frac{B_0(t)G_d}{B_{0d}}(a + b\cos\omega) \tag{5.9}$$

where G_d is the measured or generated daily solar insolation at the earth's surface in Wh/m^2 and a and b are empirically derived as follows:

$$a = 0.409 - 0.5016\sin\left(\omega_s + 60\right) \tag{5.10}$$

$$b = 0.6609 + 0.4767\sin\left(\omega_s + 60\right) \tag{5.11}$$

Equation (5.9) approximates the radiation on a flat plate at any instant in time given the daily solar insolation. This radiation has two components: beam radiation which comes from the direction of the sun, and diffuse radiation which is scattered by the atmosphere and comes from all directions. The breakdown of the radiation components can be found as follows.

Due to the atmosphere, only a fraction of the radiation reaches the earth's surface. This is referred to as the clearness index and for a day's time period it is given by:

$$K_{Td} = \frac{G_d}{B_{0d}} \tag{5.12}$$

The clearness index has been used to empirically determine the amount of diffuse radiation. Based on data from the European weather station network, the diffuse fraction of radiation was derived as:

$$F_{Dd} = \begin{cases} 0.952 \text{ for } K_{Td} \le 0.13 \\ 0.868 + 1.335K_{Td} - 5.782{K_{Td}}^2 + 3.721{K_{Td}}^3 \text{ for } 0.13 < K_{Td} \le 0.8 \\ 0.141 \text{ for } K_{Td} > 0.13 \end{cases} \tag{5.13}$$

Using this fraction, the daily diffuse insolation is given by:

$$D_d = F_{Dd}G_d \tag{5.14}$$

Given the daily diffuse insolation, the diffuse insolation at any period of time is determined using the following empirical relationship:

$$D(t) = \frac{B_0(t)}{B_{0d}}D_d \tag{5.15}$$

and the beam radiation at the earth's surface is given by:

$$B(t) = G(t) - D(t) \tag{5.16}$$

The diffuse radiation and beam radiation falling on the earth's surface along with the sun position as outlined in equations (5.1) and (5.2) can be used in the solar panel model for a given panel orientation as outlined in section 5.2.2.

5.1.2 Water Salinity Model

Water salinity varies greatly by location. For the purpose of the modular design approach, water salinity numbers are taken for each case study location from the World Ocean Atlas [96]. The water salinity will change over the course of the year due to the natural water cycle. These variations are typically less than 10%. To simplify the analysis here, average yearly values of water salinity and temperature values from a depth of 10 m are used. For system design for a specific location, measurements of the local water salinity should be taken to provide an accurate performance estimates.

5.1.3 System Demand

The water demand varies for each case and greatly affects the system design. In the case studies detailed in Chapter 6 and Chapter 7, the demand is treated differently. In the case studies in Chapter 6, the demand is assumed to be constant and known and the PVRO system is designed to meet these needs. In the case studies presented in Chapter 7, the water demand is assumed to vary according to historical water demand statistics. These statistics and predicted demand trends are detailed in Chapter 7.

5.2 Component Models

5.2.1 PV System

Photovoltaics convert light energy directly to electrical energy. A PV cell is composed of two or more layers of doped semiconducting materials as shown in Figure 5.1. When exposed to sunlight, electrons are excited from the valence band to the conduction band in the semiconducting material. The electrons then move via diffusion to the PN junction where they are separated from their corresponding holes. The electrons are then conducted by electrical contacts to an external circuit. A typical PV cell produces only a few watts of power. Cells are typically strung together in series and are encapsulated in a PV module to provide adequate voltage. These modules are then strung together in array to provide enough power for a given application.

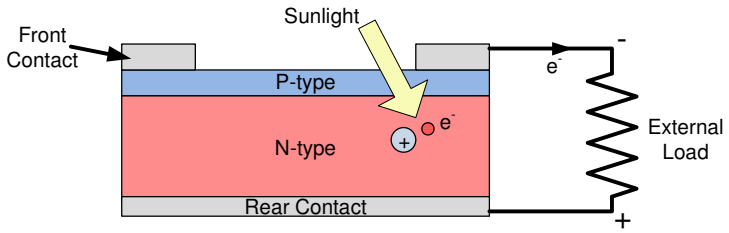

Figure 5.1: Solar cell operation.

Due to the bandgap of the semiconductor and the cell structure, photovoltaics can only convert a portion of the solar spectrum into electrical energy. The remainder of the solar energy is lost to heat. Conversion efficiencies of photovoltaic cells vary depending the material and process used to produce the cells. Many different types of semiconducting materials are used in PV cells. The majority of commercial PV modules on the market today are made of silicon (Si) which can be divided into three main categories: monocrystalline silicon, which has the highest efficiency and cost, polycrystalline silicon, which has a less ordered crystal structure and lower efficiency, and amorphous silicon, which is a thin film technology with relatively low efficiency. Other compounds that are commonly used in solar cells include cadmium telluride (CdTe), gallium arsenide (GaAs), and copper indium gallium selenide (CIGS). Common efficiencies for commercial monocrystalline silicon modules are 15-18% [123].

The basic operation of a solar cell can be represented using the classic one diode model. In this model, depicted in Figure 5.2, the current produced by a solar module is given by [124]:

$$I = I_{ph} - I_0\left[\exp\left(\frac{V + IR_s}{nk(T_{cell} + 273.15)/q}\right) - 1\right] - \frac{V + IR_s}{R_{sh}} \tag{5.17}$$

where I_{ph} is the light generated current, I_0 is the reverse saturation current which is affected by temperature, V is the panel operating voltage, I is the operating current, R_s is the panel series resistance, R_{sh} is the panel shunt resistance, n is the diode ideality factor, k is the Boltzmann constant, T_{cell} is the cell temperature in ^{o}C, and q is the charge of the electron. Note that I_0, R_s, R_{sh} and n are all panel specific parameters. All currents are in A, voltages are in V, and resistances are in Ohms. The light generated current can be represented by:

$$I_{ph} = A_{panel}\left(C_0 + C_1 T_{cell}\right) G_{PV} \tag{5.18}$$

where A_{panel} is the area of the solar panel in m^2, G_{PV} is the incoming solar radiation normal to the cell, and C_0 and C_1 are panel specific constants.

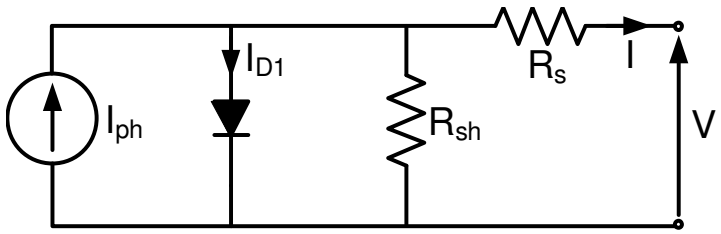

Figure 5.2. Electrical circuit representation of the one diode solar module model.

From the above equations, it is evident that the output current of the photovoltaic module is dependent on many factors including the operating voltage, the solar radiation, and the solar cell temperature. Output current and power produced by a typical solar panel for a given amount of solar radiation and different cell temperatures are shown in Figure 5.3. At each temperature or radiation level, there exists an operating voltage at which the solar panel produces its maximum amount of power. In general, connecting a load directly to a solar panel will not result in the voltage that gives maximum power output. Typically, a power converter with a maximum power point tracking algorithm is required to optimize the power output.

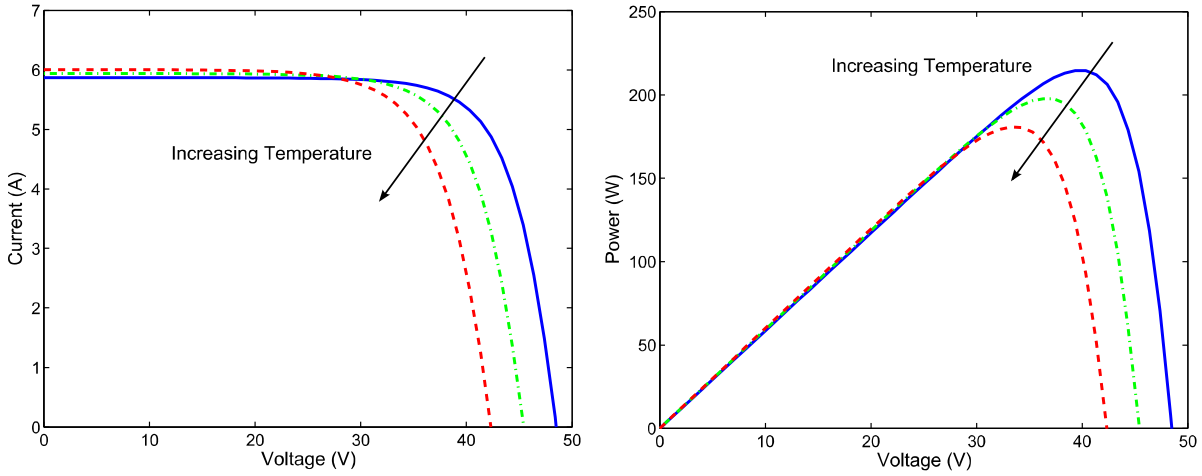

Figure 5.3. Photovoltaic panel operating curves.

The PV model which is used in the modular design approach assumes that the electronics are able to track the maximum power output for the given solar radiation. Using this assumption, the PV system model determines the power output for a given solar profile, panel type, and number of panels. For each PV module in the inventory, dimensions, efficiency, and thermal properties are extracted from the manufacturer's data sheet. Using these properties, the power produced by the PV system can be determined using:

$$P_{Solar} = n_{panel}\left[\eta_{PV} G_{PV} A_{PV} (1+\alpha(T_{cell} - 298))\right] \tag{5.19}$$

where P_{solar} is the power produced by the PV system, n_{panel} is the number of PV panels, η_{PV} panel efficiency of the PV panel considered, G_{PV} is the solar radiation incident on the PV panel, A_{PV} is the PV panel area, α is the temperature coefficient of the panel and T_{cell} is the cell temperature. The cell temperature can be estimated using the following relationship:

$$T_{cell} = T_{amb} + \frac{G_{PV}\left(NOCT - 20\right)}{800} \tag{5.20}$$

where T_{amb} is the ambient temperature in ^{o}C and $NOCT$ is the normal operating cell temperature of the model being considered in ^{o}C.

5.2.2 PV Tracking/Mounting

The amount of solar radiation being received by the solar panel depends on time of day, weather conditions, and the panel orientation. This section outlines the calculation of the panel radiation, G_{PV}, for an input solar radiation (which factors weather conditions and time of day) and panel position. One and two-axis PV tracking systems and fixed mounting configurations were also considered. Tracking systems add expense to the PV system, but can be cost effective when used in locations with clear skies.

The solar radiation calculated using the method outlined in section 5.1.1 determines the solar radiation falling on a horizontal panel over the course of the day from the daily solar insolation value. To determine the radiation falling on the PV panel, this must be translated to the panel orientation. For a given sun position, the angle between the incident solar rays and the panel position, θ_s, is given by:

$$\begin{aligned}\cos\theta_s = {} & \sin\delta\sin\phi\cos\beta - \left[sign(\phi)\right]\sin\delta\cos\phi\sin\beta\cos\alpha + \cos\delta\cos\phi\cos\beta\cos\omega \\ & + \left[sign(\phi)\right]\cos\delta\sin\phi\sin\beta\cos\alpha\cos\omega + \cos\delta\sin\alpha\sin\omega\sin\beta\end{aligned} \tag{5.21}$$

where β is the panel slope, and α is the panel azimuth. All angles are expressed in degrees.

The simplest mounting case considers fixed PV panels with the azimuth facing the equator. For this case, equation (5.21) simplifies to:

$$\cos\theta_s = \left[sign\left(\phi\right)\right]\sin\delta\sin\left(abs\left(\phi\right) - \beta\right) + \cos\delta\cos\left(abs\left(\phi\right) - \beta\right)\cos\omega \tag{5.22}$$

The one-axis tracking systems considered in these studies are all polar mount systems. In these mechanisms, the axis of rotation is aligned north-south and tilted relative to the ground by an angle, β_{PV}. To maximize the power output, the panel will rotate about the polar axis by:

$$\theta_{PV} = \begin{cases} \arctan\left(\dfrac{\sin\psi_s \cos\gamma_s}{\cos\psi_s \cos\gamma_s \sin\beta_{PV} + \sin\gamma_s \cos\beta_{PV}} \right) + c, \gamma_s > 0 \\ 0, \gamma_s \le 0 \end{cases} \tag{5.23}$$

where c is a constant associated to the quadrant of θ_{PV} as follows:

$$c = \begin{cases} -180 \text{ for} \cos\psi_s \cos\gamma_s \sin\beta_{PV} + \sin\gamma_s \cos\beta_{PV} < 0 \,\&\, \psi_s < -90 \\ 180 \text{ for} \cos\psi_s \cos\gamma_s \sin\beta_{PV} + \sin\gamma_s \cos\beta_{PV} < 0 \,\&\, \psi_s > 90 \\ 0 \text{ otherwise} \end{cases} \tag{5.24}$$

Note that θ_{PV} is limited between +/- 90^o due to the mechanism design. From this relationship, the panel slope and azimuth are calculated as follows:

$$\beta = \arccos\left(\cos\theta_{PV} * \cos\beta_{PV} \right) \tag{5.25}$$

It is assumed that two-axis tracking systems are able to follow the sun exactly. For these mechanisms, the azimuth and slope of the PV panel are given by:

$$\begin{aligned} \alpha &= \psi_s \\ \beta &= 90 - \gamma_s \end{aligned} \tag{5.26}$$

With the slope of the PV panel defined for all possible mounting mechanisms, the solar radiation incident on the panel surface can be calculated as follows. The radiation incident on the sloped PV panel has 3 components: beam radiation, diffuse radiation, and reflected radiation. The beam radiation incident on the panel, in W/m^2, is calculated using:

$$B_{PV}(t) = \frac{B(t) \max\left(0, \cos\theta_s\right)}{\cos\theta_{zs}} \tag{5.27}$$

Assuming that diffuse radiation comes equally for all directions, the amount of diffuse radiation falling on the PV panel, in W/m^2, is proportional to the panel's view factor of the sky as given by:

$$D_{PV}(t) = D(t) \frac{1 + \cos\beta}{2} \tag{5.28}$$

Finally, the reflected radiation component, in W/m^2, is given by the panel's view factor of the ground as given by:

$$R_{PV}(t) = \rho G(t) \frac{1-\cos\beta}{2} \tag{5.29}$$

where ρ represents the reflectivity of the ground. For the studies conducted here, a general number of 0.2 was assumed.

By adding together the different radiation components, the total radiation incident on the PV panels, in W/m^2, can be found.

$$G_{PV}(t) = B_{PV}(t) + D_{PV}(t) + R_{PV}(t) \tag{5.30}$$

The total solar radiation incident on the PV panel for the three different panel tracking configurations is shown in Figure 5.4. These cases are considered for a day in mid-May in Boston with the fixed panels and 1-axis tracking systems oriented at latitude tilt. It is evident that there is substantial gain from the 1-axis tracking mechanism, but only a small additional improvement is seen for the 2-axis tracking mechanism. With latitude tilt for the polar 1-axis tracking system, the largest gains are seen during the summer and winter solstice. This cost/performance tradeoff will be analyzed in the modular design approach.

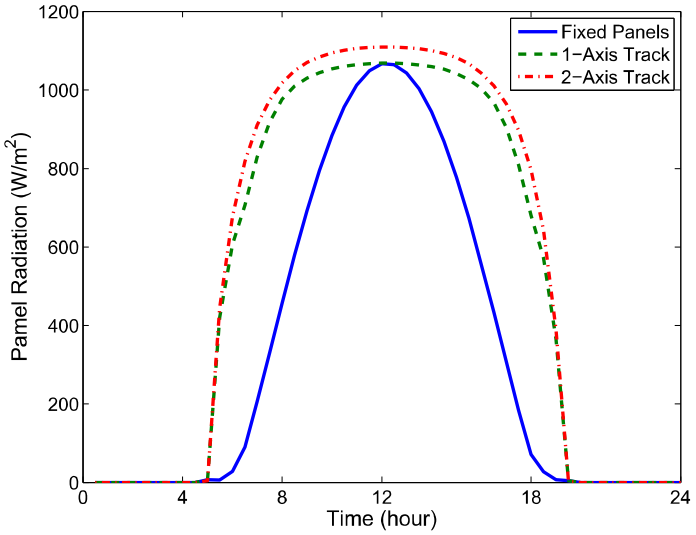

Figure 5.4. Radiation incident of PV panels with different tracking mechanisms on clear May day in Boston.

5.2.3 Motors

Two different types of motors are considered in the modular design approach, DC motors and AC motors. For low-power applications, DC motors tend to be cost effective and efficient.

As the power requirements increase, AC motors become more cost effective. The models used to describe the different types of motors used are detailed in this section.

A simple, non-dynamic, DC motor model was used. In this model, the motor torque output, τ_m, is directly proportional to the motor current as given by:

$$\tau_m = \left(I_m - I_{0,m}\right) / K_{T,m} \tag{5.31}$$

where I_m is the motor current in A, $I_{0,m}$ is the friction related current in A, and $K_{T,m}$ is the torque constant in Nm/A.

The internal motor back-EMF, V_m, is related to the motor speed, Ω_m as shown:

$$V_m = \Omega_m / K_{V,m} \tag{5.32}$$

where $K_{V,m}$ is the motor speed constant.

The motor terminal voltage, V_{motor}, can be found by adding the resistive voltage drop to the back-EMF, V_m, as shown:

$$V_{motor} = V_m + I_{motor} R_m = \frac{\Omega_m}{K_{V,m}} + I_{motor} R_m \tag{5.33}$$

where R_m is the resistance of the motor in Ohms.

Similar equations can be derived for AC motors. The sync speed of the AC motor, Ω_{sync}, in revolutions per second, is dependent on the frequency set by the drive as given by:

$$\Omega_{sync} = \frac{2 f_m}{n_{poles}} \tag{5.34}$$

where f_m is the motor frequency in Hz, and n_{poles} is the number of AC motor poles. Taking the motor slip into account, the speed of the AC motor can be written as:

$$\Omega_m = \Omega_{sync} - K_{s,m} \tau_m = \frac{2 f_m}{n_{poles}} - K_{s,m} \tau_m \tag{5.35}$$

where $K_{s,m}$ is the motor slip constant.

The motor current for the AC motor is related to the torque output as follows:

$$I_{motor} = \sqrt{I_a^2 + I_r^2} = \sqrt{\left(m_a \tau_m + b_a\right)^2 + \left(m_r \tau_m + b_r\right)^2} \tag{5.36}$$

where I_a is the active current and I_r is the reactive current. The active and reactive currents are approximated by linear functions of the motor torque where m_a and m_r are the slopes and b_a and b_r are the intercepts of the relationship. Using the active current, the power required to drive the AC motor can be calculated using:

$$P_{m,AC} = \sqrt{3} V_{m,AC} I_a \tag{5.37}$$

5.2.4 Pumps

Due to the pressures and flow rates involved in the reverse osmosis system, positive displacement pumps are commonly used. Positive displacement pumps used in reverse osmosis systems take on many different forms, such as vane pumps, progressive cavity pumps, diaphragm pumps and piston pumps. Fortunately, these pumps all have similar operating characteristics. The flow rate produced by a positive displacement pump, in L/s, is found using:

$$Q_{pump} = D_p n_p - c_{s,p} \frac{D_p}{2\pi} \frac{\Delta p_p}{\mu} - Q_{R,p} \tag{5.38}$$

where n_p is the pump speed in revolutions per second, D_p is the pump volumetric displacement in L per revolution, $c_{s,p}$ is the pump slip coefficient, μ is the dynamic viscosity of the water, Δp_p is the pressure difference across the pump in bar, and $Q_{R,p}$ is the flow loss due to inlet flow restriction in L/s.

The torque required by a positive displacement pump, in Nm, is given by:

$$\tau_p = 100 \frac{\Delta p_p D_p}{2\pi} + c_{d,p} D_p \mu n_p + c_{f,p} \frac{D_p}{2\pi} \Delta p_p + T_{c,p} \tag{5.39}$$

where $c_{d,p}$ is the coefficient of viscous drag for the pump, $c_{f,p}$ is the coefficient of friction for the pump geometry, and $T_{c,p}$ is the pump torque constant in Nm. Since the motor and pump share the same shaft, the speed and torque of the motor and pump are identical.

5.2.5 Reverse Osmosis Membranes

The reverse osmosis membranes are the essential components affecting separation. The prevalent construction used in PVRO systems are composite, spiral-wound membranes, as shown in Figure 5.5. In this configuration, permeate is driven through the membrane by the high pressure into the permeate carrier, and then spirals in to the permeate tube. The membrane itself is composed of a thin, nonporous polyamide active layer supported by a thicker, porous polysulfone backing. The membrane is configured as a cross-flow separator wherein a portion of the water is recovered. The rest leaves the membrane module as high concentrate brine.

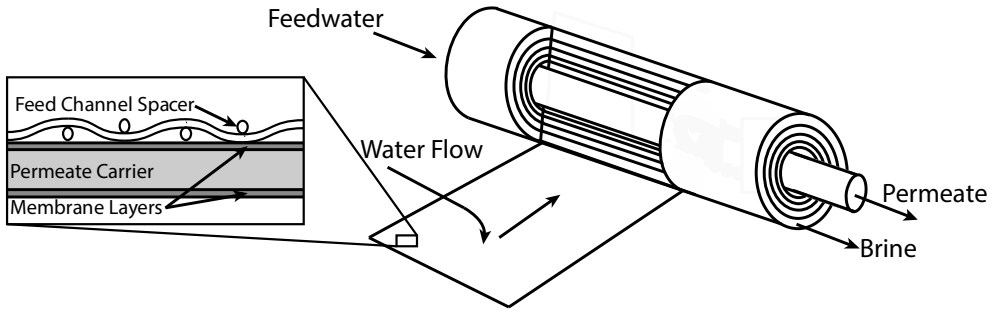

Figure 5.5. Reverse osmosis membrane configuration.

The membranes are modeled as a cross-flow separator with the permeate water well mixed. The flow rate of clean water across the membrane is proportional to pressure difference minus the osmotic pressure difference, given by

$$Q_p = K_A A_{mem} K_{TCF} \left(FF\right)\left(\Delta\bar{p} - \Delta\bar{\pi}\right) \tag{5.40}$$

where A_{mem} is the membrane surface area in m^2, K_A is the membrane permeability for water, K_{TCF} is the water permeability temperature correction factor, FF is the membrane fouling factor, $\Delta\bar{p}$ is the average pressure applied across the membrane in bar, and $\Delta\bar{\pi}$ is the average osmotic pressure applied across the membrane in bar. This equation shows that increasing the membrane area, permeability and driving pressure result in increased water production.

The osmotic pressure must be overcome to produce fresh water by reverse osmosis. The osmotic pressure varies depending on the amount of salt dissolved in the water and the composition of the salt. For the majority of seawater sources, the composition of dissolved minerals scales proportionally with overall salinity. For these cases, the following relationship is used to estimate the osmotic pressure of the water in bar [125]:

$$\pi_w = \frac{2.654\times10^{-3} C_w \left(T_w + 273.15\right)}{1000 - C_w / 1000} \tag{5.41}$$

where C_w is the water concentration in mg/L and T_w is the water temperature in °C. Using this relationship, the average osmotic pressure across the membrane can be determined using:

$$\Delta\bar{\pi} = \left(pf\right)\frac{\pi_f + \pi_b}{2} - \pi_p \tag{5.42}$$

where π_f is the osmotic pressure of the feed water, π_b is the osmotic pressure in the brine, π_p is the osmotic pressure in the permeate, and pf is the membrane polarization factor.

The membrane polarization factor accounts for the boundary layer effect next to the membrane. In this region, the salt concentration is higher and increases the osmotic pressure. For the model used in the modular design approach, the polarization factor is given by the following empirical relationship [99]:

$$pf = \exp(0.7R) = \exp\left(0.7\frac{Q_p}{Q_f}\right) \tag{5.43}$$

where R is the membrane recovery ratio, and Q_f is the feed water flow rate.

The membrane permeability increases with rising water temperature. This can greatly affect performance and has been exploited in the design of PVRO systems [126]. The temperature effect is accounted for in the model using the empirical temperature correction factor relationship given by [99]:

$$TCF = \begin{cases} \exp\left(2640\left(\frac{1}{298} - \frac{1}{273+T_f}\right)\right); T_w \geq 25^0\text{C} \\ \exp\left(3020\left(\frac{1}{298} - \frac{1}{273+T_f}\right)\right); T_w < 25^0\text{C} \end{cases} \tag{5.44}$$

where T_w is the temperature of the feed water in °C.

The pressure applied along the length of the membrane is not constant due to the pressure drop associated with water flowing through a constrained space. The average pressure applied across the membrane is found using:

$$\Delta\overline{p} = p_H - \frac{\Delta p_{fc}}{2} - p_p \tag{5.45}$$

where p_p is the pressure of the fresh water exiting the membrane in bar and Δp_{fc} is the pressure drop over the membrane module in bar, estimated empirically using [99]:

$$\Delta p_{fc} = 0.756\left(\frac{(Q_C + Q_F)}{2}\right)^{1.7} \tag{5.46}$$

where Q_b and Q_f are the brine and feed flow rates in L/s, respectively. The pressure drop over the membrane can also be used to calculate the pressure in the brine using:

$$P_C = P_F - \Delta P_{fc} \tag{5.47}$$

Since separation across an RO membrane is not perfect, some salt is also transmitted. The concentration of salt in the fresh water is given by [99]:

$$C_p = \frac{K_B S_E (pf) K_{TCF} C_{fc}}{Q_p} \tag{5.48}$$

where K_B is the membrane permeability to salt and C_{fc} is the average concentration of the water on the concentrate side of the membrane, given by:

$$C_{fc} = \frac{C_f + C_b}{2} \tag{5.49}$$

where C_f is the salt concentration in the feed water and C_b is the salt concentration in the exiting brine.

In order to solve for the pressures, flowrates and concentrations of the feed, brine, and permeate streams, two more physical relationships are required. First, the volume of water flowing through the membrane must be conserved as shown by:

$$Q_f = Q_b + Q_p \tag{5.50}$$

In addition, the salt must also be conserved, as given by:

$$Q_f C_f = Q_b C_b + Q_p C_p \tag{5.51}$$

5.2.6 Energy Recovery Devices

Different types of energy recovery devices and pressure control options were considered in the modular design approach. These devices consist of hydraulic motors coupled to electric generators, pressure exchangers, and pressure control valves. The physical models used for these systems are described in this section.

The first type of energy recovery devices considered enable direct control of the system operating pressure and water recovery ratio. These devices consist of a turbine or hydraulic motor connected to an electric generator. The equations that describe a hydraulic motor are similar to those of a positive displacement pump. The speed of the hydraulic motor in rev/s, n_{hm}, can be calculated using:

$$n_{hm} = \frac{Q_{hm} - Q_{R,hm}}{D_{hm}} - c_{s,hm} \frac{\Delta p_{hm}}{2\pi\mu} \tag{5.52}$$

where Q_{hm} is the flow through the hydraulic motor in L/s, $Q_{R,hm}$ is the flow restriction in L/s, D_{hm} is the displacement per revolution of the hydraulic motor in L/rev, $c_{s,hm}$ is the motor slip coefficient and Δp_{hm} is the pressure difference across the motor in bar.

The torque produced by the hydraulic motor in Nm, τ_{hm}, is given by:

$$\tau_{hm} = 100\frac{\Delta p_{hm} D_{hm}}{2\pi} - c_{d,hm} D_{hm} \mu n_{hm} - c_{f,hm} \frac{D_{hm}}{2\pi} \Delta p_{hm} - T_{c,hm} \tag{5.53}$$

where $c_{d,hm}$ is coefficient of viscous drag for the hydraulic motor, $c_{f,hm}$ is the friction coefficient and $T_{c,hm}$ is the hydraulic motor torque constant in Nm.

Similarly, the equations that describe the operation of the generator are parallel to the equations that describe the operation of the motor. A simple DC generator model, with resistance assumed constant, is used to estimate the system performance. The generator current in A, I_{gen}, can be expressed using the following equation:

$$I_{gen} = K_{T,gen}\left(\tau_{gen} - \tau_{f,gen}\right) \tag{5.54}$$

where τ_{gen} is the shaft torque of the generator in Nm, $\tau_{f,gen}$ is the torque required to overcome the friction in Nm, and $K_{T,gen}$ is the torque constant.

The generator terminal voltage, V_{gen}, can be found by subtracting the resistive voltage drop from the EMF term:

$$V_{gen} = \frac{\Omega_{gen}}{K_{V,gen}} - I_{gen} R_{gen} \tag{5.55}$$

where Ω_{gen} is the generator speed in rev/s, $K_{V,gen}$ is the EMF constant, and R_{gen} is the resistance of the generator in Ohms. Since the hydraulic motor and the generator are on the same shaft, the speeds and torques are identical.

The second type of energy recovery devices considered is pressure exchangers. These devices use high pressure brine to pressurize the incoming feed water. Pressure exchangers can be classified into two different categories: pressure intensifiers and isobaric devices. Pressure intensifiers, such as the Clark Pump manufactured by Spectra Watermakers or the RO-Boost manufactured by Danfoss, operate based on the principle shown in Figure 5.6. These energy recovery devices use a mechanism consisting of two pistons connected with a rod. When the piston reaches the end of travel, a reversing valve switches the brine and exhaust connections, and the piston reverses direction. The area of the rod changes the effective areas on either side of the piston, and the device adds the energy in the medium pressure feed to the energy in the concentrate, producing water at a higher pressure than the concentrate.

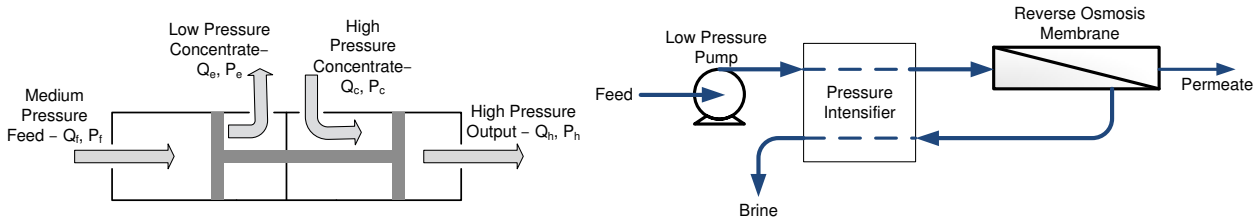

Figure 5.6. Pressure intensifier mechanics (left) and typical system configuration (right).

Isobaric devices pressurize the incoming seawater directly. These devices have different configurations. All the different pressure exchanger configurations have a constant area between brine and feedwater which results in both having the same pressure. A schematic of one of the device configurations, the Dual Work Energy Exchanger (DWEER) manufactured by Flowserve, can be seen in Figure 5.7. Since the high pressure feedwater exits the device at the same pressure as the brine, an additional pump is required to boost the pressure, as shown in Figure 5.7.

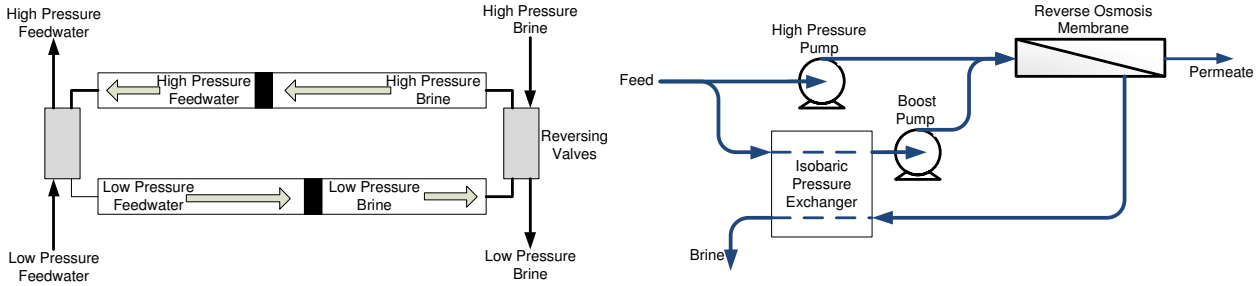

Figure 5.7. Isobaric pressure exchanger mechanics (left) and typical system configuration (right).

Fortunately, these two types of pressure exchangers can be described by the same set of equations. These are fixed displacement devices and the flow rate of the brine is related to the flow rate of the feed water by:

$$Q_{f,ER} = \varphi Q_{b,ER} \tag{5.56}$$

where $Q_{f,ER}$ is the flow of the feed through the energy recovery device in L/s, $Q_{b,ER}$ is the flow of the brine through the energy recovery device in L/s, φ is the ratio between the feed flow and the brine flow defined by the energy recovery device geometry. For pressure intensifiers, this number is greater than 1. For isobaric pressure exchangers, this number equals 1.

The pressure relationship for these devices varies with system flow rate. To simply the analysis, the pressure relationship is taken to be constant and is given by:

$$\Delta p_{f,ER} Q_{f,ER} = \eta_{ER} \Delta p_{b,ER} Q_{b,ER} \tag{5.57}$$

where $\Delta p_{f,ER}$ is the change in feed stream pressure, $\Delta p_{b,ER}$ is the change in pressure in the brine stream, and η_{ER} is the efficiency of the energy recovery device.

5.2.7 Control Electronics

The control electronics condition power from the PV panels and other power sources such as the generator in the energy recovery system for use by the system pumps. The overall power in the system must be conserved, as shown by:

$$\sum \text{Power In} = \sum \text{Power Out}$$

$$\eta_{mppt} P_{solar} + P_{gen} = \frac{\sum_{i=1}^{n_{Pumps-DC}} P_{m,DC,i}}{\eta_{DCDC}} + \frac{\sum_{i=1}^{n_{Pumps-AC}} P_{m,AC,i}}{\eta_{inv}} \tag{5.58}$$

where η_{mppt} is the efficiency of the maximum power point tracking algorithm used for the PV system, η_{DCDC} is the efficiency of the DC to DC conversion, η_{inv} is the efficiency of the inverter used for any AC motors.

The control electronics will dictate the distribution of power amongst the different system motors. In order to accommodate this, additional design variables, θ_i, are added to the optimization problem. The number of design variables added are equal to the number of pumps in the system and determine the output power as follows:

$$P_{m,DC,i} = \eta_{DCDC} \frac{\theta_i}{\sum_{i=1}^{n_{pumps}} \theta_i} \left(\eta_{mppt} P_{solar} + P_{gen} \right) \tag{5.59}$$

$$P_{m,AC,i} = \eta_{inv} \frac{\theta_i}{\sum_{i=1}^{n_{pumps}} \theta_i} \left(\eta_{mppt} P_{solar} + P_{gen} \right) \tag{5.60}$$

5.3 Graph Representation

Section 5.1 above describes individual component models. This section describes a new structure which was developed to link the component models together to represent any PVRO system configuration and estimate the overall system performance. As stated above, the models

are segmented into two parts, the PV system and the RO system, whose performance is coupled via the electrical power transmitted through the control electronics.

The RO system model must determine the water output flow rate and water quality for a given component selection, system topology, pressure operating point, power input, and input water salinity. To represent and analyze the reverse osmosis system, a graph-based model was developed. In this model, the RO system components and connecting pipes are represented using edges and the nodes are the points of connection. Each edge has an assigned type based on the component it represents and associated equations, presented in section 5.1 above, which govern the pressure, flow and water concentrations. These edge types include: pumps, reverse osmosis membranes, energy recovery devices, and pipes which serve to connect all components. An example system and its graph representation can be seen in Figure 5.8.

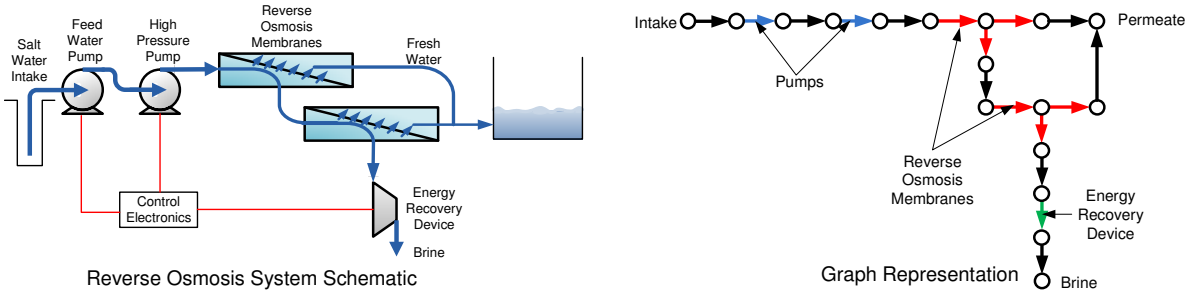

Figure 5.8: Sample reverse osmosis system and its graph representation.

This representation has advantages. First, it can easily capture any reverse osmosis system configuration using a node adjacency matrix of zeros and ones, as shown in Figure 5.9, and a vector representing the system components, which is can be implemented in a genetic algorithm optimization. Second, it allows the system equations to be uncoupled and allows for an iterative solution approach, detailed below.

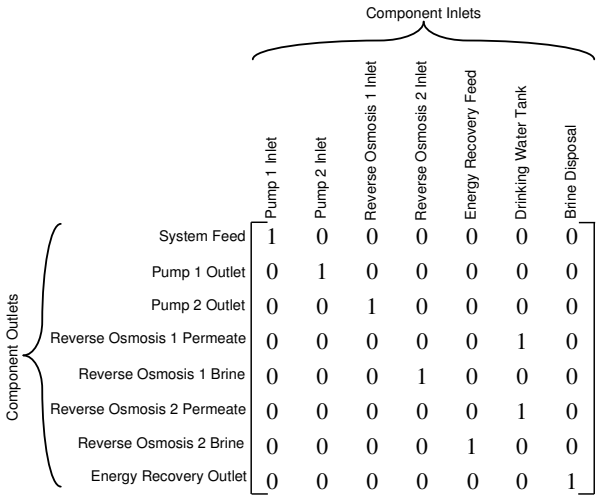

Figure 5.9: Connection matrix for sample reverse osmosis system.

For the given system connection matrix, component types, pressure operating point, and power input, the method outlined in Figure 5.10 is used to calculate the output water flowrate and concentration. This method was programmed using Matlab and starts by ordering the system nodes and generating a node-arc incidence matrix for the system graph. The incidence matrix is a $l \times m$ matrix, where l is the number of nodes and m is the number of edges. The matrix, **B**, is defined as:

$$b_{ij} = \begin{cases} 1 \text{ if edge } j \text{ enters node } i \\ -1 \text{ if edge } i \text{ leaves node } j \end{cases} \tag{5.61}$$

This matrix defines conservation of water and salt over the network as follows:

$$\mathbf{Bq} = \mathbf{q}_{in} - \mathbf{q}_{out} \tag{5.62}$$

where $\mathbf{q}$ is the vector of flows through each edge, $\mathbf{q}_{in}$ is the vector of flows entering the system at each of the node and $\mathbf{q}_{out}$ is the flow exiting the system at each node.

The node-arc incidence matrix also defines the concentration of salt over the network as follows:

$$\mathbf{B}(\mathbf{q} \circ \mathbf{c}) = \mathbf{q}_{in} \circ \mathbf{c}_{in} - \mathbf{q}_{out} \circ \mathbf{c}_{out} \tag{5.63}$$

where $\circ$ denotes component-wise multiplication of vectors, $\mathbf{c}$ is the vector of water concentrations along each edge, $\mathbf{c}_{in}$ is the vector of water concentrations entering the system at each of the node and $\mathbf{c}_{out}$ is the vector of water concentrations exiting the system at each node.

Once this graph structure is generated, an initial guess of the overall water production is made based on the power input using equation (4.11). An average system recovery rate (10% for systems which produce less than 5 m^3 per day, and 30% for all other systems) is assumed to fully define $\mathbf{q}_{in}$ and $\mathbf{q}_{out}$ for the system. Using these system flowrate guesses, a feasible system flowrate vector is determined using equation (5.62). The pressures at each of the system nodes and the concentration of water at each edge are determined using the system equations in section 5.1 and the initial flowrate guesses. This calculation neglects the membrane pressure flow calculation defined in equation (5.40) as it is used to correct the flowrates in the next step. The calculated pressures are then used to determine the flow across the membrane and the system flows are recalculated using equation (5.62). The calculated flow rate is averaged with the previous guess and the process is repeated until the change in the flow rate is less than the specified tolerance. This solution method is very robust and the process typically converges in less than 1 second.

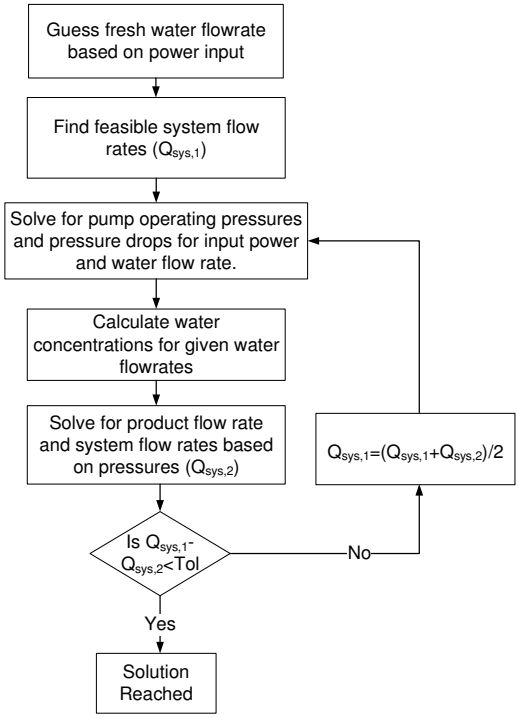

Figure 5.10: Solution method for reverse osmosis system equations.

5.3.1 Surrogate Model

The model discussed above requires several seconds to compute the water output for a single power setting. Hence, this model cannot be used directly for optimization since the

computation of the water output using a varying power input for an average year would take many minutes. Fortunately, the resulting system of equations, while non-linear, can be accurately approximated by interpolating between evaluated function points. The resulting water production for the sample PVRO system depicted in Figure 5.8 is shown in Figure 5.11.

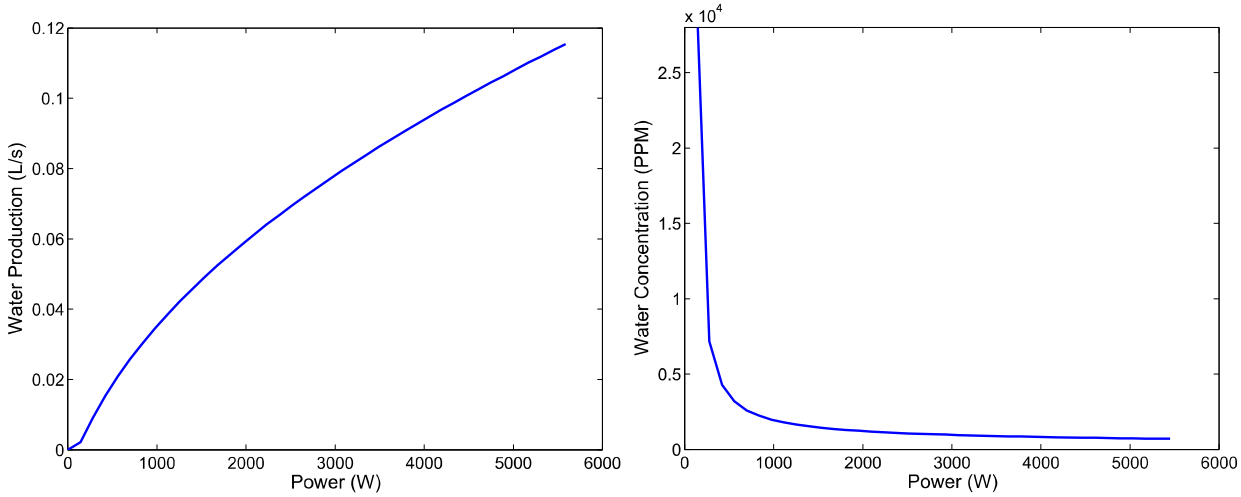

Figure 5.11: Water production and water concentration vs. power input for sample PVRO system.

To determine the number of interpolation points required, a study evaluating the error versus the number of points was performed for an array of 10 different RO system configurations. In this study, the each system was simulated for an average spring day in Boston using the full model. Then water production and output water salinity were evaluated using a different surrogate model where the system output is determined by interpolating between evaluation points of the original model output. The sample points of the original model are evenly distributed between zero system power and the maximum system power. The number of times the original model is sampled is varied to determine the number of samples required to meet a desired accuracy. Here, the criteria was set that the surrogate model have a less than 1% error.

The average percentage error in the water production and the water salinity for the surrogate model versus the number of function evaluations is shown in Figure 5.12. As expected, as the number of evaluations increases, the error goes to zero. In order to achieve <1% error, a total of 8 evaluations of the full system model at varying power levels are required. For each

PVRO system evaluated in the final stage of the modular design approach, this surrogate model, formed by 8 evaluations of the full system model, will be used to determine the system output over varying solar profiles.

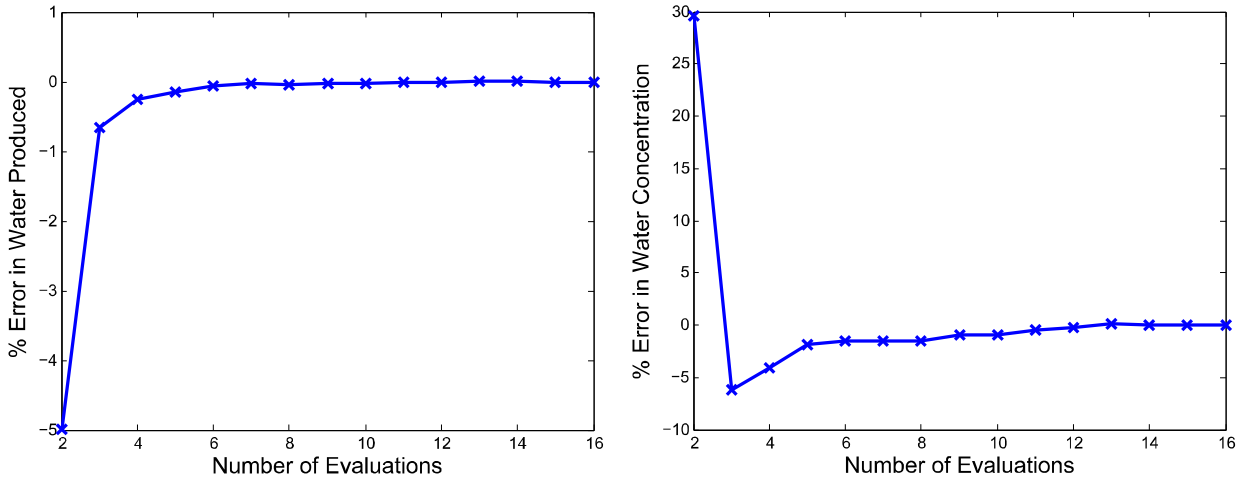

Figure 5.12: Error in water production based on number of evaluations.

The interpolation approach saves substantial computation time. The time saved varies depending on the PVRO system being evaluated and the length of the simulation. An average value of 10.2 seconds is saved for a day-long simulation of a PVRO system with an hourly time step. When simulated over the course of a year, an average time of 2.9 hours is saved. The surrogate model enables the implementation of the modular design approach.

5.4 Experimental Model Verification

5.4.1 Experimental System Description

The PVRO system modeling approach outlined above was verified using data from the MIT Experimental PVRO System. The system is modular and has been constructed on a campus rooftop (see Figure 5.13). The system schematic and model representation can be seen in Figure 5.14. It is composed of a tracking PV panel, custom control electronics, parallel DC pumps, a Clark pump energy recovery system, a reverse osmosis membrane within a pressure vessel, and plastic water tanks. The system is equipped with custom control electronics and designed to operate variably to eliminate the need for batteries. The system is fully instrumented and

computer controlled to optimize the system water output, and is designed to produce approximately 350 L of fresh water per day in Boston on a sunny summer day.

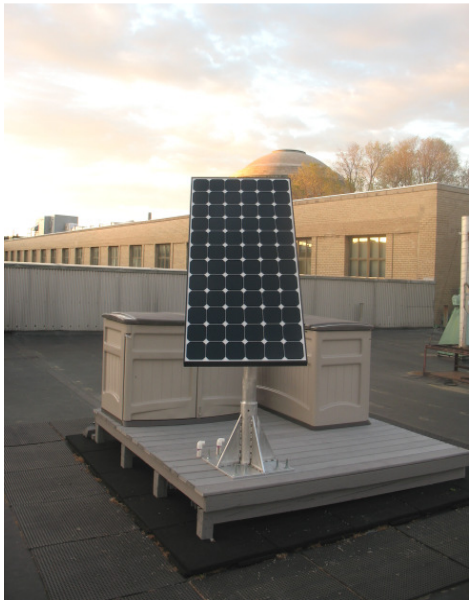

Figure 5.13: Experimental PVRO system.

The system instrumentation consists of 18 different sensors that provide sufficient information for model validation and control feedback (see Figure 5.14). Sensors include thermistors for measuring solar panel, feed water, and ambient air temperature, flow sensors, salinity sensors, pressure transducers, and sensors for measuring solar panel orientation. The sensors are connected via custom electronics to the data acquisition and control computer, shown in Figure 5.15.

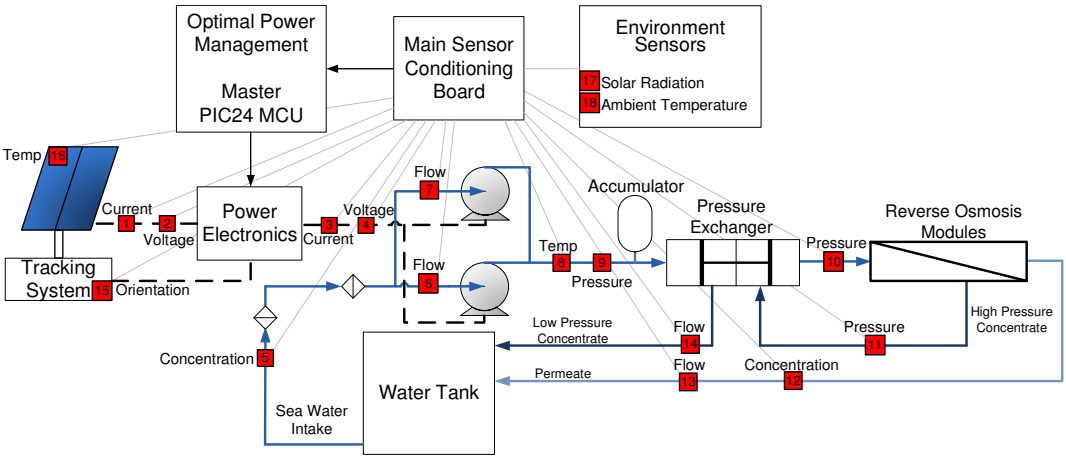

Figure 5.14: Experimental PVRO system layout.

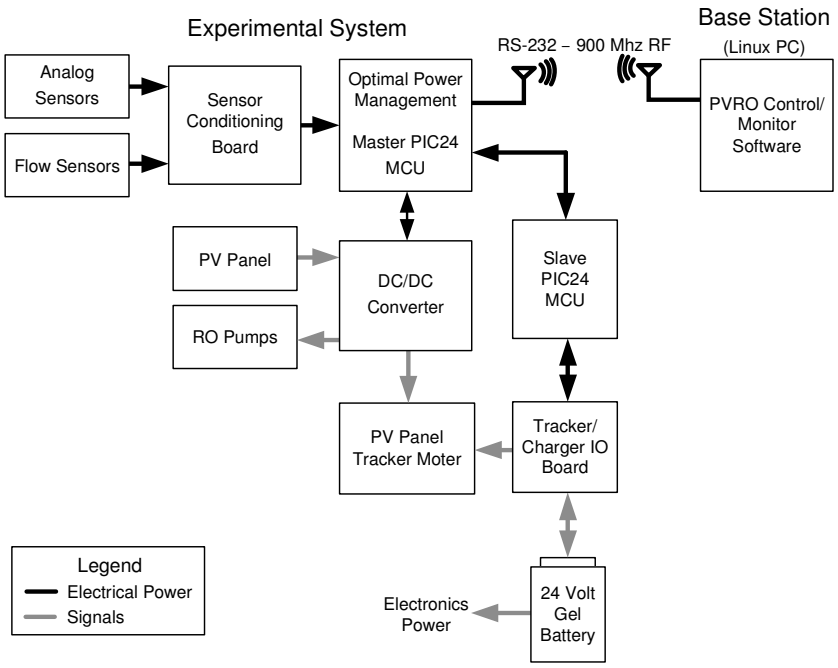

Figure 5.15: MIT experimental PVRO system electronics.

Two PIC24 microcontrollers in a Master/Slave configuration are used to acquire sensor data through a sensor conditioning board, and to perform computation and control tasks. The Master PIC24 is used to control a DC/DC step down converter that receives power from the solar panels and converts it to the voltage desired by the two DC boost pumps. This electrical system configuration was designed with student Roman Geykman [127]. Custom control software was developed to track the maximum power point of the solar panel throughout variable solar radiation and temperature conditions and maximize the system water production. The Slave PIC24 is used to drive the solar panel tracker motors. The Master PIC24 also communicates with a base station PC running Linux over a wireless modem. The base station is used to record the acquired data and to display it in real time.

The water type used for the experimental system greatly affects the system performance. The seawater salinity varies from location to location, but the reference value commonly used is 35.164 g of salts per kg of seawater [128]. The majority of seawater in the world has water salinities close to this value, although there are areas in the Arabian Gulf and Red Sea where salinities can exceed 45 g/kg [2]. Since the MIT experimental system is located far from any natural salt water source, surrogate seawater was used to test the performance of the

experimental system. This water was mixed using NaCl with the concentration adjusted to ensure the solution has the same osmotic pressure as seawater. This method is commonly used by reverse osmosis membrane manufacturers in system testing [14]. The water concentration used in the experiments was 32800 mg/L or 32125 g/kg. This concentration results in an osmotic pressure of 25.8 bar, equivalent to the osmotic pressure of standard seawater.

The PVRO system was tested over a range of operating conditions to evaluate the system performance. The power produced and panel efficiency for different radiation levels over a spring day is shown in Figure 5.16. As is expected, the power production is roughly linear with respect to the input solar radiation. Also, the efficiency of the panels is roughly constant over the majority of the day. Slight variations in the efficiency occur due to temperature effects and the dynamics of the maximum power point tracking.

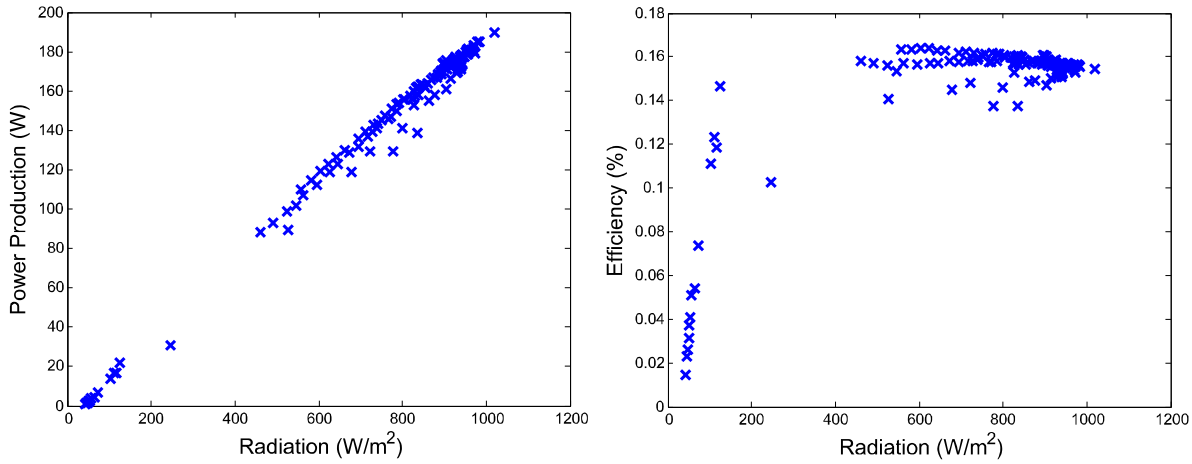

Figure 5.16: Power produced by PV panels.

The overall reverse osmosis system efficiency was also evaluated to benchmark the performance of the system against data in literature. Since the system has been designed to operate variably to account for differing levels of solar radiation without the need for batteries, the system will have different specific power consumptions for different input power levels. The specific power consumption is shown in Figure 5.17. The system requires a certain amount of energy, approximately 20 W, to overcome static friction in the system mechanical components and generate a water pressure higher than 25.8 bar required for desalination. Once this initial level is reached, the experimental system operates efficiently and is able to produce water with a specific energy consumption of 2.7 to 4 kWh/m^3. While this is much higher than the

thermodynamic limit of 0.8 kWh/m^3 for the 9% water recovery ratio (this number is 0.7 kWh/m^3 as the recovery ratio goes to 0), this is very efficient for such a small scale system. Typical specific energy consumption of large scale reverse osmosis plants is between 3 to 5 kWh/m^3 [6]. It should be noted that energy numbers for large plants include plant overhead, pretreatment, and brine disposal that are not accounted for here. When only considering desalination, power consumptions of new, highly-efficient plants have been shown to reach values of 2.5 kWh/m^3 [129].

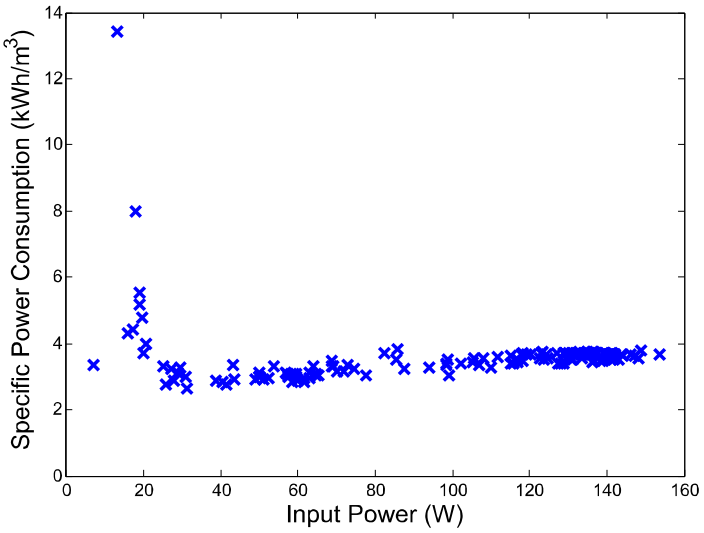

Figure 5.17: Specific power consumption of experimental PVRO system.

5.4.2 Model Representation

A graph-based model was generated for the MIT Experimental PVRO system using the approach detailed in section 5.3. This graph is shown in Figure 5.18. The system consists one tracking Sunpower 230W solar panel, two Shurflo 8050-243-169 pumps and DC motors, one DOW Filmtec SW30-2540 reverse osmosis membrane, and a Clark Pump energy recovery device manufactured by Spectra Watermakers. Parameters of the system components are outlined in Table 5.1.

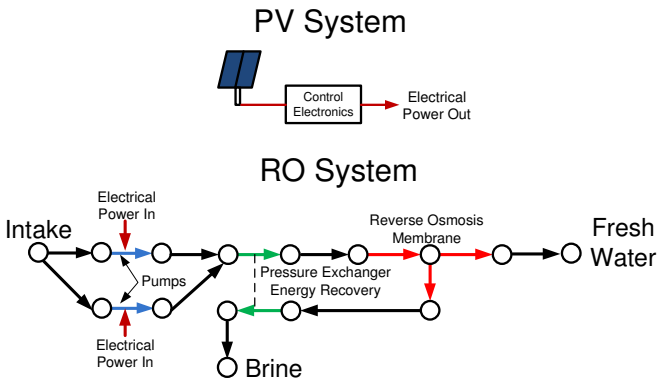

Figure 5.18: Graph representation of MIT experimental PVRO system.

Table 5.1: Model parameters of MIT Experimental PVRO system.

Component	Parameter	Value
Sunpower 230W Solar Panel [23]	Solar panel efficiency, η_{PV}	18.5 %
	Solar panel area, A_{PV}	1.23 m^2
	Solar panel temperature coefficient, α	0.38 %/K
	Normal operating cell temperature, *NOCT*	45 °C
Shurflo 8050-243-169 Pump & DC Motor	Pump coefficient of viscous drag c_d	3.803 x10^{-4} N-m/bar-L
	Pump friction coefficient, c_f	4.033 N-m/bar-L
	Pump slip coefficient, c_s	3.361 x10^{-10}
	Pump volumetric displacement per revolution, D	2.60 x10^{-3} L/rev
	Motor friction related current, I_0	0.65 A
	Motor torque constant, K_T	2.252 A/N-m
	Motor speed constant, K_V	1.824 rev/V-s
	Motor resistance, R_m	0.1546 Ω
	Pump torque constant, T_c	0.05 Nm
DOW Filmtec SW30-2540 Reverse Osmosis Membrane [24]	Membrane water permeability, K_A	3.714x10^{-4} L/m^2-bar-s
	Membrane salt permeability, B	5.842x10^{-5} L/m^2-s
	Membrane area, S_E	2.6 m^2
Other System Parameters	Feed water salt concentration, C_f	32800 mg/L
	Clark pump recovery ratio, R_t	0.090

5.4.3 Model Validation

Data from a partly cloudy summer day was used to validate the modeling approach. The solar profile used as an input to the model is shown in Figure 5.19. The resulting water production for the experimental system and the model prediction is shown in Figure 5.20. There is a very good agreement between the data and model values, with an error of less than 8%. This shows that the graph modeling approach and the simplified analysis method accurately predict system water production.

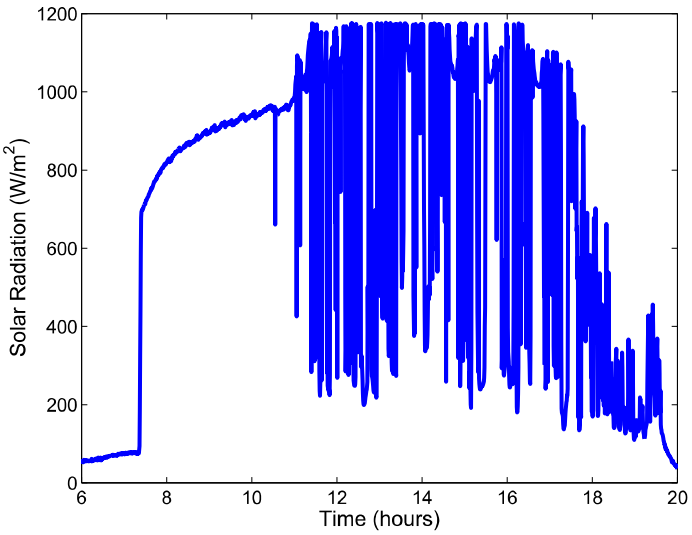

Figure 5.19: Solar radiation input for model validation.

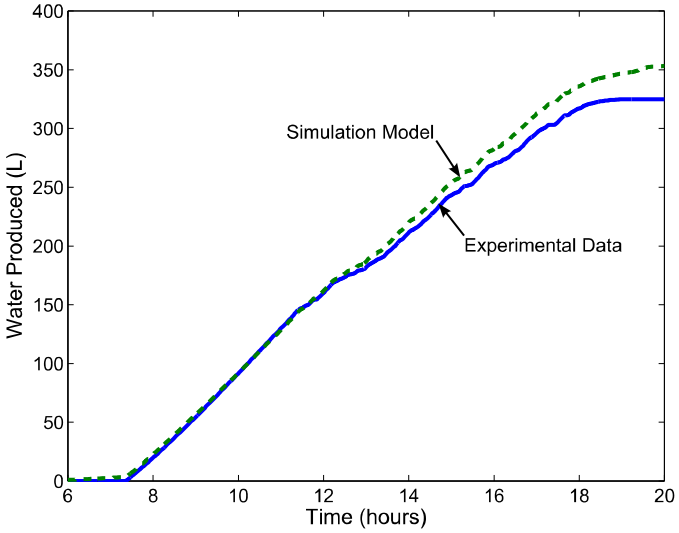

Figure 5.20: Experimental validation of modeling approach.

The specific energy consumption of the experimental system was compared to the values determined in the model. For a wide operating range, the model accurately predicts the overall system performance. This shows that the physical models detailed in section 5.2 capture the important system characteristics and are appropriate for use with the modular design approach.

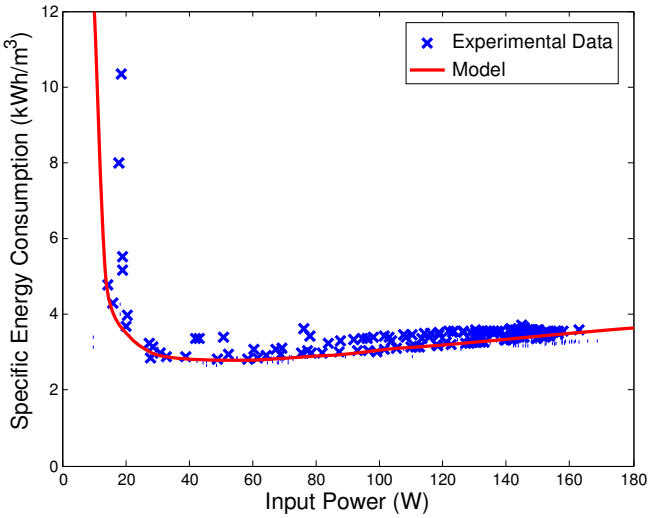

Figure 5.21: Model specific energy consumption.

5.5 Economic Models

As stated in section 4.1, the goal of the modular design approach as applied to PVRO systems is to configure the lowest lifetime cost system that is able to meet the fresh water demands of a particular location. Therefore, a set of economic models are required to estimate the overall system cost. These models are described here.

5.5.1 Total Costs

The equivalent annualized cost method used in Chapter 3 is applied here to compare the economics of different PVRO systems. The costs are separated into capital system costs and operating costs. The total annualized costs are given by:

$$A_{PVRO} = A_{CC} + A_{Op} \tag{5.64}$$

Using the total annual cost, the total water cost can be estimated using the following:

$$C_w = \frac{A_{PVRO}}{V_w} \tag{5.65}$$

where V_w is the amount of water produced by the system during an average year.

5.5.2 Capital Costs

The capital costs of a PVRO desalination system are given by:

$$C_{PVRO} = C_{Infra} + C_{PV} + C_{RO} \tag{5.66}$$

where C_{Infra} is the capital cost of the system infrastructure, C_{PV} is the capital cost of the PV system and C_{RO} is the capital cost of the RO system.

The infrastructure capital costs encompass a wide array of items such as system installation, site preparation, brine disposal system, water intake, and water distribution system. These costs will vary greatly from location to location. For the purpose of the case studies done in this thesis, these costs are accounted for by scaling the costs of RO plant as follows:

$$C_{\text{infra}} = \varphi_{\text{infra}} C_{RO} \tag{5.67}$$

where φ_{infra} is the cost of the infrastructure relative to the reverse osmosis components. Based on literature surveying installed reverse osmosis systems, this value is taken to be 1.71 [102].

The photovoltaic system costs include the cost associated with the PV panels, the mounting system and the control electronics. They are calculated using:

$$C_{PV} = \sum_{i=1}^{N_{PV\_type}} n_{PV,i} C_{PV,i} + C_{mount} + C_{elec} \tag{5.68}$$

where $n_{PV,i}$ is the number of panels of type i which are included in the system configuration, $C_{PV,i}$ is the cost of panel I, C_{mount} is the cost of the mounting system, and C_{elec} to the cost of the electrical components. The mounting cost is directly calculated based on the mounting component type and the number of panels. Different types of electronics modules are not considered in this thesis. Equation 3.29 is used to calculate the cost associated with the electronics, repeated here [105]:

$$C_{elec} = 0.72 W_p \tag{5.69}$$

where W_p is the power rating of the PV array in Watts.

The reverse osmosis system capital costs are given by:

$$C_{RO} = C_{\text{Pre}} + C_{RO\_comp} + C_{Post} \tag{5.70}$$

where C_{Pre} is the pre-treatment system cost, C_{RO_comp} is the cost of the reverse osmosis components, and C_{post} is the cost is cost of the post-treatment system and water storage.

Pre-treatment systems are often required for reverse osmosis systems to ensure that system components, such as the membranes, do not degrade prematurely. While completely

characterizing reverse osmosis pretreatment options is beyond the scope of this thesis, including these components in the overall cost analysis is required for accuracy. For this work, it is assumed that the capital cost of the pre-treatment components is proportional to the overall reverse osmosis system cost as follows:

$$C_{\mathrm{Pre}} = \varphi_{\mathrm{Pre}} C_{RO\_comp} \tag{5.71}$$

where φ_{Pre} is the cost of the pretreatment relative to the reverse osmosis components. Based on literature surveying installed reverse osmosis systems, this value is taken to be 0.35 [102].

The costs associated with the reverse osmosis components are directly taken from the components selected during the modular design approach. The total component cost is calculated using:

$$C_{RO\_comp} = C_{mem} + C_{press} + C_p + C_{motor} + C_{er} + C_{connect} \tag{5.72}$$

where C_{mem} is the total cost of membranes selected for the system, C_{press} is the total cost of pressure vessels required to hold those membranes, C_p is the total cost of the system pumps, C_{motor} is the total cost of the system motors, C_{er} is the total cost of the system energy recovery devices, and $C_{connect}$ is the total cost of the component piping and other connections.

The costs associated with post-treatment systems are typically low when compared with with other system costs. The chemical post-treatment system cost is estimated based on literature values. In addition to chemical post-treatment, investment is also required for water storage to supply water when the system is not operating due to cloudy weather. The overall post-treatment cost is given by:

$$C_{post} = \varphi_{post} C_{RO\_comp} + C_{storage} \tag{5.73}$$

where φ_{post} is the cost of the post-treatment chemical system relative to the reverse osmosis components and $C_{storage}$ is the cost of the water storage component selected by the modular design approach. Based on literature surveying installed reverse osmosis systems, φ_{post} is taken to be 0.03 [102].

The capital costs are converted into annualized costs using Equation 3.21, presented again here:

$$A_{cc} = \frac{i(1+i)^n}{(1+i)^n - 1} C_{PVRO} \tag{5.74}$$

where i is the interest rate, and C_{PVRO} is the total PVRO system capital cost.

5.5.3 Operating and Maintenance Costs

The total annual operational cost for the photovoltaic reverse osmosis system is given by:

$$A_{Op} = A_l + A_{chem} + A_{r,RO} \tag{5.75}$$

where A_l is the annual labor cost, A_{chem} is the annual chemical cost, and A_r is the annual cost of component replacement in $.

The annual cost of the labor will be highly dependent on the system location. Here, it is assumed the labor cost can be expressed as:

$$A_l = 365\gamma V_{cap} \tag{5.76}$$

where γ is the specific operating labor cost in $/m^3-day, and V_{cap} is average system production in m^3/day. In this analysis, the specific operating labor cost was $3.00/$m^3$-day [93].

The chemical costs are also location specific as the pre-treatment chemicals are dependent on local water conditions. The total annual cost of treatment chemicals is given by:

$$A_{chem} = 365kV_{cap} \tag{5.77}$$

where k is the average cost of chemicals $/$m^3$. In this analysis, the treatment chemical cost per m^3 was $0.033 [94].

From time-to-time, system components will require replacement. The major components that will require regular replacement are the reverse osmosis membranes. Less frequently, pumps, motors, energy recovery units, pre- and post-treatment systems and control electronics will require replacement. The replacement rates assumed are specified in Table 5.2. Using the replacement rates, the annual replacement cost is given by:

$$A_r = C_{PV}RR_{PV} + C_{elec}RR_{elec} + C_{mem}RR_{mem} + C_pRR_p + C_{motor}RR_{motor} + C_{er}RR_{er} + C_{pre}RR_{pre} + C_{post}RR_{post} \tag{5.78}$$

where RR represents the replacement rate of each component.

Table 5.2: Assumed replacement rate of PVRO system components.

Component	Annual Replacement Rate
PV Components	4%
Control Electronics	10%
Membranes	20%
Pumps	10%
Motors	10%
Energy Recovery Units	10%
Pre-treatment	10%
Post-treatment	10%

5.6 Summary

This section developed the physical system and economic models used for the modular design of PVRO systems. Physics-based models are developed for individual system components. The component models are implemented in a graph-based system model to represent any PVRO system configuration. A surrogate model of the solar radiation to water production relationship is developed to increase calculation speed for different solar profiles. This model is validated using an experimental PVRO system that was constructed as a part of this research. The model use is demonstrated in the case studies in Chapters 6 and 7.

CHAPTER

6

DETERMINISTIC CASE STUDIES

A series of case studies were performed to study the performance of the modular design approach applied to PVRO systems. To simplify the analysis, initial case studies were performed with deterministic solar radiation inputs and system demands. These case studies are detailed in this chapter.

6.1 Problem Description

Several representative case studies were conducted to demonstrate the modular design approach. Systems were designed for four different locations with a seawater source and for one location with a brackish water source. The location details are shown in Table 6.1. These locations provide a range of different water salinities and solar insolation values. The objective of this design process is to minimize the net present cost of the PVRO system assuming a system life of 25 years and a 4% interest rate. Both system capital costs and maintenance costs are included as described in section 5.5. The system must meet the specified water demand and produce water which is below the drinkable salinity level of 500 ppm as outlined by the World Health Organization [130].

Table 6.1: Locations used for deterministic modular design case studies.

Location	Water Salinity (ppm)	Average Yearly Solar Insolation ($kWh/m^2/day$)
Albuquerque, NM	3000*	5.79
Boston, MA	32664	4.21
Brisbane, Australia	35438	5.31
Cape Haiten, Haiti	36275	6.05
Limassol, Cyprus	39182	6.25

*Brackish Groundwater

6.1.1 System Inventory

Systems are designed for different average water demands, ranging between 1 m^3/day and 20 m^3/day. To accommodate the wide range of system requirements, a large component inventory was constructed. Figure 6.1 shows this inventory. It consists of 6 different types of motors, 8 different types of pumps, 8 different reverse osmosis membranes, 8 different types of PV panels, 3 different PV panel mounting/tracking configurations, 2 different hydraulic motors, 2 different generators, 5 pressure exchange energy recovery devices, and one pressure control valve.

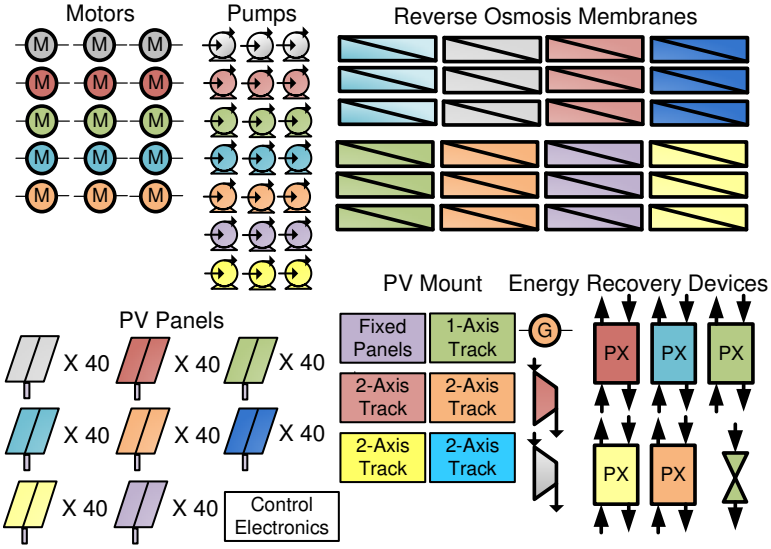

Figure 6.1: Inventory used for case studies.

The inventory details are presented in Table 6.2 through Table 6.7. Individual component specifications are derived from manufacturers' datasheets and costs are given by local component distributers.

Table 6.2: PV panel inventory used for case studies [131].

PV Panels	Quantity	Power Rating (W)	Efficiency	Temperature Factor (%/K)	NOCT (ºC)	Cost
Model 1 – First Solar – FS-385	40	85	11.8%	0.25	45	$399
Model 2 – First Solar – FS-280	40	80	11.8%	0.25	45	$299
Model 3 – Sunpower – 315W	40	315	19.3%	0.38	45	$999
Model 4 – Trina Solar – TSM-230PA05	40	230	14.1%	0.45	46	$529
Model 5 – Trina Solar – TSM-225PA05	40	225	14.1%	0.45	46	$399
Model 6 – Sanyo – HIT-N220A01	40	220	17.4%	0.336	44	$619
Model 7– Suntech – STP205-24UD	40	205	13.9%	0.47	45	$408
Model 8 – Suntech – STP295-24VDC	40	295	15.2%	0.4	45	$587

Table 6.3: PV panel mounting inventory used for case studies [132].

PV Panels	Tracking Type	Average Power Use (W)	Max Array Area Per Mount (m^2)	Cost
Model 1 – No Tracking	None	0	11.6	$500
Model 2 – Wattsun-AZ-125	1 – Axis	1.5	11.6	$3985
Model 3 – Wattsun-AZ-125	2 – Axis	1.5	11.6	$4710
Model 4 – Wattsun-AZ-225	2 - Axis	1.5	15.7	$7250
Model 5 – Wattsun-AZ-225	2 - Axis	1.5	17.6	$7645
Model 5 – Wattsun-AZ-225	2 - Axis	1.5	20.9	$8175

Table 6.4: RO membrane inventory used for case studies [133].

RO Membranes	Quantity	Water Type	Water Permeability (L/m^2-bar-s)	Salt Permeability (L/m^2 -s)	Area (m^2)	Max Pressure (bar)	Cost
Model 1 – Dow SW30XLE-400i	3	Seawater	4.25×10^{-4}	1.93×10^{-5}	37	83	$990
Model 2 – Dow SW30HRLE-400i	3	Seawater	3.48×10^{-4}	1.59×10^{-5}	37	83	$982
Model 3 – Dow SW30-2540	3	Seawater	4.22×10^{-4}	5.84×10^{-5}	2.8	69	$188
Model 4 – Dow SWHRLE-4040	3	Seawater	3.50×10^{-4}	2.02×10^{-5}	7.9	83	$435
Model 5 – AM M-B2540A	3	Brackish Water	9.95×10^{-4}	1.09×10^{-4}	2.8	41	$163
Model 6 – AM M-B4040AHF	3	Brackish Water	1.31×10^{-3}	1.44×10^{-4}	7.5	41	$303
Model 7– Koch 4820HR	3	Brackish Water	5.94×10^{-4}	2.51×10^{-5}	7.5	41	$343
Model 8 – Koch 8822HR-400	3	Brackish Water	6.09×10^{-4}	2.55×10^{-5}	7.5	41	$844

Table 6.5: Motor inventory used for case studies [134].

Motor	Quantity	Motor Type	Max Power (HP)	Rated RPM	Max Efficiency	Cost
Leeson 116698.00	3	AC Motor	5	3600	93.6 %	$845
Leeson G141121.00	3	AC Motor	10	3600	89.3 %	$1319
Leeson 170615.60	3	AC Motor	15	3600	92.4%	$2141
Shurflo 8050-243-169	3	DC Motor	1/6	3600	80.2%	$150
Leeson 108014.00	3	DC Motor	0.5	1750	81.7 %	$754
Leeson 108022.00	3	DC Motor	1	1750	83.7 %	$968

Table 6.6: Pump inventory used for case studies [135].

Pumps	Quantity	Volumetric Displacement (mL/rev)	Max Rated RPM	Max Pressure (bar)	Cost
Danfoss APP 0.8	3	5.1	3450	80	$700
Danfoss APP 1.8	3	10.0	3450	80	$4239
Danfoss APP 2.5	3	15.3	3450	80	$4782
Danfoss APP 3.5	3	20.5	3450	80	$7452
Shurflo 8050-243-169	3	2.6	3450	10	$150
Procon 140 GPH	3	5.3	1725	17.3	$152
NRD PRG 10	3	13.1	1725	18	$190

Table 6.7: Pressure exchange energy recovery inventory used for case studies.

Energy Recovery Unit	Quantity	Max Brine Flow (L/h)	Feed to Brine Flow Ratio	Average Efficiency	Cost
ERI PX-30S	1	6800	1	90%	$6000
Spectra Clark Pump	1	760	1.08	95%	$3500
Spectra Clark Pump	1	1160	1.18	95%	$4500
Flowserve DWEER	1	12000	1	95%	$8000
Pressure Control Valve	1	1000	N/A	N/A	$45
Pressure Control Valve	1	10000	N/A	N/A	$171

In addition to the component costs outlined above, there are costs associated with the pressure vessels required to hold the individual reverse osmosis membranes. In the

representation chosen, the pressure vessel itself is not one of the design choices, but is contingent on the selection of the reverse osmosis membrane configuration. The pressure vessel costs are outlined in Table 6.8.

Table 6.8: Costs of membrane pressure vessels used in case studies [136].

Water Type	Membrane Diameter	Number of 40" Long Membranes		
		1	2	3
Brackish Water	**2.5"**	$144	N/A	N/A
	4"	$294	$356	$418
Seawater	**2.5"**	$244	N/A	N/A
	4"	$539	$611	$685
	8"	$1190	$1338	$1453

6.1.2 Power Source

Solar radiation varies greatly over the course of the year due to changing seasons and local weather. To account for these variations, an average sunny day and an average cloudy day are simulated for each of the four seasons. The average values of solar insolation for cloudy and sunny days are determined from historical solar radiation data [8]. Using the method outlined in section 5.1.1, the solar profile is determined for a typical sunny and cloudy day for each season. Example solar radiation profiles for a sloped photovoltaic panel in Boston, MA are shown in Figure 6.2.

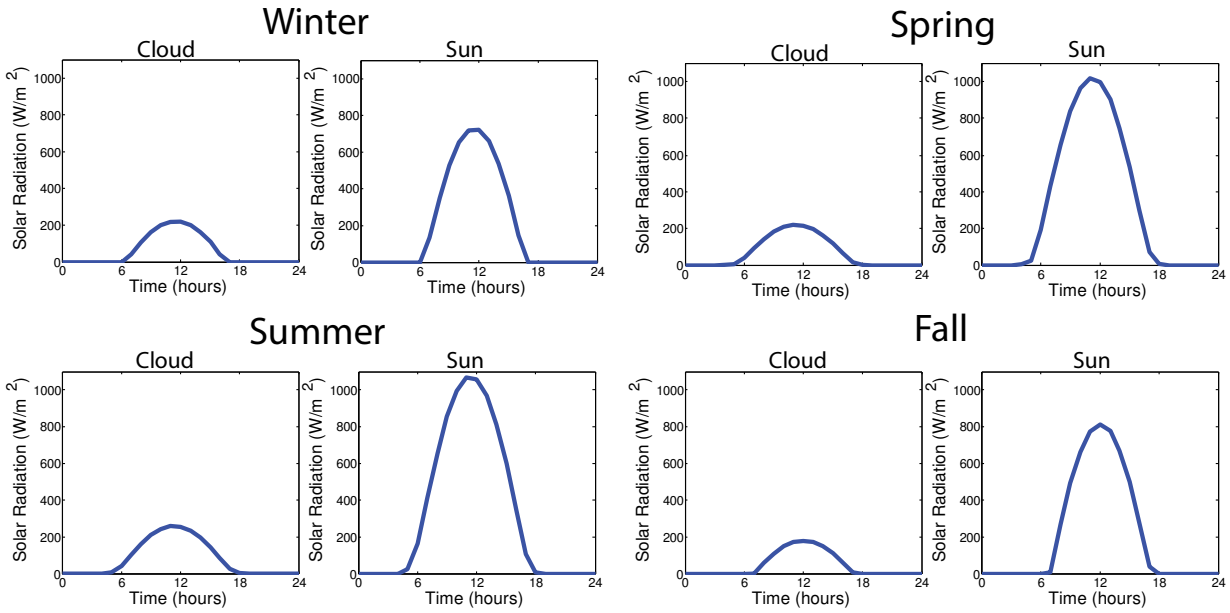

Figure 6.2: Typical solar profile used for case studies.

The PVRO system is simulated over these eight average days. The number of typical days in each season is determined from the average seasonal solar insolation using the following relationship:

$$H_i = \frac{n_{sun,i}}{n_{total,i}} H_{sun,i} + \left(1 - \frac{n_{sun,i}}{n_{total,i}}\right) H_{cloud,i} \tag{6.1}$$

where H_i is the average solar insolation in season i, $H_{sun,i}$ is the solar insolation on a sunny day during season i, $H_{cloud,i}$ is the solar insolation on a cloudy day during season i, $n_{sun,i}$ is the number of sunny days in season i, and $n_{total,i}$ is the total number of days in season i.

6.1.3 System Demand

The system demand is simplified for the deterministic case studies. Here, the system must meet the demand measured as an average daily water production. Average system demands between 1 m^3 per day and 20 m^3 per day are examined. Although using an average system demand simplifies the analysis, in reality, the system demand and water production will vary on a daily basis. Any system design must be able to accommodate these variations. This effect is accounted for in the case studies presented in Chapter 7.

Using the water produced on each of the typical days, the average daily water production is determined from the number of sunny and cloudy days in each season using:

$$V_{ave} = \frac{1}{365} \sum_{i=1}^{4} \left[n_{sun,i} V_{sun,i} + n_{cloud,i} V_{cloud,i} \right] \tag{6.2}$$

where $V_{sun,}$ is the water production on a sunny day in season i, and $V_{cloud,i}$ is the water production on a cloudy day in season i.

6.2 Optimization Setup

The modular design algorithm was implemented using Matlab. Starting with the inventory specified in section 6.1.1, the number of possible system configurations is decreased by applying the module, subassembly, and topology filters using the approach detailed in chapter 4. The final step in the modular design algorithm is to optimize the system over the reduced design space. Modular systems are composed of discrete components, making the optimization problem difficult. To add to the complexity, the cost function and constraints are non-linear, resulting in a

mixed integer nonlinear program (MINLP). Different optimization routines have been developed that can accommodate MINLPs such as Branch and Bound, genetic algorithms and simulated annealing. Any optimization algorithm can be used with the modular design approach. For the PVRO system, the topology must also be optimized, adding to the number of discrete variables and the complexity. This large number of discrete variables can easily be incorporated into a genetic algorithm, which is used here.

The genetic algorithm optimization routine is coupled to a detailed system model as shown in Figure 6.3. For the PVRO system design, the number of design variables depends on the individual location and requirements. For the cases studied, this ranges between 20 and 50 design variables. These variables represent the number of different components (integer design variables), the type of each component (integer design variables), the reverse osmosis system connections (binary design variables), reverse osmosis system operating pressure (discrete variable), and pump power division (discrete variable).

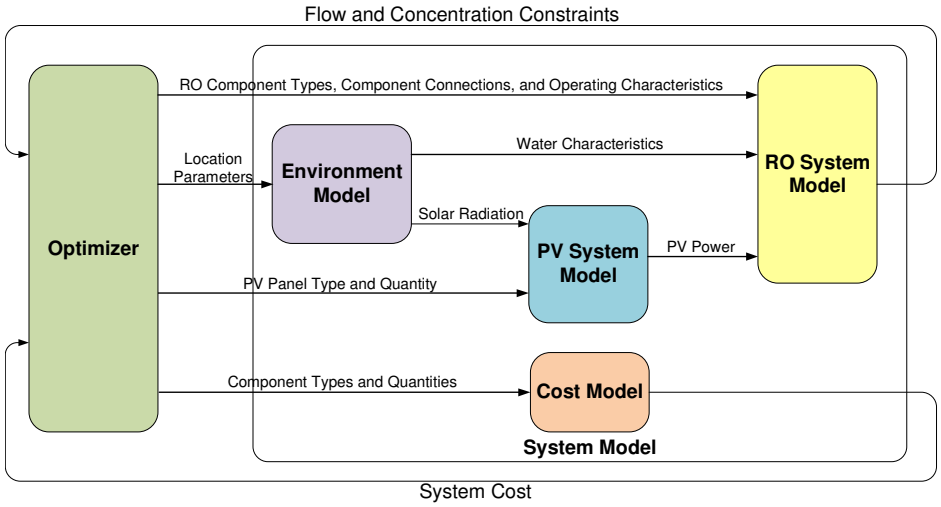

Figure 6.3: Optimization and model setup for PVRO design problem.

The design goal is to minimize the lifecycle cost of the PVRO system while meeting the water volume requirements, water quality requirements, and system pressure and flowrate limitations. The problem statement is written as follows:

$$
\begin{aligned}
&\text{minimize } f(\mathbf{x},\mathbf{y}) \\
&\text{subject to } \mathbf{g}(\mathbf{x},\mathbf{y}) = 0 \\
&\qquad V_{ave} > V_{\min} \\
&\qquad C_{ave} < 500\text{ppm} \\
&\qquad \mathbf{p} < \mathbf{p}_{\max} \\
&\qquad \mathbf{q} < \mathbf{q}_{\max} \\
&\qquad \mathbf{y}_{\min} \le \mathbf{y} \le \mathbf{y}_{\max} \\
&\qquad \mathbf{x} \in \{0,1\} \\
&\qquad \mathbf{y} \in I
\end{aligned}
\tag{6.3}
$$

where $f(\mathbf{x},\mathbf{y})$ represents the system cost as outlined in section 5.5.1, $\mathbf{g}(\mathbf{x},\mathbf{y})$ represents the system equations outlined in section 5.3, $\mathbf{x}$ represents the reverse osmosis system connections, and $\mathbf{y}$ represents the remainder of the design variables.

For genetic algorithms, constraints are incorporated using penalty functions. The overall fitness function for the PVRO design problem becomes:

$$
\begin{aligned}
fitness = A_{PVRO} + \kappa_{all}(j+5)(&\kappa_p \max(0, \mathbf{p} - \mathbf{p}_{\max}) + \kappa_q \max(0, \mathbf{q} - \mathbf{q}_{\max}) \\
&+ \kappa_V \max(0, V_{\min} - V_{ave}) + \max(0, Cp - 500))
\end{aligned}
\tag{6.4}
$$

where κ_{all} represents the scaling factor on the constraint violation, κ_p is the scaling factor of the pressure violations, κ_q is the scaling factor on flowrate violations, κ_V is the scaling factor on water production violations, and j is the number of generations. The scaling factors are used to scale the violations to the same order of magnitude.

As stated above, the genetic algorithm was chosen because it can accommodate the discrete design variables and the non-linear system equations. A genetic algorithm is a heuristic optimization method that mimics the behavior of natural selection. It uses a population of individuals which represent different system configurations. The population is evaluated at each iteration to determine their fitness. The fittest individuals are then selected to produce the next generation of individuals. The next generation is produced by mating selected individuals. The process continues until the termination criteria are met. This termination criterion is typically specified in terms of the number of generations since the latest cost improvement. More details on genetic algorithms are available in [118].

The main downside of genetic algorithms is that their execution takes considerable amounts of computation since the cost function must be evaluated for every individual in each generation. Even with the simplifications made, the computation time for one system power level

of the PVRO system model is on the order of seconds, and the time required to compute the average water production in on the order of minutes. The genetic algorithm parameters must be carefully selected to ensure that the computation time is reasonable.

A set of design studies were conducted to select the parameters of the genetic algorithm optimization. In these design studies, the parameters of the genetic algorithm were varied for the example case of designing a 1 m^3 system in Boston, MA. Different sampling methods can be used to study these effects, such as Latin Hypercubes and one-factor-at-a-time. For these cases, the one-factor-at-a-time approach was used to gain intuition.

Table 6.9 shows the starting point for the one-factor-at-a-time sampling. Each case was run three times to ensure that the random nature of the genetic algorithm optimization isn't dominating the results. The difference in genetic algorithm performance for different population sizes is shown in Figure 6.4. As the population size increases, the overall system cost decreases but the computation requirements increase. To balance this, a population size of 60 individuals was used in the case studies and the remainder of the genetic algorithm parameter study.

Table 6.9: Starting point for genetic algorithm parameters.

Parameter	Value
Population Size	80
Elite Count	10% of Population Size
Crossover Fraction	50%
Maximum Number of Generations	100
Mutation Probability	1%

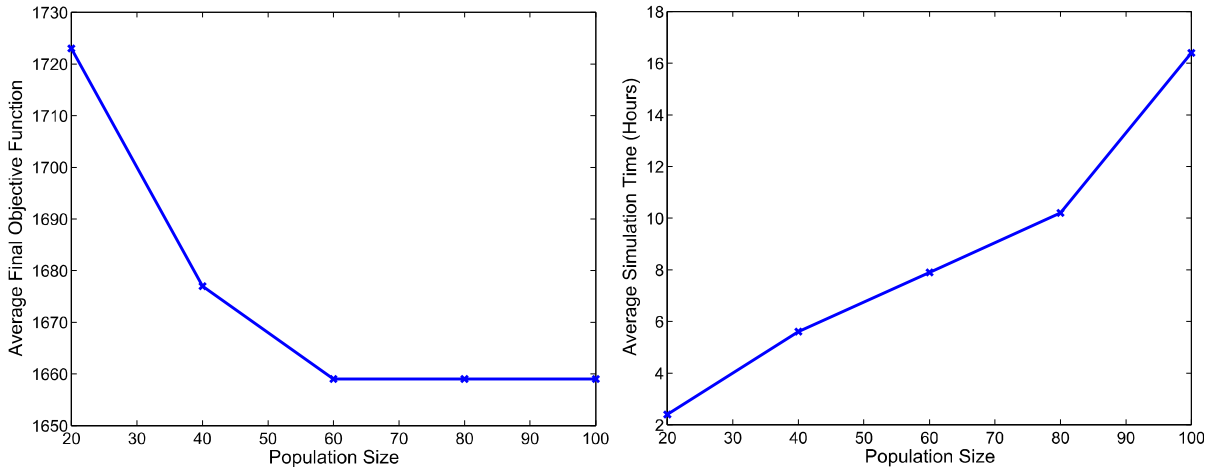

Figure 6.4: Optimization performance for different population sizes.

Similar studies were conducted for the elite count, the number of individuals that are directly transferred the next generation. The elite individuals are those that have the best fitness.

The variation in the overall cost and computation time required when the elite count is varied is shown in Figure 6.5. Based on the simulation results, an elite count of 6, or 10% of the population was chosen for the case studies and the remainder of the genetic algorithm parameter study.

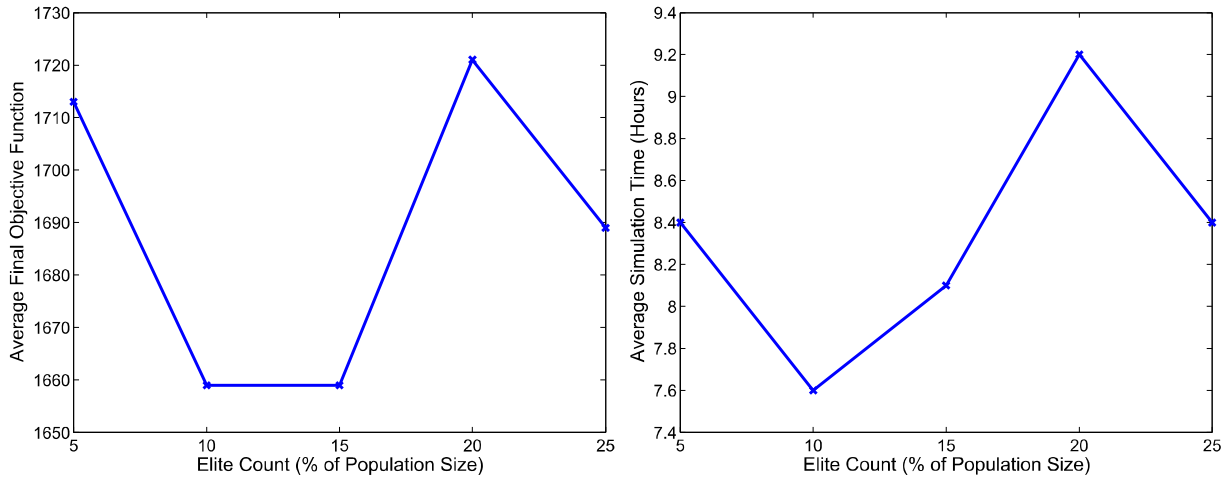

Figure 6.5: Optimization performance for different elite count.

The effect of the variation of crossover probability was also studied. The crossover probability determines the likelihood that children are produced through mating of two pairs of the previous generation. If no children are produced, the parents are directly carried into the next generation. The variation in overall system cost and computation time required when the crossover probability is varied is shown in Figure 6.7. Based on the results, a value of 0.7 was used for the modular design case studies and the remainder of the genetic algorithm parameter study.

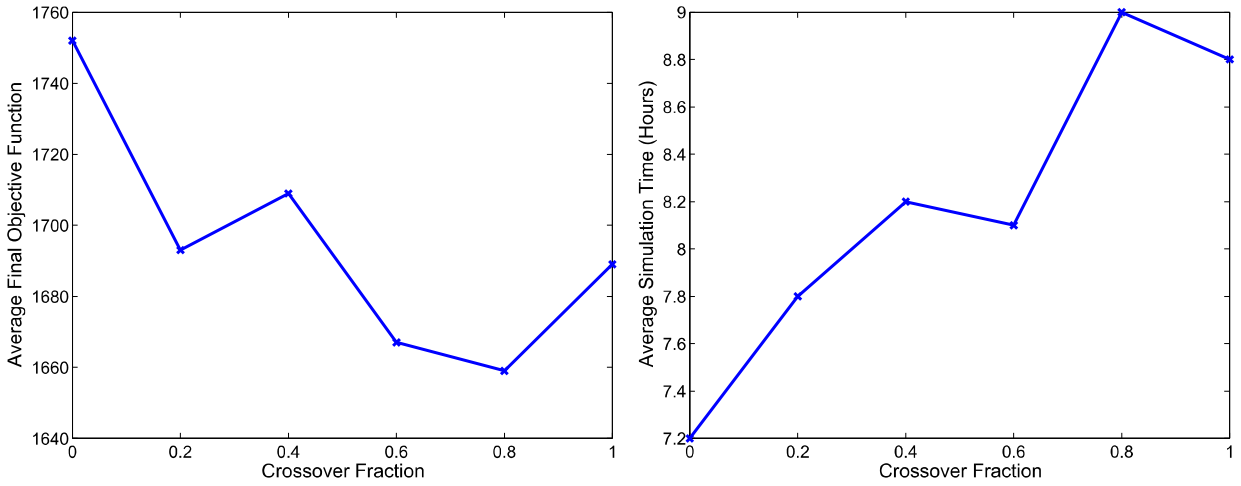

Figure 6.6: Optimization performance for different crossover fraction.

Once the children are generated, the genetic algorithm performs a mutation operation. In this operation, bits in the system representation are randomly flipped. The probability of these bits being flipped was varied to study the effect. The variation in system cost and convergence time for different probability of mutation is shown in Figure 6.7. Based on these results, a value of 2% was selected for the modular design case studies and the remainder of the genetic algorithm parameter study.

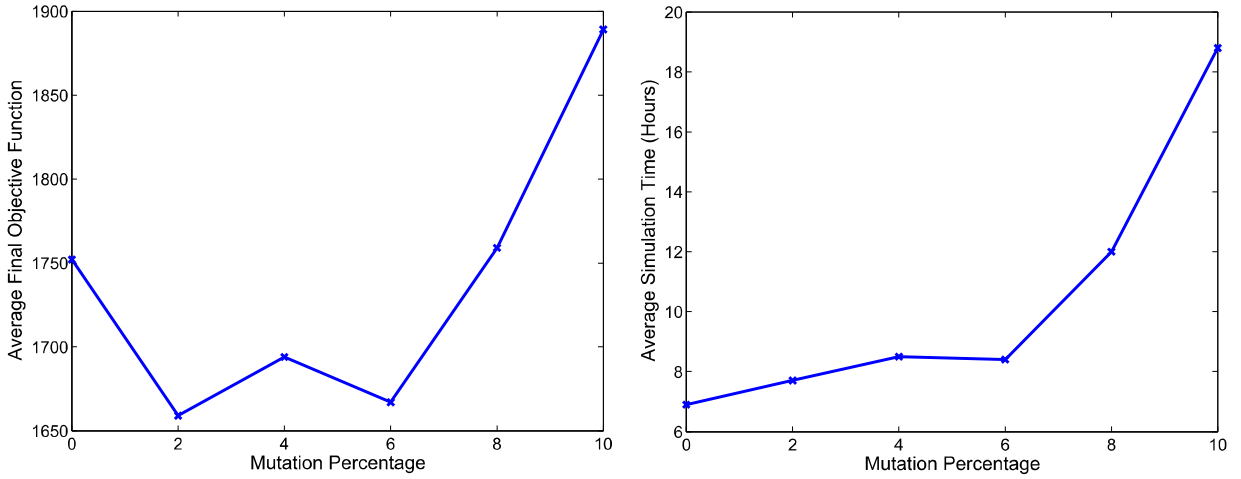

Figure 6.7: Optimization performance for different mutation percentage.

Genetic algorithms have no clear stopping point, so criteria such as the maximum number of generations and the number of generations since the last fitness function improvement are commonly used to terminate the algorithm. Here, the effect of varying the termination criteria of the number of stalled generations is studied. The results are shown in Figure 6.8. Based on these results, a value of 30 generations was selected for the modular design case studies. The final parameters selected for the modular design case studies are shown in Table 6.10.

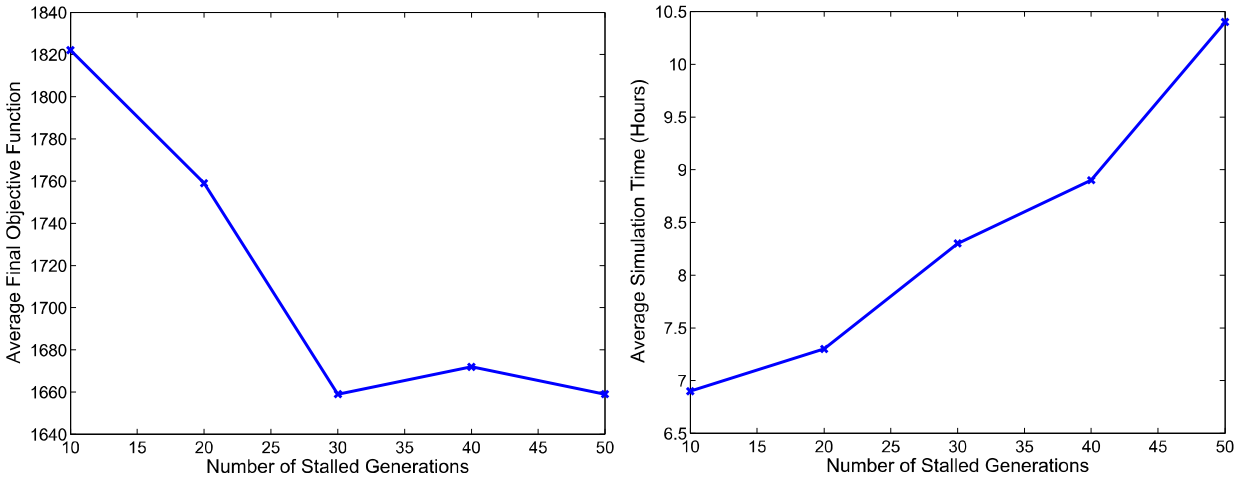

Figure 6.8: Optimization performance for different termination criteria.

Table 6.10: Parameters used for genetic algorithm in modular design studies.

Parameter	Value
Population Size	60
Elite Count	10% of Population Size
Crossover Fraction	70%
Number of Generations for Convergence	30
Maximum Number of Generations	100
Mutation Probability	2%

6.3 Optimization Results

6.3.1 Varied Location

Table 6.11 shows the results for a 1 m^3 system designed for the following locations: Albuquerque, NM, Boston, MA, Brisbane, Australia, Cape Haïtien, Haiti and Limassol, Cyprus. The configurations are similar for most locations except for Limassol, Cyprus, where an energy recovery device was excluded from the design. Energy recovery devices, especially for small-scale applications, are expensive. Cyprus has an abundant solar resource, so the power produced

by the PV panels is less expensive. As a result, the most cost-effective design is a less efficient system with more PV panels. This is not an obvious tradeoff and it would be difficult for a non-expert to capture this subtlety.

Water costs for systems designed using the modular design approach are in the range reported by other researchers developing photovoltaic reverse osmosis systems, shown in Table 3.7. The calculated water costs for the systems designed using the modular design approach are at lower end of the reported range, as expected since the system is optimized for system cost. Another factor which contributes to low water costs when compared to previously reported numbers is the dramatic reduction in the cost of installed small-scale photovoltaic systems ($\leq$5 kW_p), which dropped by \$3.40/W_p or 30% between 2000-2010 [137].

Table 6.11: Results of modular design approach for 1 m^3 systems in various locations.

System Location	System Stats	System Configuration	Component Details	
Albuquerque (Brackish Water)	**Lifetime Cost: $36668** Capital Cost: $12834 Water Cost: $3.78/$m^3$	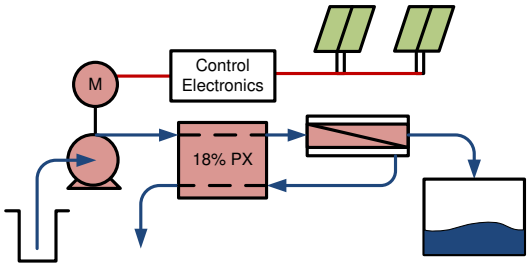	Panel Panel Mounting Motor Pump Energy Recovery Membrane	Trina Solar 225 W Panels Fixed Panels Leeson 0.5 HP Motor Procon 140 GPH Pump 18% Spectra Clark Pump 2.5" Diameter, 40" long, Applied Membranes M-B2540AHF
Boston	**Lifetime Cost: $43874** Capital Cost: $17104 Water Cost: $4.71/$m^3$	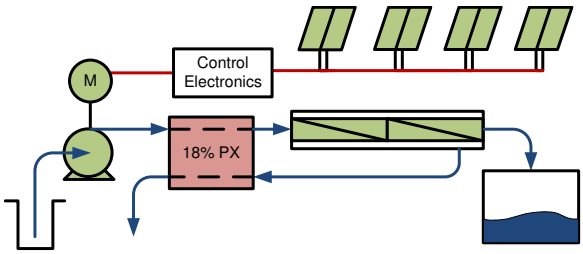	Panel Panel Mounting Motor Pump Energy Recovery Membrane	Trina Solar 225 W Panels Fixed Panels Leeson 1 HP Motor NRD PRG 10 Vane Pump 18% Spectra Clark Pump 4" Diameter, 40" long, Dow SWHRLE
Brisbane	**Lifetime Cost: $40663** Capital Cost: $15088 Water Cost: $4.41 /$m^3$	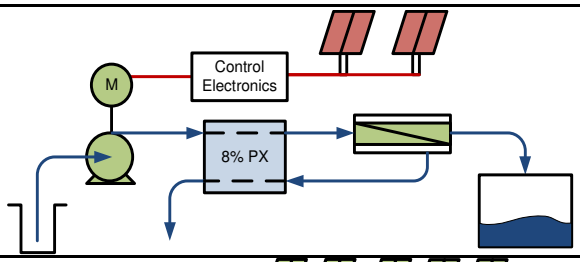	Panel Panel Mounting Motor Pump Energy Recovery Membrane	Suntech 295 W Panels Fixed Panels Leeson 1 HP Motor NRD PRG 10 Vane Pump 8% Spectra Clark Pump 4" Diameter, 40" long, Dow SWHRLE
Limassol, Cyprus	**Lifetime Cost: $39943** Capital Cost: $18324 Water Cost: $3.93/$m^3$	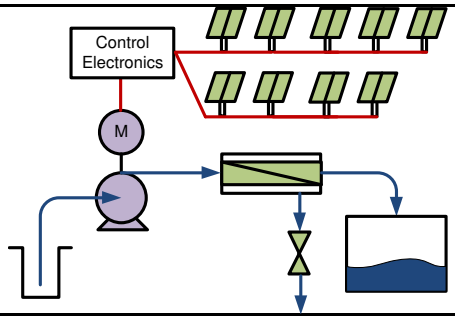	Panel Panel Mounting Motor Pump Energy Recovery Membrane	Trina Solar 225 W Panels Fixed Panels Leeson 5 HP Motor Danfoss APP 0.8 None 4" Diameter, 40" long, Dow SWHRLE
Haiti	**Lifetime Cost: $40663** Capital Cost: $15088 Water Cost: $4.03/$m^3$	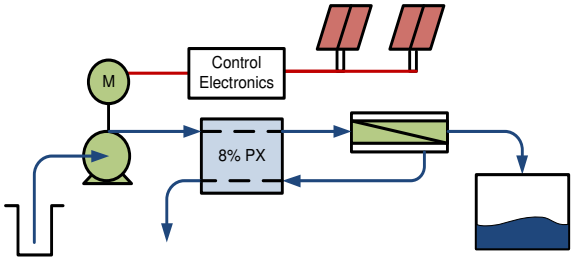	Panel Panel Mounting Motor Pump Energy Recovery Membrane	Suntech 295 W Panels Fixed Panels Leeson 1 HP Motor NRD PRG 10 Vane Pump 8% Spectra Clark Pump 4" Diameter, 40" long, Dow SWHRLE

To demonstrate both the effectiveness of the modular design approach and the location dependency, the performance of the system designed to produce an average of 1 m^3 average in Haiti was simulated in Boston. The results for this system were compared to those of the system designed for Boston. The system simulation for an average spring day is shown in Figure 6.9. The system tailored for Boston produces 1.09 m^3 of water on the spring day, while the system tailored for Haiti is only produces 0.69 m^3 of water.

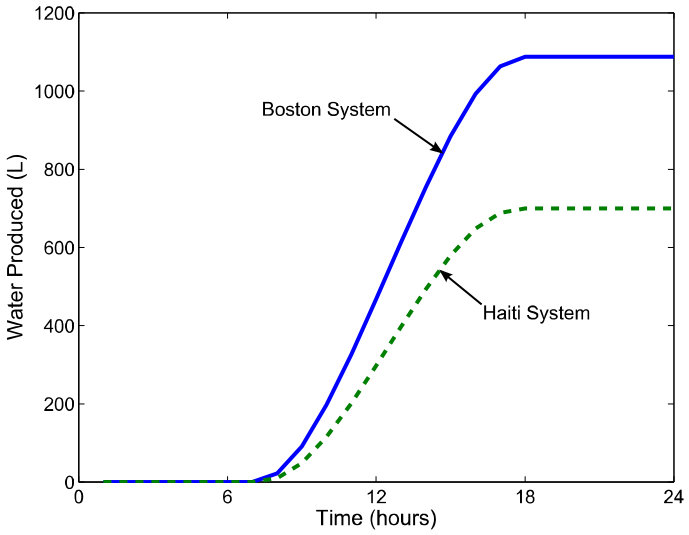

Figure 6.9: Comparison of two systems simulated in Boston.

Over the course of the year, the system optimized for Boston is able to produce 1.03 m^3 of water per day on average at a cost of \$4.71/m^3. The system optimized for Haiti produces 0.65 m^3 of water per day on average at a cost of \$6.85/m^3. The algorithm effectively designs a system for a location and demand.

6.3.2 Varied System Size

Different scale systems were designed for Boston, MA. The results for systems which produce 1 m^3, 5 m^3 and 20 m^3 of water per day are shown in Table 6.12. The system configuration becomes more complex as the water demand increases. The effect of economies of scale can be seen. For the 1m^3 system, the water cost is \$4.71/m^3. For the 20 m^3 system, the water cost decreases to \$3.01/m^3. This demonstrates the modular design algorithm is effective at designing systems of different sizes.

Table 6.12: Results of modular design approach for various size systems in Boston, MA.

System Location	System Stats	System Configuration	Component Details	
1 m^3	**Lifetime Cost: $43874** Capital Cost: $17104 Water Cost: $4.71/$m^3$	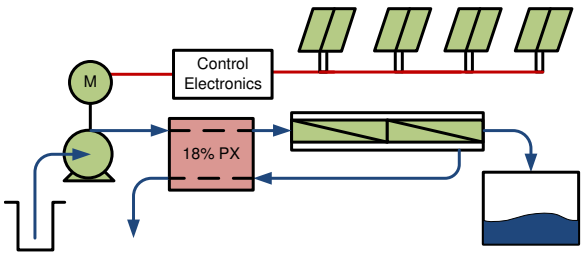	Panel Panel Mounting Motor Pump Energy Recovery Membrane	Trina Solar 225 W Panels Fixed Panels Leeson 1 HP Motor NRD PRG 10 Vane Pump 18% Spectra Clark Pump 4" Diameter, 40" long, Dow SWHRLE
5 m^3	**Lifetime Cost: $160672** Capital Cost: $49562 Water Cost: $3.45 /$m^3$	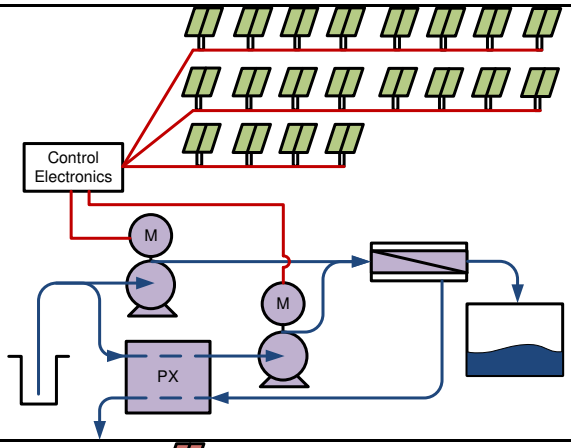	Panel Panel Mounting Motor Pump Energy Recovery Membrane	Trina Solar 225 W Panels Fixed Panels 2 x Leeson 5 HP Motor 2 x Danfoss APP 2.5 ERI PX-30S 8" Diameter, 40" long, Dow SWHRLE
20 m^3	**Lifetime Cost: $547279** Capital Cost: $120761 Water Cost: $3.01/$m^3$	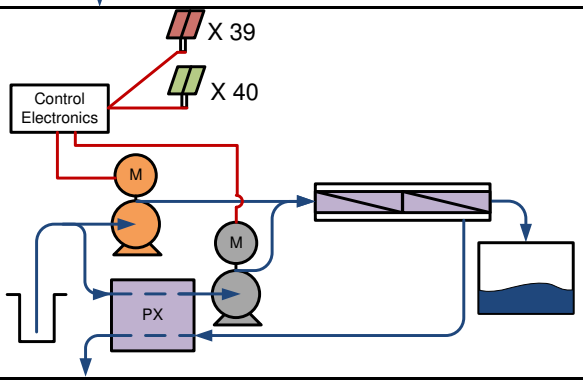	Panel Panel Mounting Motors Pumps Energy Recovery Membrane	39 x Suntech 295 W Panels 40 x Trina Solar 225 W Panels Fixed Panels Leeson 15 HP Motor, Leeson 10 HP Motor Danfoss APP 3.5 Danfoss APP 2.5 Flowserve DWEER 2 x 8" Diameter, 40" long, Dow SW30XLE-400i

6.3.3 Cost Sensitivity

The cases conducted above assume a discount rate of 4% and a system life of 25 years. These factors can vary depending on the economic climate and the maintenance abilities of the communities in which the systems are implemented. To show the trends in water cost due to these factors, a sensitivity study was conducted. The results for this study are shown in Table 6.13. For the baseline case of 4% interest and a 25 year system life, the overall cost of water produced by the system is \$4.71/m^3. At the other end of the spectrum, a system that has an 8% interest rate and lasts 10 years produces water at a cost of \$7.23/m^3, a cost increase of over 50%. This shows that the choosing the correct values is critical for accurate cost modeling. Future

work could implement the modular design approach with uncertainty in these two cost parameters.

Table 6.13: Sensitivity of water cost for various interest rates and system lifetimes for 1m^3 Boston, MA system.

		Interest Rate		
		4%	**6%**	**8%**
System Life	**25 Years**	\$4.71/m^3	\$5.13/m^3	\$5.59/m^3
	20 Years	\$4.99/m^3	\$5.40/m^3	\$5.84/m^3
	15 Years	\$5.48/m^3	\$5.87/m^3	\$6.28/m^3
	10 Years	\$6.47/m^3	\$6.84/m^3	\$7.23/m^3

6.3.4 Varied Inventory

The modular design approach can also be used by companies to determine if new components will make an impact on the overall market. In order to validate that claim, a case study was conducted with a new component added to the inventory. The new component is a pressure exchange device, the RO-Boost, manufactured by Danfoss. It operates on the same principles as the Clark Pump manufactured by Spectra Watermakers, and has a 13% recovery ratio. Based on personal communication, this device would likely be priced at \$2499 per unit.

This expanded inventory was used to design a system a new 1 m^3 PVRO system for Cyprus. With the original inventory, the most cost effective system design did not include an energy recovery device, see Table 6.11. The total lifetime cost of the system using the original inventory is \$39943 and the water cost is \$3.92/m^3. When the expanded inventory is used, the new design includes the Danfoss energy recovery device. The total lifetime cost of the new configuration is \$38,139 and the total water cost is \$3.87/m^3. The configurations are shown in Figure 6.10.

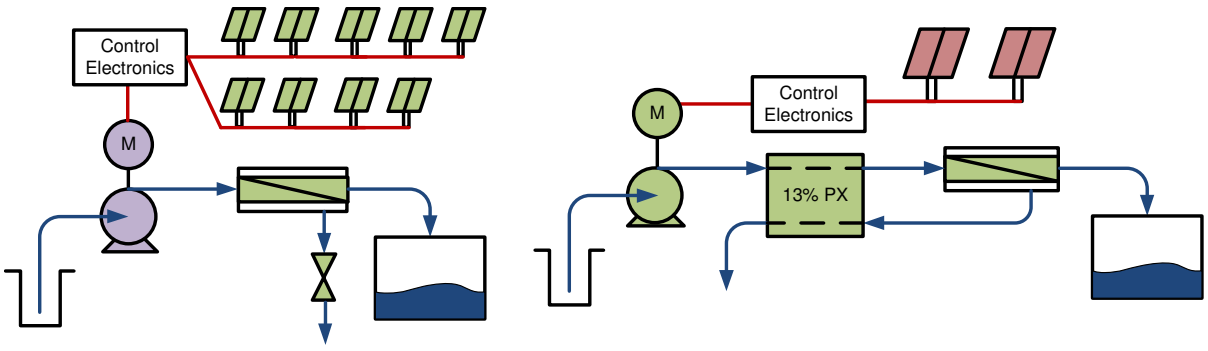

Figure 6.10: System designed in Cyprus using original inventory (left) and expanded inventory (right).

6.3.5 Convergence Properties

The case study results show that the modular design approach is effective when used to configure systems for different locations and different water demand requirements. The computation time and convergence properties of process must also be considered. Since the proposed solution is meant for design of PVRO systems by non-experts, all cases were conducted on a regular desktop computer containing an Intel 2.8 GHz Dual Core processor and 4 GB of RAM. The total CPU time required for an individual case ranged from 5.2 hours to 32.7 hours, with an average time of 16.1 hours. The designs are not generated instantaneously, but total computation time is not unreasonable.

The convergence properties of the genetic algorithm optimization were also studied. The genetic algorithm optimization process is heuristic, so there is no guarantee that the optimizer will converge to a minimum. Convergence was studied by repeating the 1 m^3 system optimization for Boston 10 times. A sample convergence pattern for one of these cases can be seen in Figure 6.11. In this case, the final system configuration is reached by a path which includes infeasible system configurations that don't meet the water production requirements. In the end, the optimizer determines a low-cost feasible solution.

In the 10 cases conducted, the optimization converges to the same, lowest-cost configuration 7 times. This lowest cost solution has an equivalent annual cost of $2,809 or a net present cost of $43,874. The cases that didn't converge to this configuration also had low overall costs, with the maximum case having an equivalent annual cost of $2,876 and a net present cost of $44,923.

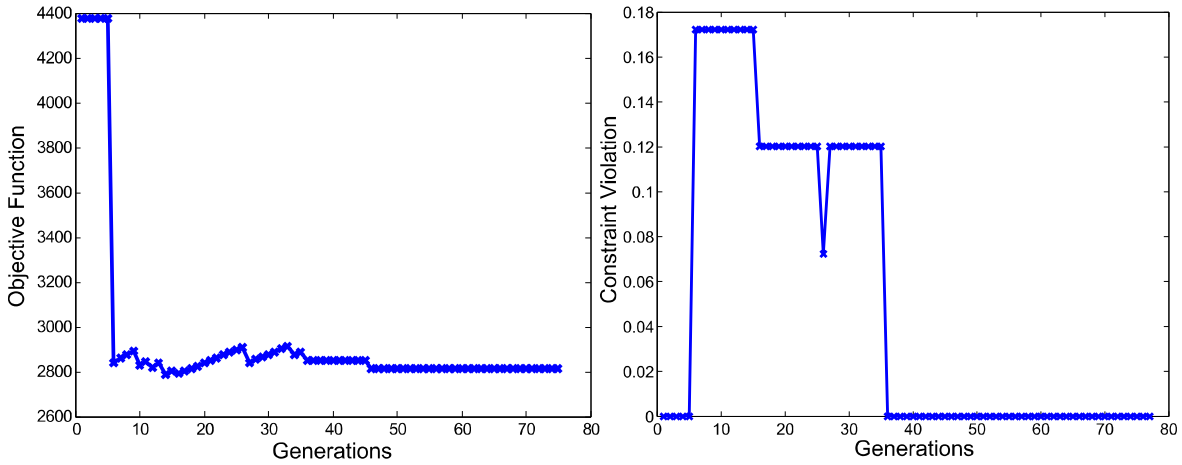

Figure 6.11: Convergence of PVRO design for 1 m^3 system in Boston.

6.4 Summary

This section presented case studies for the design of PVRO systems using the modular design approach. The approach uses filters to limit the size of the design space and then uses a genetic algorithm to optimize the system design. The parameters of the genetic algorithm are selected based on a study presented in this section. It is shown that the approach is able to tailor systems for a wide range of locations and water demands from a large system inventory. In addition, it is shown that the approach is able to repeatedly generate low-cost configurations for a given application.

CHAPTER

7

ACCOMMODATING VARIATIONS

The previous chapter demonstrated that the modular design approach can be used to configure PVRO systems under deterministic environmental conditions. However, the solar radiation and water demand vary considerably from year-to-year and a PVRO design must meet the water demand in spite of such uncertainty. This chapter presents two approaches to accommodate these variations during the design phase, and case studies to evaluate their performance.

7.1 Problem Description

In this chapter, the variations in the water demand and solar insolation are incorporated into the design. The overall design goal remains the same: determine the PVRO system with the lowest lifetime cost that meets the water demand of an individual location. When considering these variations, the sequence of events and the water storage becomes important. The design requirements are slightly different for the problems in this chapter. Instead of meeting an average daily water production requirement, the water demand must be met with a specified probability. The problem statement for this case becomes:

$$
\begin{aligned}
&\text{minimize } f(\mathbf{x},\mathbf{y}) \\
&\text{subject to } \mathbf{g}(\mathbf{x},\mathbf{y}) = 0 \\
&\qquad LOWP < LOWP_{\max} \\
&\qquad C_{\text{tank}} < 500\text{ppm} \\
&\qquad \mathbf{p} < \mathbf{p}_{\max} \\
&\qquad \mathbf{q} < \mathbf{q}_{\max} \\
&\qquad \mathbf{y}_{\min} \le \mathbf{y} \le \mathbf{y}_{\max} \\
&\qquad \mathbf{x} \in \{0,1\} \\
&\qquad \mathbf{y} \in I
\end{aligned}
\tag{7.1}
$$

where C_{tank} represents the concentration of the desalinated water in the storage tank, and *LOWP* represents the loss-of-water probability as given by:

$$LOWP = \frac{\#\,hours, \text{water not supplied}}{total\,\#\,hours} \tag{7.2}$$

Details of the *LOWP* calculation for the different design methods are presented in the following section.

The PVRO component inventory used for these design problems is identical to the inventory specified in section 6.3.3. However, since the sequence in which the events occur is important, the size of water storage plays a large role, so this cost is considered separately. The overall cost of water storage varies greatly since these units are usually constructed locally for each system. The assumed costs used in these studies are from approximated tank costs for developing world applications and are listed in Table 7.1 [138].

Table 7.1: Water tank details.

Tank Volume	Cost
1 m^3	$200
2 m^3	$300
5 m^3	$600
10 m^3	$1000
20 m^3	$1600
40 m^3	$3000
60 m^3	$5000

Bacterial contamination and algal growth of stored water is a common concern. To alleviate these effects; water storage will be limited to 10 times the average daily water consumption. In addition, it is assumed that the water is chlorinated to maintain drinkability. The cost of the post-treatment chlorination system is factored into the infrastructure costs described in section 5.5.2.

7.2 Stochastic Modeling Approach

The first method evaluates the PVRO systems using a time-series simulation. This section describes these simulation models.

7.2.1 Simulation Model

The time-series model used to evaluate the loss-of-water probability for a given PVRO system is shown in Figure 7.1. In this model, the graph method described in section 5.3 is used to

develop a simple relationship for the system production as a function of input power. This relationship is used to determine the loss-of-water probability for a given water demand and solar input profile.

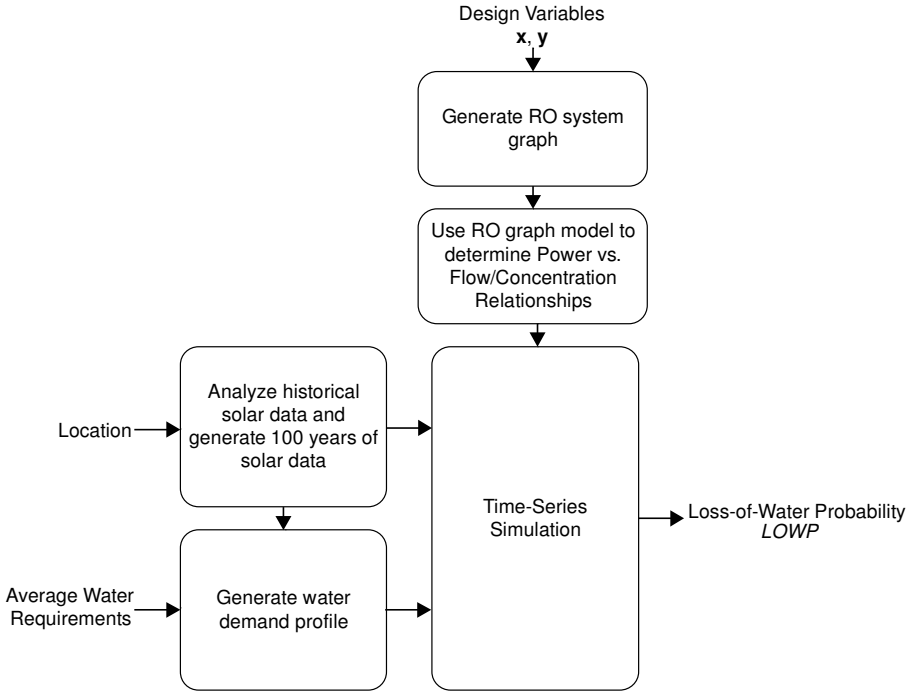

Figure 7.1: Stochastic modeling approach.

The flowrate and concentration of the water being produced by the PVRO system are determined at each time step. These values are used to update the volume of stored water as follows:

$$V_t = V_{t-1} + \frac{(Q_t + Q_{t-1}) - (D_t + D_{t-1})}{2}\Delta t \tag{7.3}$$

where Q_t is the water being produced by the PVRO system at time t, and D_t is the water demand at time t and Δt is the time step length. A one hour time-step is used for all simulations. The volume in the tank is limited by the tank capacity, V_{tank} as follows:

$$0 \le V_t \le V_{\text{tank}} \tag{7.4}$$

If the tank is empty, the water demand is not met during the time-period.

Since the salt concentration of the produced by the system varies with the power input, the salt concentration in the water tank must also be updated at each step as follows:

$$C_{\text{tank,t}} = \begin{cases} \dfrac{V_{t-1}C_{\text{tank},t-1} + (Q_t + Q_{t-1})(C_{prod,t} + C_{prod,t-1})\Delta t / 4}{V_{t-1} + (Q_t + Q_{t-1})/2}, V_{t-1} + (Q_t + Q_{t-1})/2 > 0 \\ 0, \text{ otherwise} \end{cases} \quad (7.5)$$

This expression assumes that all the water is withdrawn from the tank at the end of the time period. If the concentration in the tank exceeds the maximum allowable value of 500 ppm, the water quality limit set by the World Health Organization [130], the water demand is not met.

The system is simulated over a 100-year time period. This length of simulation was chosen because it has been shown that long-term simulations are required to provide reliable loss-of-load probabilities for photovoltaic systems [139]. The models used to generate the solar data and water demand data for the 100-year time period are described below. To initialize the simulation, the water tank is assumed to be half-full and the water concentration is assumed to be 250 ppm. Since simulations are run for long time periods, the initial state of the water in the tank has little effect.

Due to the seasonal water demand and solar energy cycles, the PVRO system is only seriously stressed during one period of the year. Therefore, the analysis can be simplified by only considering this time period. A series of case studies are conducted only considering the most critical month and are compared to the results using the full-year analysis.

7.2.2 Solar Radiation Model

Solar data is available for any location over a 21-year time horizon from the NASA Surface Meteorology and Solar Energy Database [8]. Unfortunately, data from this time period is not sufficient to ensure a loss-of-water probability lower than 0.01. In order to simulate the system performance over a longer time period, representative solar data is generated. A first-order Markov chain model is used to generate the solar data is based on a method outlined by Richardson [140]. As shown in Figure 7.2, the model has two states: mostly sunny or mostly cloudy days. The characteristics of this model can be extracted from solar insolation data.

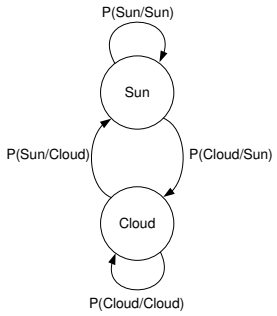

Figure 7.2: Markov model of solar radiation.

The sunny and cloudy days have distinctly different levels of solar insolation. The mean insolation values for sunny and cloudy days over a 21-year time horizon in Boston, MA are shown in Figure 7.3. A first-order Fourier series is used to smooth the seasonal solar insolation for the sunny and cloudy days as follows:

$$\bar{H}_{sun}(d) = \frac{a_{0,sun}}{2} + a_{1,sun}\cos\frac{2\pi d}{365} + b_{1,sun}\sin\frac{2\pi d}{365} \tag{7.6}$$

$$\bar{H}_{cloud}(d) = \frac{a_{0,cloud}}{2} + a_{1,cloud}\cos\frac{2\pi d}{365} + b_{1,cloud}\sin\frac{2\pi d}{365} \tag{7.7}$$

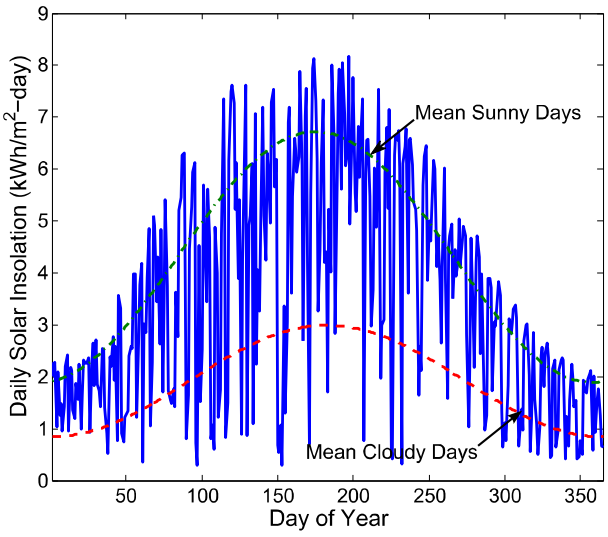

Figure 7.3: Solar insolation profile for Boston, MA.

One of the characteristics that define the Markov chain model is the state transition probabilities. The probabilities are determined by counting the number of transitions over the 21-

year history for the site. These transition probabilities vary over the course of the year and were fit using a first-order Fourier series:

$$P(d) = \frac{a_{0,P}}{2} + a_{1,P}\cos\frac{2\pi d}{365} + b_{1,P}\sin\frac{2\pi d}{365} \tag{7.8}$$

The probability of transitioning from a sunny day to a sunny day and a cloudy day to a cloudy day for Boston, MA is shown in Figure 7.4. The other transition probabilities are determined as follows:

$$\begin{aligned} P(sun/cloud) &= 1 - P(cloud/cloud) \\ P(cloud/sun) &= 1 - P(sun/sun) \end{aligned} \tag{7.9}$$

where *P(cloud/cloud)* is the probability of having a cloudy day after a cloudy day, *P(sun/cloud)* is the probability of having a sunny day after a cloudy day, *P(sun/sun)* is the probability of having a sunny day following a sunny day, and *P(cloud/sun)* is the probability of having a cloudy day after a sunny day.

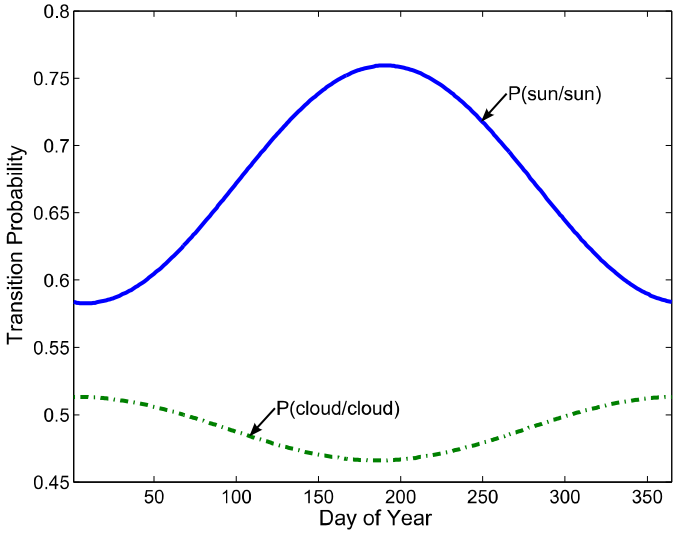

Figure 7.4: Transition probabilities for Boston, MA.

The characteristics of the solar insolation time series are determined from the Markov chain characteristics. The first step reduces the measured solar insolation sequence to residual elements. The residual is calculated as follows:

$$\chi(d) = \begin{cases} \dfrac{H(d) - \bar{H}_{sun}(d)}{\sigma_{sun}(d)}, X(d) = sun \\ \dfrac{H(d) - \bar{H}_{cloud}(d)}{\sigma_{cloud}(d)}, X(d) = cloud \end{cases} \tag{7.10}$$

where $H(d)$ is the measured solar insolation on day d, $\bar{H}_{sun}(d)$ is the mean solar insolation on day d when the day is sunny, $\sigma_{sun}(d)$ is the standard deviation of the solar insolation on day d when the day is sunny, $\bar{H}_{cloud}(d)$ is the solar insolation on day d when the day is cloudy, $\sigma_{cloud}(d)$ is the standard deviation of the solar insolation on day d when the day is cloudy, and $X(d)$ is the state of day d. This translation results in a stationary, zero-mean, unit variance sequence. An example residual sequence for Boston, MA is shown in Figure 7.5.

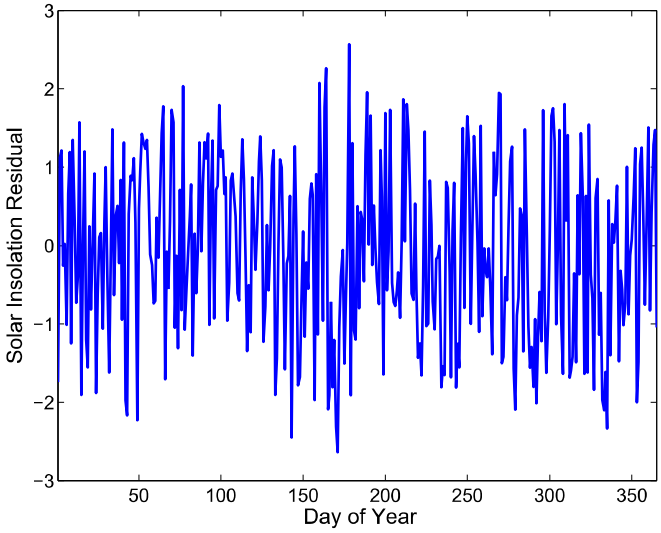

Figure 7.5: Solar insolation residual for Boston, MA.

A general model is developed from the properties of the solar insolation residuals. Figure 7.6 shows the autocorrelation of the solar insolation residuals for Boston, MA. From the figure, it is evident that there is statistically significant correlation between the value of the residual from one day to the next. As such, a first-order autoregressive model is used to represent the residuals:

$$\chi(i+1) = a\chi(i) + b\varepsilon(i) \tag{7.11}$$

where a is given by the value of the first-order lag in the autocovariance function, b is given by:

$$b = 1 - a^2 \tag{7.12}$$

and $\varepsilon(i)$ is unit variance, white noise. For Boston, MA, a takes on a value of 0.19 and b takes on a value of 0.96. These values can be calculated for any location by analyzing the solar insolation sequence.

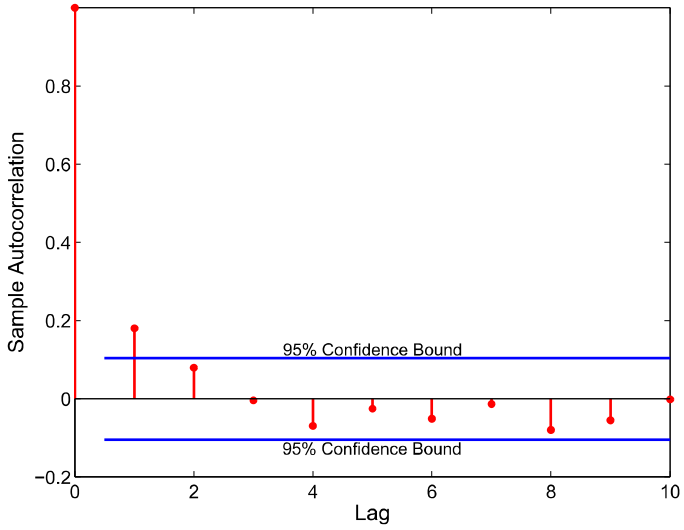

Figure 7.6: Solar insolation residual autocorrelation for Boston, MA.

Using the characterization of the solar insolation above, the simulated solar insolation sequence for the PVRO system is generated using the following process:

1. The initial state (sunny or cloudy) is generated based on the overall day state probability on January 1.
2. The sequence of day states is generated using the Markov chain model and transition probabilities.
3. The sequence of residuals is generated using the first-order autoregressive model in equation (7.11).
4. The residuals are translated back to daily solar insolation values depending on the state of the day, as given by:

$$H(i) = \begin{cases} \sigma_s \chi(i) + \bar{H}_s(i), X(i) = s \\ \sigma_c \chi(i) + \bar{H}_c(i), X(i) = c \end{cases} \tag{7.13}$$

5. The hourly insolation sequences are then generated from the daily solar insolation using the method specified in 5.1.1.

Figure 7.7 shows an example of a generated solar insolation sequence for Boston, MA. The characteristics of the generated sequence match the solar characteristics of the measured characteristics of the solar insolation shown in Figure 7.3.

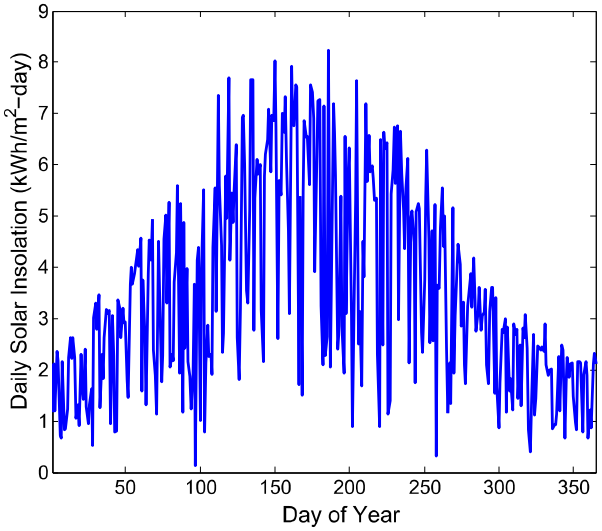

Figure 7.7: Generated solar insolation sequence for Boston, MA.

7.2.3 System Demand Model

Researchers have shown that solar radiation is related to water demand, but their models typically include many climatic variables unknown for the locations being studied here [141]. It is also expected that there may be some coupling between the amount of water stored and the water demand where residents would ration water usage when supply is low. However, given the data available, estimating and accounting for this effect is not possible here but can be considered in future work.

Due to the lack of climatic variables that are used in many water demand models, a system demand model was determined using a process similar to that used to determine the solar radiation. The demand on a water system varies over the course of the year. In the water demand model developed here, the water demand is assumed to consist of a deterministic seasonal component and a random component as shown:

$$V_d(d) = V_{d,seas}(d) + V_{d,rand}(d) \tag{7.14}$$

The seasonal component is determined by fitting a Fourier series to the data:

$$V_{d,seas}(d) = \frac{a_{0,V_d}}{2} + \sum_{i=1}^{k}\left[a_{i,V_d} \cos\left(\frac{2\pi i d}{365}\right) + b_{i,V_d} \sin\left(\frac{2\pi i d}{365}\right)\right] \tag{7.15}$$

To analyze the variations in water demand, data was solicited from the Massachusetts Water Resources Authority. Data was obtained for 2005-2010 and the average value was fit with a Fourier series to determine the seasonal component. Since only the first harmonic had a significant contribution, higher order terms were ignored. The 2005 water demand and the calculated seasonal component are shown in Figure 7.8.

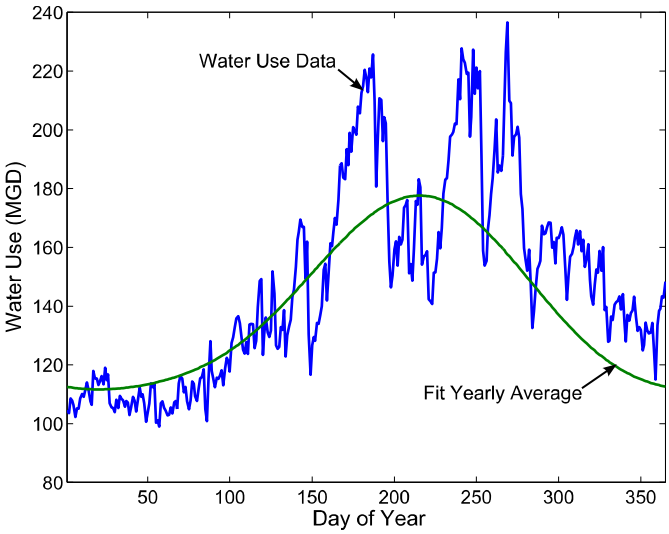

Figure 7.8: Water use and yearly average in Boston, MA.

The residuals of the water use data were calculated using the following relationship:

$$\chi_{demand}(d) = \frac{D(d) - \bar{D}(d)}{\sigma_D(d)} \tag{7.16}$$

where $D(d)$ is the measured water demand on day d, $\bar{D}(d)$ is the mean demand on day d, $\sigma_D(d)$ is the standard deviation of the demand on day d. Since the water demand is taken relative to the yearly average, regardless of the state of the day, the solar radiation residual is calculated without regard of the day state as follows:

$$\chi_{solar} = \frac{H(d) - \bar{H}(d)}{\sigma_H(d)} \tag{7.17}$$

where $\bar{H}(d)$ is mean solar radiation on day d, and $\sigma_H(d)$ is the standard deviation of the solar radiation on day d.

The residuals of the water demand and solar insolation for 2005 are shown in Figure 7.9. Periods of high solar insolation often coincide with periods of high water use. This suggests that the water demand model should depend on the level of solar insolation. Therefore, both the water residual autocorrelation and cross-correlation between the water demand and solar insolation are examined.

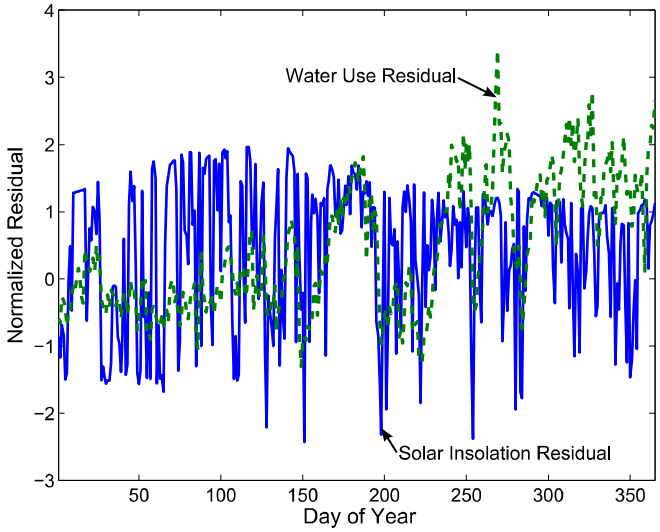

Figure 7.9: Normalized water demand and solar insolation residuals.

The autocorrelation of the water demand residuals can be seen in Figure 7.10. Statistically significant correlation between the values of the residuals from one day to the next is evident. This indicates that an autoregressive term should be included in the water demand model.

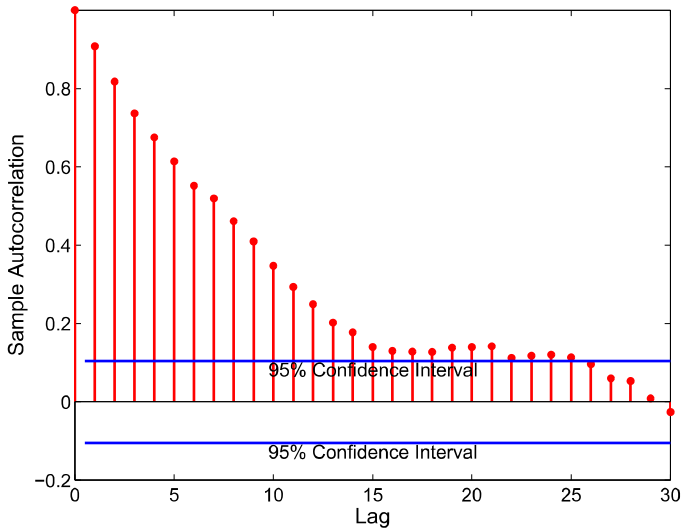

Figure 7.10: Water demand residual autocorrelation.

The cross-correlation function between the solar insolation and the water demand is shown in Figure 7.11. This indicates evidence of a lagged relationship between the solar insolation and the water demand. However, since each of the sequences is autocorrelated, this cross-correlation may be misleading. To determine if the signals are correlated, each signal is pre-whitened [142].

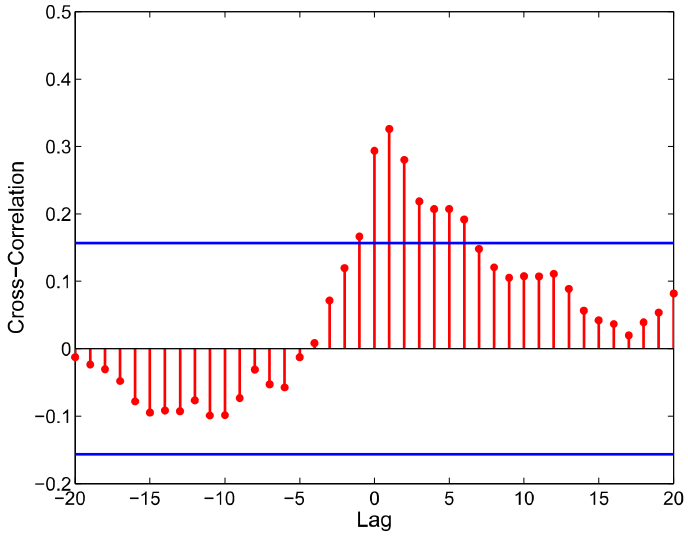

Figure 7.11: Cross-correlation between solar insolation and water demand residuals.

The water demand and solar insolation sequences are pre-whitened using the simple first-order filter:

$$Y'(d) = Y(d) - \alpha Y(d-1) \tag{7.18}$$

where α is the first order lag of the solar insolation autocorrelation function. The autocorrelation of the whitened solar insolation function is shown in Figure 7.12. The only statistically significant occurs at a lag of 0, indicating that the resulting signal is nearly white.

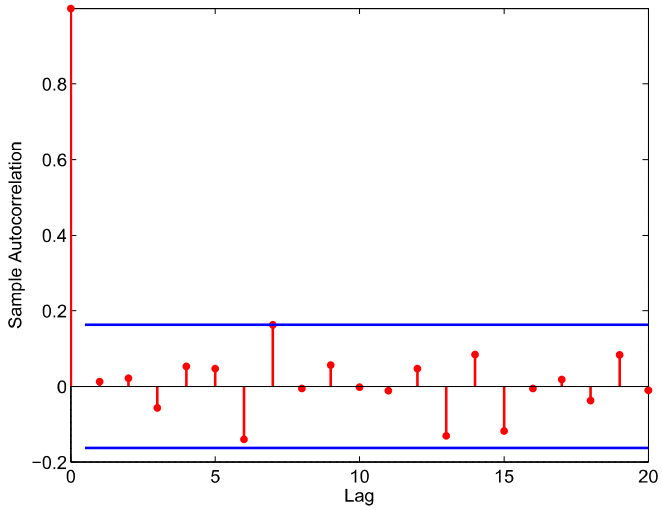

Figure 7.12: Autocorrelation of whitened daily solar insolation sequence.

The cross-correlation of the two whitened signals, see Figure 7.13, shows that a correlation exists between the solar insolation and the water demand. Significant correlations exist at lags of 0 and 1. Based on these results, different models are fit to the water demand data.

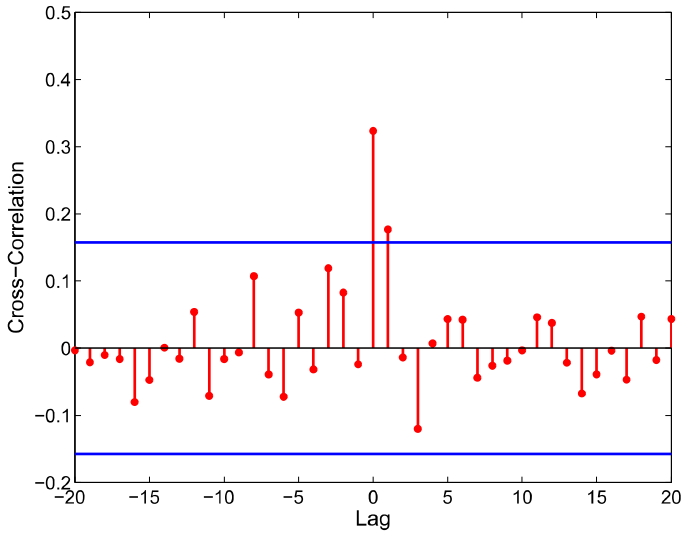

Figure 7.13: Whitened cross-correlation between solar radiation and water use.

The variable component of demand is modeled using an autoregressive distributed lag system that depends on current and previous values of the solar insolation residuals as well as the previous values water use:

$$V_{d,rand}(d) = \sum_{i=1}^{m} \alpha_i V_{d,rand}(d-i) + \sum_{i=0}^{n} \beta_i \left[H(d-i) - \overline{H}(d-i) \right] + \alpha_0 + u(d) \tag{7.19}$$

where $u(d)$ is a noise input. The coefficients α and β are determined by fitting the data. Table 7.2 shows testing results of three different model configurations. The tests show that there is only a small amount of accuracy gained by including a lag input for the solar insolation. As a result, the final model used is given by:

$$V_{d,rand}(d) = \alpha_1 V_{d,rand}(d-1) + \beta_0 \left[H(d) - \overline{H}(d) \right] + \alpha_0 + u(d) \tag{7.20}$$

The coefficients are selected for each season and the values used in simulation are shown in Table 7.3. The agreement between the model and the measured data is shown in Figure 7.14.

Table 7.2: Water demand models tested.

Case	Conditions	MSE	R^2	Chi-Squared Value
1	m=0, n=0	199.6	0.840	0.369
2	m=1, n=0	121.6	0.901	0.251
3	m=1, n=1	121.1	0.903	0.248

Table 7.3: Demand model coefficients.

Coefficient	Jan 1 – April 30	May 1 – Aug 31	Sept 1 – Dec 31
α_0	-0.169	-1.184	-0.198
α_1	0.982	0.828	0.859
B_0	2.41×10^{-4}	3.46×10^{-3}	1.63×10^{-3}

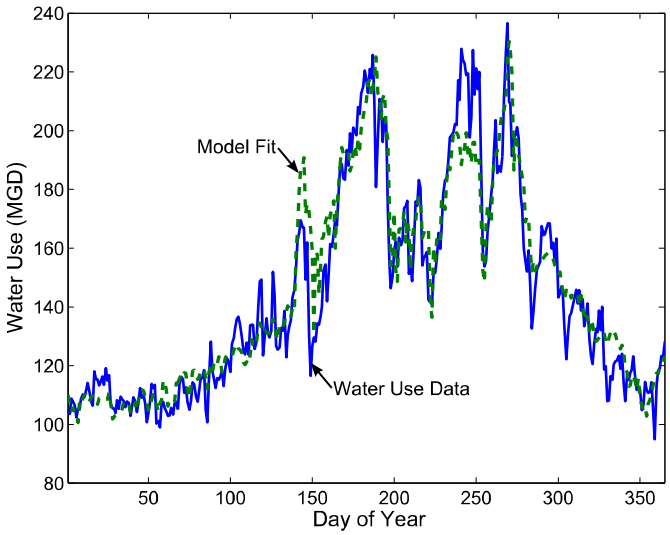

Figure 7.14: Water use and the model fit.

The model developed above is tailored for Boston, but the general model representation can be used to develop models for other locations. Ideally, demand data is available for analysis at every location to allow for estimation of the model coefficients. Unfortunately, this is not always the case. By making the assumption that the relationship between water demand and solar insolation is the same in other locations, the demand model can be scaled to determine the water demand for other locations and system sizes. The demand scaling factor is given by:

$$\phi = \frac{a_{0,V_d}}{2V_{d,ave}} \tag{7.21}$$

where $a_{0,Vd}$ is the Fourier coefficient for the analyzed water data, and $V_{d,ave}$ is the average water demand for the case of interest. With the scaling factor, the demand for the individual application is given by:

$$V_{d,app}(d) = \phi V_d(d) = \phi V_{d,seas}(d) + \phi V_{d,rand}(d) \tag{7.22}$$

The above analysis provides the amount of water used over the course of a day. However, a shorter time step is needed to determine if the PVRO system is able to instantaneously meet the water demand. All cases considered here use an hourly time-step to determine system performance. An average daily water use profile was developed based on [141]. The average profile for a small family, shown in Figure 7.15, has usage peaks in the morning and evening. For simulation, this hourly profile is scaled based on the daily water demand as follows:

$$V_{d,hour}(d,h) = V_{d,app}(d)\frac{V_{d,base}(h)}{\int_0^{24} V_{d,base}(h)\,dh} \tag{7.23}$$

where $V_{d,base}(h)$ is the baseline hourly water demand specified in Figure 7.15.

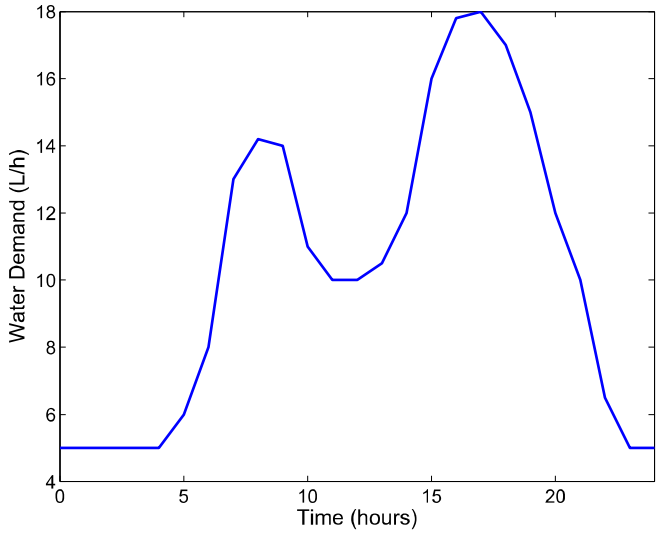

Figure 7.15: Assumed hourly water demand profile.

7.3 Stochastic Modeling Case Studies

A series of case studies were conducted to test the stochastic modeling approach and to demonstrate the effect of various loss of water probabilities. In these case studies, a PVRO system capable of providing an average water production of 1 m^3 in Boston, MA, was designed. Two sets of studies are conducted: one that considers the entire year and one that only considers the month during which the system is most stressed.

7.3.1 Full Year Simulations

In the full-year simulations, the stochastic solar radiation model and water demand model described above are used to generate typical profiles for 100 years. The method described in section 7.2.1 is used to analyze the system loss-of-water probability. The inventory specified in section 6.3.3 is used to configure the lowest lifecycle cost system. As in the deterministic case studies, a system lifetime of 25-years and an interest rate of 4% are assumed.

Cases are run for varying loss-of-water probabilities to illustrate the economic impact of more reliable PVRO systems. Designs are generated for loss-of-water probabilities ranging from

0.01% to 10%. A Pareto plot of the loss-of-water probability versus the resulting lifetime PVRO system costs is shown in Figure 7.16. Different methods can be used in multi-objective optimization to generate Pareto plots. Here, the plot is generated by specifying the required loss of water probability and optimizing a system to meet the requirement. It is evident as probability of meeting demand increases, so does system cost. Here, the overall expense increases by almost 30%. The additional expense for higher reliability may not be justified in some locations if there are other backup water options available, so the appropriate level of reliability is also location dependent. As the higher loss of water probabilities are reached, the Pareto plot levels off. This occurs due to constraints of the discrete inventory. As the loss-of-water probability increases, the systems become smaller and there are fewer components and subsystems which can be decreased or eliminated while meeting the system requirements.

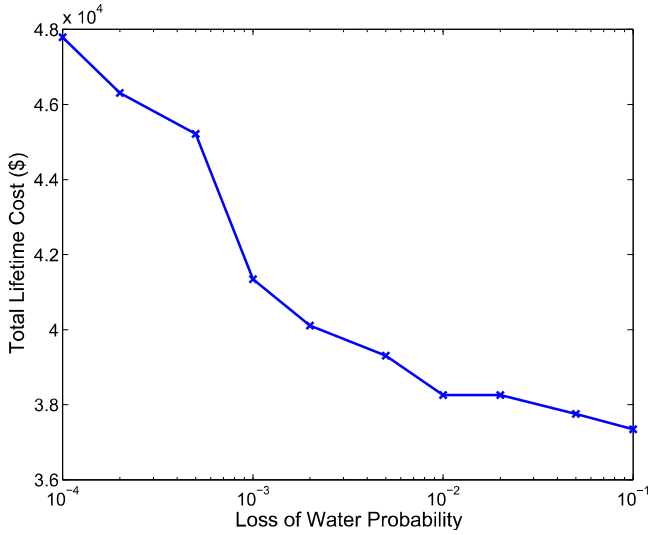

Figure 7.16: Pareto plot of lifetime system cost versus loss-of-water probability.

Table 7.4 details system configurations resulting from different loss-of-water probability constraints. As the loss of water probability increases, the overall system cost and complexity decrease. For the low probability levels, the system configurations are different. The inventory has a limited number of small-scale energy recovery devices. The small-scale energy recovery devices in the inventory are unable to provide the required flowrates to meet the demands due to the component operational limits and are not included in the final system configuration as a result. For the remaining configurations, the number of membranes and PV panels decrease as the probability increases, resulting in lower system costs.

Table 7.4: Results of modular design approach for 1 m^3 systems with various LOWP.

Loss of Water Probability	System Stats	System Configuration	Component Details	
0.01%	**Lifetime Cost: $47788** Capital Cost: $23563 Average Cost of Water: $5.24/$m^3$	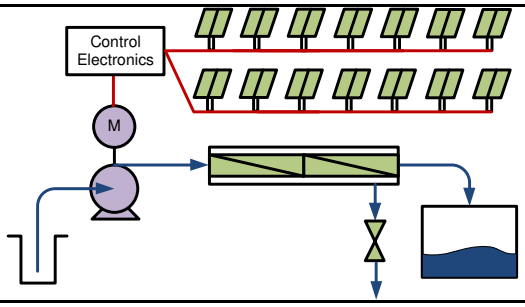	Panel Panel Mounting Motor Pump Energy Recovery Membrane Water Tank Size	Trina Solar 225 W Panels Fixed Panels Leeson 5 HP Motor Danfoss APP 1.8 None 4" Diameter, 40" long, Dow SWHRLE 10m^3
0.1%	**Lifetime Cost: $41344** Capital Cost: $17247 Average Cost of Water: $4.53/$m^3$	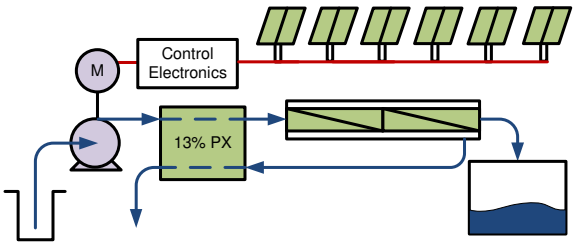	Panel Panel Mounting Motor Pump Energy Recovery Membrane Water Tank Size	Trina Solar 225 W Panels Fixed Panels Leeson 1 HP Motor NRD PRG 10 Vane Pump 13% Danfoss RO Boost 4" Diameter, 40" long, Dow SWHRLE 10m^3
1%	**Lifetime Cost: $38262** Capital Cost: $12687 Average Cost of Water: $4.19/$m^3$	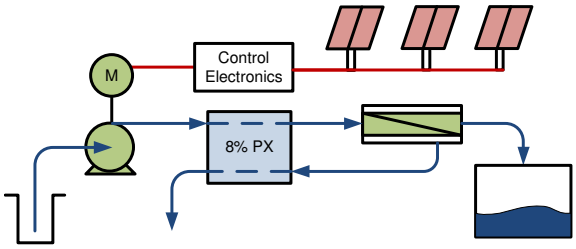	Panel Panel Mounting Motor Pump Energy Recovery Membrane Water Tank Size	Suntech 295 W Panels Fixed Panels Leeson 1 HP Motor NRD PRG 10 Vane Pump 8% Spectra Clark Pump 4" Diameter, 40" long, Dow SWHRLE 5m^3
10%	**Lifetime Cost: $37344** Capital Cost: $11769 Average Cost of Water: $4.09/$m^3$	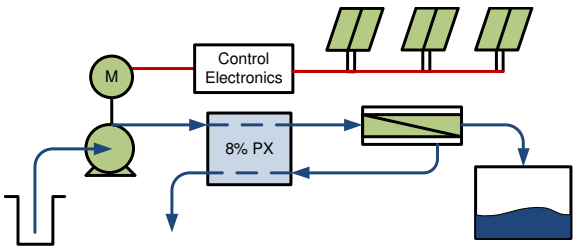	Panel Panel Mounting Motor Pump Energy Recovery Membrane Water Tank Size	Trina Solar 225 W Panels Fixed Panels 1 HP Leeson Motor NRD PRG 10 Vane Pump 8% Spectra Clark Pump 4" Diameter, 40" long, Dow SWHRLE 5m^3

7.3.2 Critical Month Simulations

In the critical month of case studies, the stochastic solar radiation model and water demand model described above are used to generate typical profiles for 100 years, which are used to determine the months of highest water stress. Since the amount of water produced is proportional to the solar insolation is the month in which the system is most stressed. The water demand/solar

insolation ratio is determined for every month over the 100-year period, and the month with the highest ratio is selected for each year. This ratio varies by location. Figure 7.17 shows the system demand ratio over one year for the 1 m^3 Boston system, as well as the long-term average. The average over the 100-year time window indicates that December is the critical period and is used in the simulations.

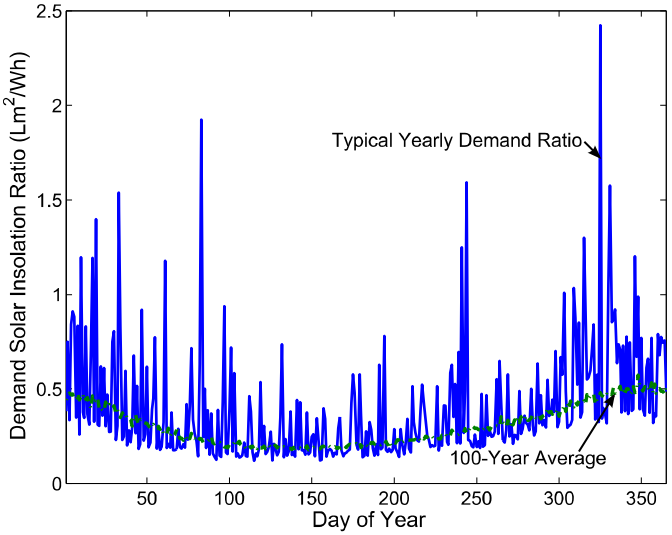

Figure 7.17: Demand solar insolation ratio for sample year and 100-year average.

The method described in section 7.2.1 is used to analyze the system loss-of-water probability. The loss-of-water probability for the entire year is estimated using two methods to provide an upper and lower bound. Since simulation data is only provided for the critical month, the lower bound on the year-long loss-of-water probability is determined by assuming all other time periods are able to satisfy demand. The upper bound on the year-long loss-of-water probability is determined by assuming all other months during the year provide the same level of performance. The inventory specified in section 6.3.3 is again used to configure the lowest lifecycle cost system and a system lifetime of 25-years and an interest rate of 4% are again assumed.

Designs are generated for loss-of-water probabilities ranging from 0.1% to 10%. A Pareto plot showing the how the total lifetime cost varies with loss of water probability is shown in Figure 7.18. Both methods for estimating the year-long loss-of-water probability are shown. The results show that the assumption that the rest of the year the system is able to provide water fails as these cases consistently result in lower-cost configurations than the full-year simulations. This

indicates the system is stressed at other points of the year. The failure in assuming the non-simulated months are able to meet demand is especially evident at high loss of water probabilities. For this case, at a probability of 10%, the system does not need to provide any water during the critical month to meet the design requirements. As a result, the system is configured to meet the minimum requirements of a valid system.

The cases where the loss-of-water probability for the unsimulated portion of the year is assumed to be the same as the critical month result in solutions that are more expensive than the full-year cases. This is expected as the system is sized to the worst month. As the loss-of-water probability increases, the distance between the upper bound and the full-year simulation cases narrows. This occurs since the systems get smaller as the probability increases and accordingly, there are fewer system design choices.

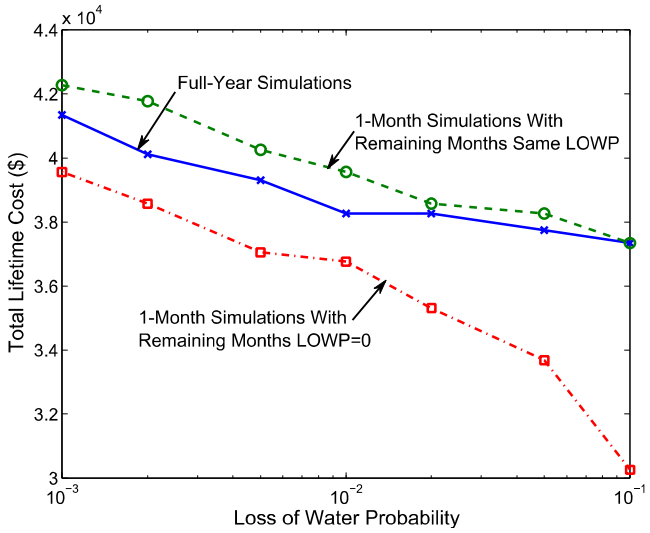

Figure 7.18: Pareto plot of lifetime system cost versus loss-of-water probability.

The overall computation time for the month long cases is greatly reduced. The computation time required on a normal desktop computer ranged from 22.3 to 43.1 hours with an average value of 28.5 hours. However, greater reduction in computation time is still desired.

7.4 Calculation of Loss-of-Water Probability Using Historical Data

Section 7.3 presented a simulation-based approach to estimate the loss-of-water probability for a given system design. While this approach was shown to be effective, the computation time

required for a single optimization ranges between 3-5 days on a standard desktop computer. A faster method is needed.

To decrease the computation time required, an analytic method for computing the *LOWP* is developed by using the knowledge of the solar insolation and water demand distributions to determine the distribution of the net change in stored water. The amount of water in storage is represented by a number of discrete states. The probability of transitioning between these states during a day is determined using the tank volume change distribution. Using this representation, the loss of water probability can be determined analytically.

Several simplifying assumptions are applied in order to estimate the *LOWP* using the data from the month with the highest solar demand. First, it is assumed that the solar radiation and water demand on a given day are independent of the values on previous days. It is also assumed that the critical water storage level is reached at the end of the day.

The solar insolation during the critical month is analyzed first. The daily data from a 21-year time period is obtained for any location using the NASA Surface Meteorology Database [8]. This data can be analyzed to determine a solar insolation histogram. An example for the month of December in Boston, MA can be seen in Figure 7.19.

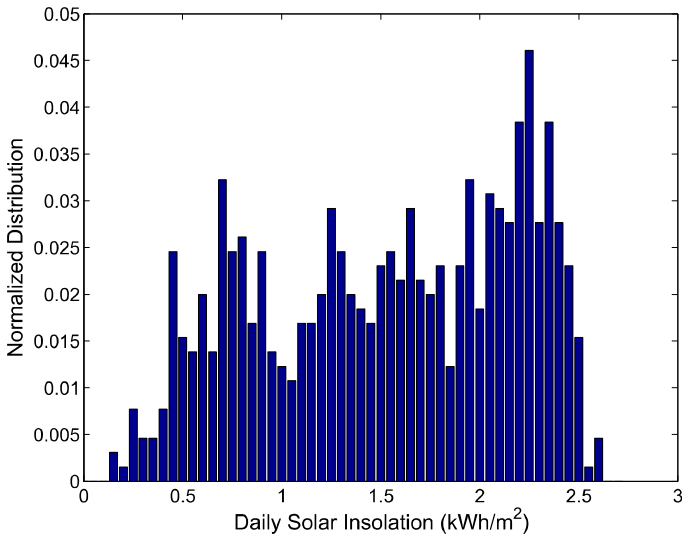

Figure 7.19: Normalized histogram of Boston daily solar insolation in December.

Next, the probability distribution is generated from the solar insolation distribution for a given PVRO system. Hourly solar radiation profiles are generated using the standard outlined in section 5.1.1 and the relationship between solar insolation and water production is calculated

[122]. The daily water production distribution is directly calculated from the daily solar insolation distribution using this relationship. Figure 7.20 shows the relation between solar insolation and water production for a small PVRO system in Boston, as well as the resulting water production distribution for the critical month of December.

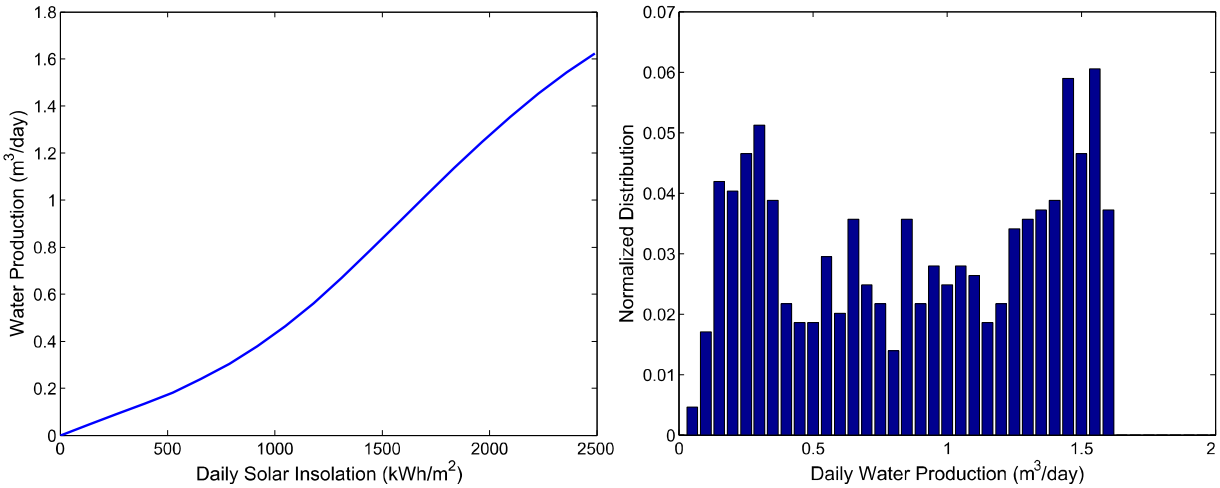

Figure 7.20: Daily water production for a small PVRO system in Boston and the normalized histogram of daily water production in December.

Variation in the water demand is then considered. A histogram of the water demand over the month of December is generated from the collected data from the Massachusetts Water Resources Authority. Individual histograms are generated for different levels of solar radiation to account for correlation between the two random variables. The water demand histograms for a 1 m^3 system located in Boston during the month of December are shown in Figure 7.21. The correlation between water demand and solar insolation is low during the month of December, but is included here to illustrate the general method. Other locations may have higher correlation. As mentioned above, there may be other effects which are not accounted for here due to lack of information, such as coupling between water tank level and system demand.

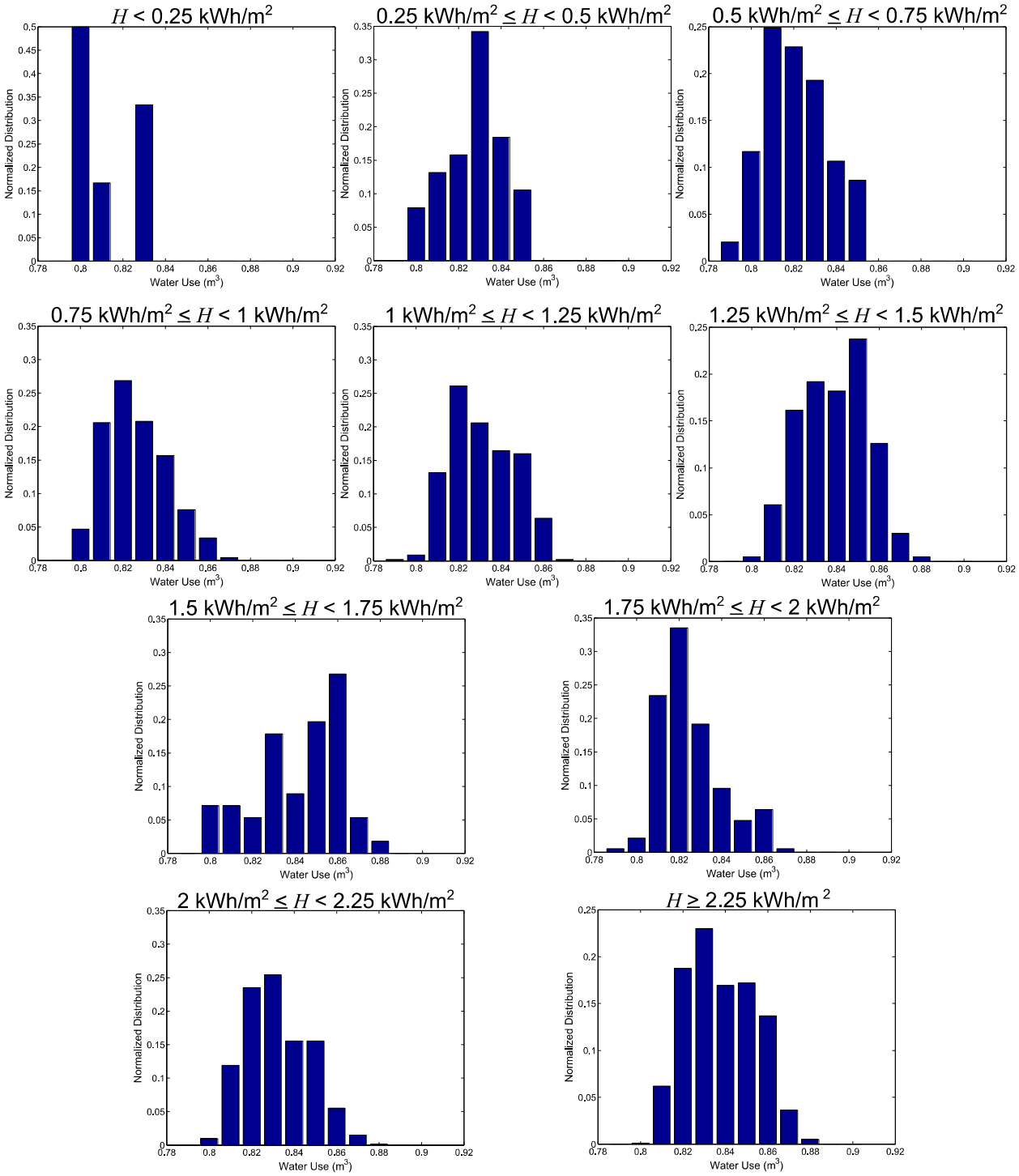

Figure 7.21: Normalized histograms of daily water demand in December for different ranges of solar insolation.

Once distributions for the solar insolation and water demand are generated, the distribution of the change in water tank level is calculated. The water production is calculated for each level

of solar insolation. The distribution in the water tank level is calculated by comparing water production and water use for that insolation level. The probability of a given change in water tank level is calculated by summing over all insolation levels as follows:

$$P(V_1 \le \Delta V_{\text{tank}} < V_2) = \sum_{H=H_1}^{H_{N_H}} P(V_{prod,1} \le V_{prod} < V_{prod,2} \mid H) P(V_{use,1} \le V_{use} < V_{use,2} \mid H)$$
$$\text{s.t. } V_{prod,1} - V_{use,2} > V_1 \ \& \ V_{prod,2} - V_{use,1} < V_2 \tag{7.24}$$

where ΔV_{tank} is the change in tank water level, V_{prod} is the volume of water produced and V_{use} is the volume of water used. The resulting distribution for the example case of a 1 m^3 system in Boston is shown in Figure 7.22.

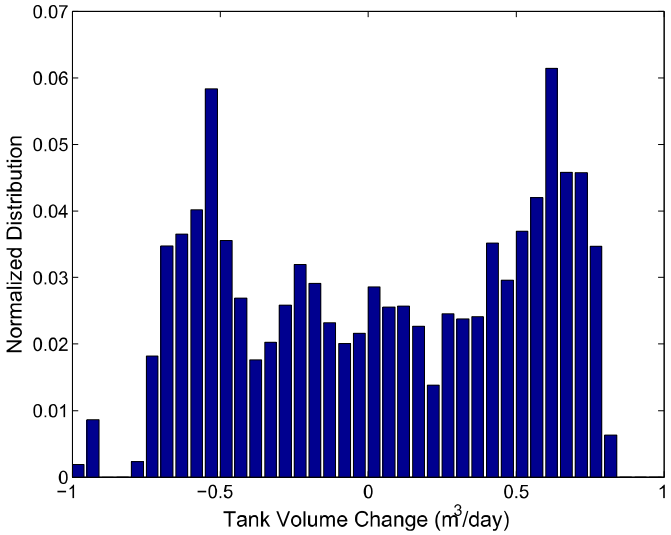

Figure 7.22: Normalized histogram of daily tank volume change for a 1 m^3 PVRO system in Boston during the month of December.

The tank is discretized into N levels, with level 1 being an empty tank and level N being a full tank. Given the probability distribution of water in the tank on day i, the distribution on day $i+1$ can be determined using the following:

$$\boldsymbol{\pi}_{i+1} = \mathbf{A}\boldsymbol{\pi}_i \tag{7.25}$$

where $\mathbf{A}$ is the transition probability matrix and $\boldsymbol{\pi}$ is and N x 1 vector representing the probability water volume in the being at a given level. The entries of $\mathbf{A}$ are given by the tank volume change probability as follows:

$$
\begin{aligned}
A_{1,1} &= \sum_{i=\Delta V_{\min}}^{0} P(\Delta V = i) \\
A_{1,2} &= \sum_{i=\Delta V_{\min}}^{-V_t} P(\Delta V = i) \\
&\vdots \\
A_{2,1} &= P(\Delta V = V_t) \\
A_{2,2} &= P(\Delta V = 0) \\
A_{2,3} &= P(\Delta V = -V_t) \\
&\vdots \\
A_{N,N-1} &= \sum_{i=V_t}^{\Delta V_{\max}} P(\Delta V = i) \\
A_{N,N} &= \sum_{i=0}^{\Delta V_{\max}} P(\Delta V = i)
\end{aligned}
\qquad \text{u(7.26)}
$$

where V_t is the size of the discretization of the tank volume.

Given a known initial volume of a half-full tank, the probability distribution of the tank storage level can be determined throughout the course of the month. This is done for the example of 1 m^3 system in Boston starting with a half-full 5 m^3 tank, and the resulting tank volume distributions are shown in Figure 7.23. Due to the limits of the tank size, spikes occur in the probability distribution when the tank is empty (0 m^3) and when the tank is at full capacity (5 m^3). Since the initial volume is unknown, the steady state value is utilized to determine the system loss-of-water probability. The steady state distribution can be determined using:

$$\left(\mathbf{I} - \mathbf{A}\right)\boldsymbol{\pi}_{ss} = 0 \qquad (7.27)$$

The system loss of water probability is given by the probability that the system is in the lowest state in the steady state condition. For the example case, the loss-of-water probability is 0.81%.

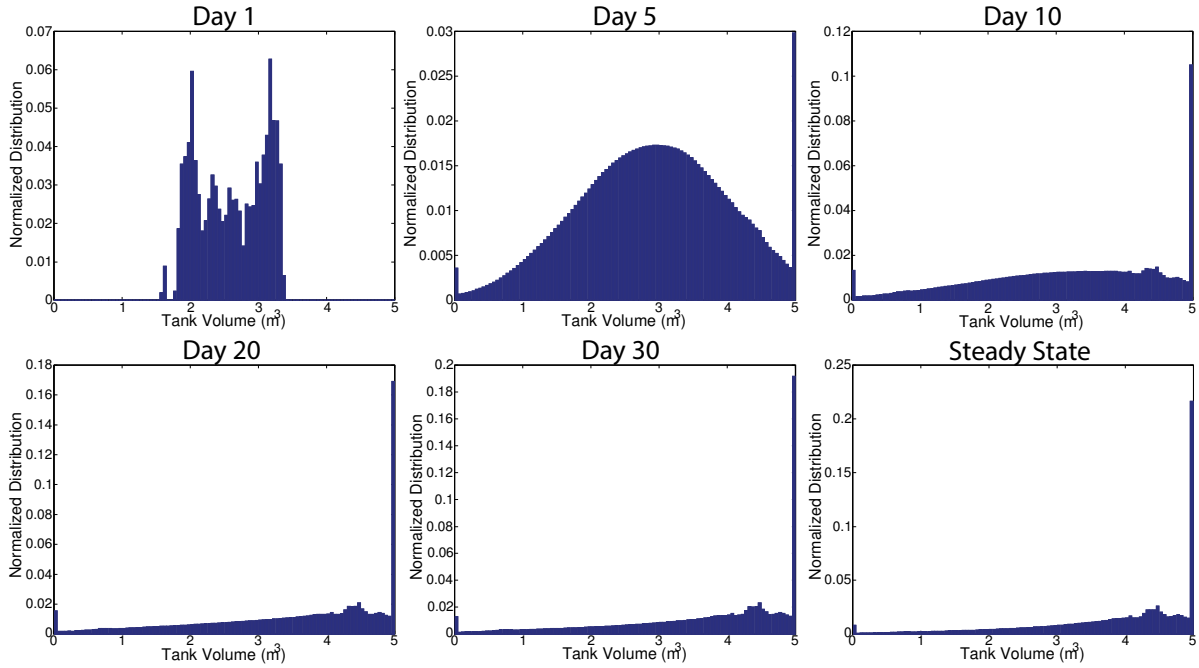

Figure 7.23: Evolution of water tank storage distribution in December.

This method can be used to calculate the loss-of-water probability in the final optimization stage of the modular design approach for PVRO systems. This approach substitutes for the time-series simulations. Case studies for this approach are presented below.

7.5 Direct Calculation Case Studies

Case studies were conducted using the direct calculation of the loss-of water probability. The problem statement remains the same as the cases presented in section 7.3. The inventory specified in section 6.3.3 is again used to configure the lowest lifecycle cost system, and a system lifetime of 25-years and an interest rate of 4% are assumed. Cases are run for varying loss-of-water probabilities to see the tradeoff between cost and reliability. Designs are generated for loss-of-water probabilities between 0.01% and 10%. A Pareto plot of the loss-of-water probability versus the resulting lifetime PVRO system costs can be seen in Figure 7.24 and resulting system configurations can be seen in Table 7.5. It can be seen that the results are very similar to the full-year simulation case studies. The resulting systems are typically larger since they are sized according to the worst period of the year.

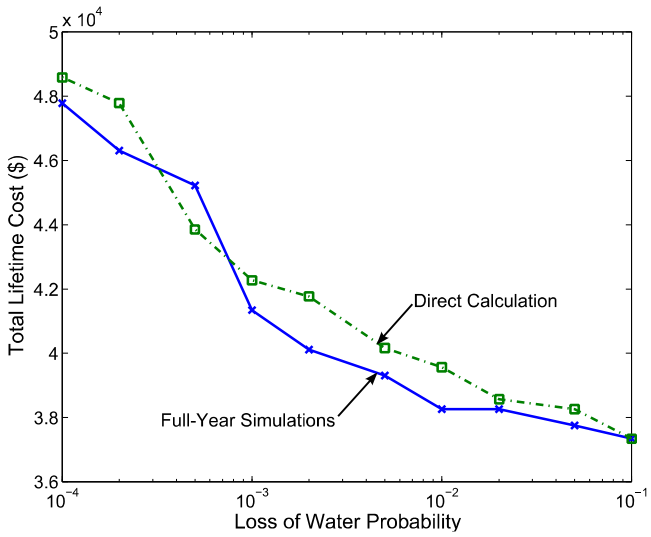

Figure 7.24: Pareto plot of lifetime system cost versus loss-of-water probability for direct LOWP calculation approach.

Table 7.5: Results of modular design approach for 1 m^3 systems when using the direct LOWP calculation.

Loss of Water Probability	System Stats	System Configuration	Component Details	
0.01%	**Lifetime Cost: $48586** Capital Cost: $24092 Average Cost of Water: $5.32/$m^3$	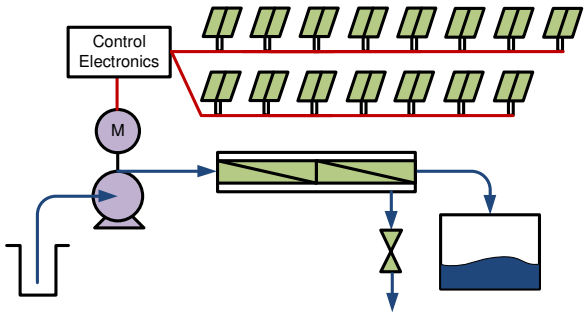	Panel Panel Mounting Motor Pump Energy Recovery Membrane Water Tank Size	Trina Solar 225 W Panels Fixed Panels Leeson 5 HP Motor Danfoss APP 1.8 None 4" Diameter, 40" long, Dow SWHRLE 10m^3
10%	**Lifetime Cost: $37344** Capital Cost: $11769 Average Cost of Water: $4.09/$m^3$	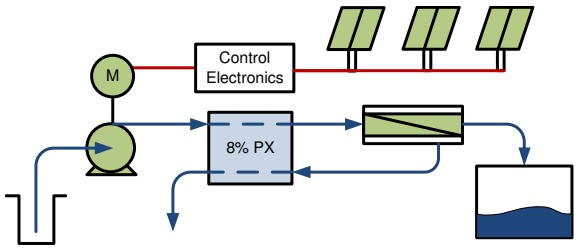	Panel Panel Mounting Motor Pump Energy Recovery Membrane Water Tank Size	Trina Solar 225 W Panels Fixed Panels 1 HP Leeson Motor NRD PRG 10 Vane Pump 8% Spectra Clark Pump 4" Diameter, 40" long, Dow SWHRLE 5m^3

For the cases considered, the direct calculation method typically results in a higher cost system cost than the full-year simulation. This matches intuition as the system components are

sized to meet demand in the worst month. An exception occurs at a loss-of-water probability of 0.05%. The resulting system configurations for this case can be seen in Figure 7.25. It is seen that the resulting system topologies are different. This occurs due to the limited one month time-window which is considered during the direct calculation approach. During this worst month, which is the winter for the case studied, the system demand and water production flowrates are lower. As a result, the system components which can meet demand during this month may reach their operational limits when system flowrates are required to be higher during the summer months. This is the case with the energy recovery device and a different configuration is required when the full year is considered.

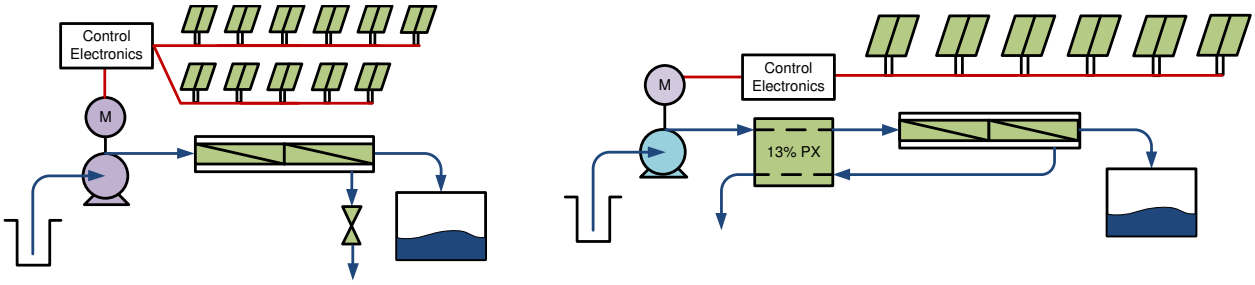

Figure 7.25: Systems designed for LOWP = 0.05% using full-year simulations (left) and direct calculation of LOWP in the critical month (right).

The computation time for this method is also greatly reduced from the full-year simulation method. In the cases studied, the total computation time on a computer with an Intel 2.8 GHz Dual Core processor and 4 GB of RAM ranged between 18.3 and 31.7 hours with an average of 22.5 hours. This method decreases the computation time required, and can be used to design systems with the required loss-of-water probability. For the majority of cases studies, the direct *LOWP* calculation method provides similar results to the full-year simulations. Due to simplifications made, checks should be implemented to ensure the resulting system can meet the required *LOWP* during the remaining portion of the year.

CHAPTER

8

SUMMARY AND CONCLUSIONS

8.1 Summary

This thesis describes an approach for automatically designing systems composed of modular components. Engineering principles are used to limit the scope of the design problem. Optimization methods are then used to determine the modular system configuration. The application considered in detail here is the design of PVRO systems for small communities. The methods are formulated to be robust to uncertainties in system requirements. Software tools can be created from the modular design methods developed in this research to enable modular system design by non-experts.

Chapter 1 presents the motivation for this research. Clean drinking water is a major issue for many locations and PVRO systems can provide a possible solution. PVRO systems are composed of modular components, so designing a system for an individual location is beyond the expertise available in many parts of the world. For a given modular inventory, a large number of possible system configurations exist. Methods which enable non-experts to custom configure PVRO systems for individual locations can make this technology accessible to many parts of the world.

Chapter 2 presents relevant literature on the topics of PVRO systems and modular design methods. PVRO systems have been designed and deployed in many regions. These systems are custom designed for individual locations and water demands. No general design methods have been developed for PVRO, although they exist for other applications including robotics, electronic circuits, and computer programs. These methods are application specific and do not consider many aspects important for PVRO system design, such as accommodating a large component inventory, complex system physics, and variations in the system environment.

Chapter 3 presents a PVRO feasibility study that was conducted to determine the potential impact of this research. The feasibility study compares the economics of PVRO systems to those of diesel reverse osmosis systems and transported water for a wide range of locations. It shows that PVRO systems are economically viable for many small communities located in equatorial regions. It also shows the area where PVRO is economically viable will increase as the system costs decrease. Decreasing the system costs can be accomplished using by using modular design methods.

Chapter 4 presents the details of the modular design approach. Engineering principles are used to reduce the system design space, and optimization methods are then used to configure a modular system for an individual application. The method is applied in a design space study for a PVRO system, where it greatly reduces the size of the design space. A parallel example is presented for the design of a hybrid car. The design studies show that this method has great potential and can be applied to many modular systems.

Chapter 5 presents the PVRO system models used in the modular design approach. Physics-based models are developed for individual system components. A new method of representing different reverse osmosis system configurations is developed which uses a graph to indicate the component connections. This graph representation is implemented in Matlab to calculate the PVRO system production for given solar input. A surrogate model of the solar radiation to water production relationship is developed to increase calculation speed for different solar profiles. This model is validated using an experimental PVRO system that was constructed as a part of this research.

Chapter 6 presents the implementation of the modular design approach for PVRO system design using deterministic solar radiation inputs and demands. The approach is able to tailor systems for a wide range of locations and water demands from a large system inventory. The validity of these solutions is demonstrated by simulating a custom designed system in the wrong location. A final case study demonstrates that the method can be used to determine if new components are capable of impacting the market.

Chapter 7 presents the implementation of the modular design approach for PVRO systems using variable solar insolation and water demand. Two methods that use historical solar insolation and water demand to account for variations are presented. The first method characterizes the historical data and develops models to synthetically generate data, then

simulates the system over a period of 100 years to determine the loss-of-water probability. In the second method, distributions of solar radiation and water demand are calculated from historical data and used to directly calculate the probability of running out of water in the worst month of the year. Modular design cases were conducted for both methods. The full-year simulation method is able to design systems for varying loss-of-water probabilities, but the computation time required is over 3 days for every case considered. The direct calculation method is shown to yield similar results to the full-year simulation method, and the computation time is greatly reduced to less than 1 day in many instances. The direct calculation method can be used to quickly estimate the failure probability of many systems with variable inputs.

8.2 Suggestions for Future Work

This thesis presents a general design approach for modular systems and studies its application to the design of PVRO systems in detail. There are many interesting opportunities for future research on both the design approach and the application of PVRO systems.

A major challenge with reverse osmosis desalination is proper pre-treatment of the incoming feedwater. In certain locations, the feedwater may contain bacteria or salts that are near their saturation limits. This is of particular concern when designing brackish water systems. This research did not consider the effects and costs associated with different pre-treatment systems. Modeling these aspects and adding them to the modular design approach will greatly aid system designers.

As PVRO systems age, the performance of individual components will degrade. These effects may result in much lower PVRO system production as the components reach the end of their lives. The effects of degradation can be incorporated into the system models for to ensure that the designed system is able to meet the demands over the entire system life.

Another design issue that may be incorporated into a modular design approach is accommodating component failure. Many of the system configurations produced by the modular design implementation will fail if one key component fails. Failure of the system may have terrible consequences. Developing a method to analyze the effects of component failure and address them during the design can be an interesting extension of this work.

In some locations where PVRO systems are economically viable, the system would not be required to provide all the water for community. For example, locations in the developing world

may already have rainwater catchments in place. Rainwater systems complement PVRO systems since they provide water during inclement weather. Designing these complementary systems provides a different set of challenges and would be an interesting avenue for future research.

This thesis developed a method to directly calculate the probability of failing to provide adequate water from statistical solar radiation and water use data. The method made simplifying assumptions to allow for the calculation. The main simplifications are that the system is only stressed during one-month of the year and that the solar radiation and water use are independent of previous values. As a result, this method provides an estimate of the loss-of-water probability. The method should be expanded to ensure conditions outside the critical month are considered. In addition, development of an expanded approach that considers day-to-day persistence of solar radiation and demand will improve the accuracy of loss-of-water probability calculation and make it useful for future design applications.

Another promising avenue of research is the implementation of the PVRO technology from this research in the developing world. For a PVRO system to have a long-term impact on a community in the developing world, it must be properly operated and maintained. Developing a control system with a robust user interface that identifies potential system issues will be essential to the successful implementation of these systems. In addition, effective training programs and maintenance programs will be required. The technical and social aspects of deploying such systems provide interesting avenues for future research.

REFERENCES

[1] World Health Organization and Unicef, "Progress on Sanitation and Drinking Water: 2010 Update," World Health Organization and Unicef, Geneva, Switzerland, 2010.

[2] H. T. El-Dessouky and H. M. Ettouney, *Fundamentals of salt water desalination*. Amsterdam; New York: Elsevier, 2002.

[3] F. Trieb and H. Müller-Steinhagen, "Concentrating solar power for seawater desalination in the Middle East and North Africa," *Desalination,* vol. 220, pp. 165-183, 2008.

[4] F. Trieb*, et al.*, "Concentrating Solar Power for Seawater Desalination," German Aerospace Center (DLR), Stuttgart, 2007.

[5] S. A. Kalogirou, "Seawater desalination using renewable energy sources," *Progress in Energy and Combustion Science,* vol. 31, pp. 242-281, 2005.

[6] E. Tzen and R. Morris, "Renewable energy sources for desalination," *Solar Energy,* vol. 75, pp. 375-379, 2003.

[7] United Nations, "World Water Day 2007 Brochure - Coping With Water Scarcity," 2007.

[8] National Aeronautics and Space Administration. Surface Meteorology and Solar Energy: A renewable energy resource web site (release 6.0) [Online]. Available: http://eosweb.larc.nasa.gov/sse/

[9] Center for Renewable Energy Systems (CRES), "Desalination guide using renewable energies. THERMIE – DG XVII," European Commission Report, Greece, 1998.

[10] M. S. Mohsen and J. O. Jaber, "A photovoltaic-powered system for water desalination," *Desalination,* vol. 138, pp. 129-136, 2001.

[11] E. S. Hrayshat, "Brackish water desalination by a stand alone reverse osmosis desalination unit powered by photovoltaic solar energy," *Renewable Energy,* vol. 33, pp. 1784-1790, 2008.

[12] E. S. Mohamed and G. Papadakis, "Design, simulation and economic analysis of a stand-alone reverse osmosis desalination unit powered by wind turbines and photovoltaics," *Desalination,* vol. 164, pp. 87-97, 2004.

[13] E. S. Mohamed*, et al.*, "A direct coupled photovoltaic seawater reverse osmosis desalination system toward battery based systems — a technical and economical experimental comparative study," *Desalination,* vol. 221, pp. 17-22, 2008.

[14] A. M. Thomson, "Reverse-Osmosis Desalination of Seawater Powered by Photovoltaics Without Batteries," Ph.D., Loughborough University, Loughborough, U.K., 2003.

[15] M. Thomson and D. Infield, "A photovoltaic-powered seawater reverse-osmosis system without batteries," *Desalination,* vol. 153, pp. 1-8, 2003.

[16] J. Went*, et al.*, "The energy demand for desalination with solar powered reverse osmosis units," *Desalination and Water Treatment,* vol. 21, pp. 138-147, 2010.

[17] A. Schies*, et al.*, "Operating control strategies and dimensioning of photovoltaic-powered reverse osmosis desalination plants without batteries," *Desalination and Water Treatment,* vol. 21, pp. 131-137, 2010.

[18] S. Dallas*, et al.*, "Efficiency analysis of the Solarflow – An innovative solar-powered desalination unit for treating brackish water," *Renewable Energy,* vol. 34, pp. 397-400, 2009.

[19] S. F. Cheah, "Photovoltaic Reverse Osmosis Desalination System," ITN Energy Systems, Inc., Littleton, CO2004.
[20] D. B. Riffel and P. C. M. Carvalho, "Small-scale photovoltaic-powered reverse osmosis plant without batteries: Design and simulation," *Desalination,* vol. 247, pp. 378-389, 2009.
[21] A. Joyce*, et al.*, "Small reverse osmosis units using PV systems for water purification in rural places," *Desalination,* vol. 137, pp. 39-44, 2001.
[22] D. Herold*, et al.*, "Small scale photovoltaic desalination for rural water supply - demonstration plant in Gran Canaria," *Renewable Energy,* vol. 14, pp. 293-298, 1998.
[23] D. Herold and A. Neskakis, "A small PV-driven reverse osmosis desalination plant on the island of Gran Canaria," *Desalination,* vol. 137, pp. 285-292, 2001.
[24] Z. Al Suleimani and V. R. Nair, "Desalination by solar-powered reverse osmosis in a remote area of the Sultanate of Oman," *Applied Energy,* vol. 65, pp. 367-380, 2000.
[25] E. Tzen*, et al.*, "Autonomous reverse osmosis units driven by RE sources experiences and lessons learned," *Desalination,* vol. 221, pp. 29-36, 2008.
[26] E. Tzen*, et al.*, "Design of a stand alone PV - desalination system for rural areas," *Desalination,* vol. 119, pp. 327-333, 1998.
[27] E. Tzen*, et al.*, "Design and development of a hybrid autonomous system for seawater desalination," *Desalination,* vol. 166, pp. 267-274, 2004.
[28] Spectra Watermakers, "SSW 3500 Datasheet," 2009.
[29] S. Abdallah*, et al.*, "Performance of a photovoltaic powered reverse osmosis system under local climatic conditions," *Desalination,* vol. 183, pp. 95-104, 2005.
[30] B. S. Richards and A. I. Schäfer, "Photovoltaic-powered desalination system for remote Australian communities," *Renewable Energy,* vol. 28, pp. 2013-2022, 2003.
[31] M. Thomson and D. Infield, "Laboratory demonstration of a photovoltaic-powered seawater reverse-osmosis system without batteries," *Desalination,* vol. 183, pp. 105-111, 2005.
[32] P. C. M. de Carvalho*, et al.*, "Control method of a photovoltaic powered reverse osmosis plant without batteries based on maximum power point tracking," in *Transmission and Distribution Conference and Exposition: Latin America, 2004 IEEE/PES*, 2004, pp. 137-142.
[33] I. de la Nuez Pestana*, et al.*, "Optimization of RO desalination systems powered by renewable energies. Part I: Wind energy," *Desalination,* vol. 160, pp. 293-299, 2004.
[34] D. Voivontas*, et al.*, "A tool for the design of desalination plants powered by renewable energies," *Desalination,* vol. 133, pp. 175-198, 2001.
[35] K. Bourouni*, et al.*, "Design and optimization of desalination reverse osmosis plants driven by renewable energies using genetic algorithms," *Renewable Energy,* vol. 36, pp. 936-950, 2011.
[36] M. Wilf and C. Bartels, "Optimization of seawater RO systems design," *Desalination,* vol. 173, pp. 1-12, 2005.
[37] M. Wilf and K. Klinko, "Optimization of seawater RO systems design," *Desalination,* vol. 138, pp. 299-306, 2001.
[38] A. Malek*, et al.*, "Design and economics of RO seawater desalination," *Desalination,* vol. 105, pp. 245-261, 1996.

[39] A. Gambier, *et al.*, "Dynamic Modeling of a Simple Reverse Osmosis Desalination Plant for Advanced Control Purposes," in *American Control Conference, 2007. ACC '07*, 2007, pp. 4854-4859.
[40] M. M. El-Halwagi, "Synthesis of reverse-osmosis networks for waste reduction," *AIChE Journal,* vol. 38, pp. 1185-1198, 1992.
[41] N. Voros, *et al.*, "Optimization of reverse osmosis networks for seawater desalination," *Computers & Chemical Engineering,* vol. 20, Supplement 1, pp. S345-S350, 1996.
[42] M. G. Marcovecchio, *et al.*, "Global optimal design of reverse osmosis networks for seawater desalination: modeling and algorithm," *Desalination,* vol. 184, pp. 259-271, 2005.
[43] Y. Saif, *et al.*, "Global Optimization of Reverse Osmosis Network for Wastewater Treatment and Minimization," *Industrial & Engineering Chemistry Research,* vol. 47, pp. 3060-3070, 2008/05/01 2008.
[44] Y.-Y. Lu, *et al.*, "Optimum design of reverse osmosis system under different feed concentration and product specification," *Journal of Membrane Science,* vol. 287, pp. 219-229, 2007.
[45] Y.-y. Lu, *et al.*, "Optimum design of reverse osmosis seawater desalination system considering membrane cleaning and replacing," *Journal of Membrane Science,* vol. 282, pp. 7-13, 2006.
[46] F. Vince, *et al.*, "Multi-objective optimization of RO desalination plants," *Desalination,* vol. 222, pp. 96-118, 2008.
[47] F. Maskan, *et al.*, "Optimal design of reverse osmosis module networks," *AIChE Journal,* vol. 46, pp. 946-954, 2000.
[48] A. Abbas, "Model predictive control of a reverse osmosis desalination unit," *Desalination,* vol. 194, pp. 268-280, 2006.
[49] A. R. Bartman, *et al.*, "Nonlinear Model-Based Control of an Experimental Reverse-Osmosis Water Desalination System," *Industrial & Engineering Chemistry Research,* vol. 48, pp. 6126-6136, 2009/07/01 2009.
[50] A. Gambier, *et al.*, "Fault-tolerant control of a small reverse osmosis desalination plant with feed water bypass," in *American Control Conference (ACC), 2010*, 2010, pp. 3611-3616.
[51] A. Gambier, *et al.*, "Optimal control of a reverse osmosis desalination plant using multi-objective optimization," in *Computer Aided Control System Design, 2006 IEEE International Conference on Control Applications, 2006 IEEE International Symposium on Intelligent Control, 2006 IEEE*, 2006, pp. 1368-1373.
[52] A. R. Bartman, *et al.*, "Minimizing energy consumption in reverse osmosis membrane desalination using optimization-based control," *Journal of Process Control,* vol. 20, pp. 1261-1269, 2010.
[53] A. Poullikkas, "Optimization algorithm for reverse osmosis desalination economics," *Desalination,* vol. 133, pp. 75-81, 2001.
[54] C. Guria, *et al.*, "Multi-objective optimization of reverse osmosis desalination units using different adaptations of the non-dominated sorting genetic algorithm (NSGA)," *Computers & Chemical Engineering,* vol. 29, pp. 1977-1995, 2005.
[55] D. Rus and M. Vona, "Crystalline Robots: Self-Reconfiguration with Compressible Unit Modules," *Auton. Robots,* vol. 10, pp. 107-124, 2001.

[56] M. Yim, *et al.*, "PolyBot: a modular reconfigurable robot," in *Robotics and Automation, 2000. Proceedings. ICRA '00. IEEE International Conference on*, 2000, pp. 514-520 vol.1.
[57] S. Farritor, *et al.*, "A systems-level modular design approach to field robotics," in *Robotics and Automation, 1996. Proceedings., 1996 IEEE International Conference on*, 1996, pp. 2890-2895 vol.4.
[58] N. Rutman, "Automated design of modular field robots," M.S., Mechanical Engineering, Masssachusetts Institute of Technology, Cambridge, MA, 1995.
[59] G. S. Hornby, *et al.*, "Generative representations for the automated design of modular physical robots," *Robotics and Automation, IEEE Transactions on,* vol. 19, pp. 703-719, 2003.
[60] C. Leger, "Automated Synthesis and Optimization of Robot Configurations: An Evolutionary Approach," The Robotics Institute, Carnegie Mellon University, Pittsburgh, PA, 1999.
[61] J. R. Koza, *et al.*, "Automated synthesis of analog electrical circuits by means of genetic programming," *Evolutionary Computation, IEEE Transactions on,* vol. 1, pp. 109-128, 1997.
[62] J. R. Koza, *et al.*, "Automated WYWIWYG design of both the topology and component values of electrical circuits using genetic programming," presented at the Proceedings of the First Annual Conference on Genetic Programming, Stanford, California, 1996.
[63] J. D. Lohn and S. P. Colombano, "A circuit representation technique for automated circuit design," *Evolutionary Computation, IEEE Transactions on,* vol. 3, pp. 205-219, 1999.
[64] E. S. Ochotta, *et al.*, "Synthesis of high-performance analog circuits in ASTRX/OBLX," *Computer-Aided Design of Integrated Circuits and Systems, IEEE Transactions on,* vol. 15, pp. 273-294, 1996.
[65] J. F. Miller, *et al.*, "Principles in the Evolutionary Design of Digital Circuits—Part I," *Genetic Programming and Evolvable Machines,* vol. 1, pp. 7-35, 2000.
[66] E. M. Sentovich, *et al.*, "Sequential circuit design using synthesis and optimization," in *Computer Design: VLSI in Computers and Processors, 1992. ICCD '92. Proceedings., IEEE 1992 International Conference on*, 1992, pp. 328-333.
[67] J. R. Koza, *Genetic programming: on the programming of computers by means of natural selection*: MIT Press, 1992.
[68] J. R. Koza, *Genetic Programming II: Automatic Discovery of Reusable Programs*: MIT Press, 1994.
[69] A. Garrard and E. S. Fraga, "Mass exchange network synthesis using genetic algorithms," *Computers & Chemical Engineering,* vol. 22, pp. 1837-1850, 1998.
[70] D. R. Lewin, *et al.*, "A generalized method for HEN synthesis using stochastic optimization – I. General framework and MER optimal synthesis," *Computers & Chemical Engineering,* vol. 22, pp. 1503-1513, 1998.
[71] B. Gross and P. Roosen, "Total process optimization in chemical engineering with evolutionary algorithms," *Computers & Chemical Engineering,* vol. 22, Supplement 1, pp. S229-S236, 1998.
[72] M. Cantoni, *et al.*, "Genetic algorithms and Monte Carlo simulation for optimal plant design," *Reliability Engineering & System Safety,* vol. 68, pp. 29-38, 2000.

[73] M. Mack, "Solar power for telecommunications," *The Telecommunication Journal of Australia,* vol. 29, pp. 20-44, 1979.
[74] R. N. Chapman, "A simplified technique for designing least cost stand-alone PV/storage systems," in *19th IEEE Photovoltaic Specialists Conference*, New Orleans, LA, 1987.
[75] M. Sidrach-de-Cardona and L. Mora López, "A simple model for sizing stand alone photovoltaic systems," *Solar Energy Materials and Solar Cells,* vol. 55, pp. 199-214, 1998.
[76] H.-G. Beyer and B. Sendhoff, "Robust optimization – A comprehensive survey," *Computer Methods in Applied Mechanics and Engineering,* vol. 196, pp. 3190-3218, 2007.
[77] L. L. Bucciarelli Jr, "Estimating loss-of-power probabilities of stand-alone photovoltaic solar energy systems," *Solar Energy,* vol. 32, pp. 205-209, 1984.
[78] L. L. Bucciarelli Jr, "The effect of day-to-day correlation in solar radiation on the probability of loss-of-power in a stand-alone photovoltaic energy system," *Solar Energy,* vol. 36, pp. 11-14, 1986.
[79] A. D. Bagul*, et al.*, "Sizing of a stand-alone hybrid wind-photovoltaic system using a three-event probability density approximation," *Solar Energy,* vol. 56, pp. 323-335, 1996.
[80] J. M. Gordon, "Optimal sizing of stand-alone photovoltaic solar power systems," *Solar Cells,* vol. 20, pp. 295-313, 1987.
[81] H. L. Macomber*, et al.*, "Photovoltaic stand-alone systems: preliminary engineering-design handbook," DOE/NASA/0195-1; NASA-CR-165352; Other: ON: DE82000678 United StatesOther: ON: DE82000678Thu Feb 07 15:45:28 EST 2008NTIS, PC A11/MF A01.ERA-07-014040; EDB-82-028230English, 1981.
[82] E. Koutroulis*, et al.*, "Methodology for optimal sizing of stand-alone photovoltaic/wind-generator systems using genetic algorithms," *Solar Energy,* vol. 80, pp. 1072-1088, 2006.
[83] S. Diaf*, et al.*, "A methodology for optimal sizing of autonomous hybrid PV/wind system," *Energy Policy,* vol. 35, pp. 5708-5718, 2007.
[84] A. Bilton*, et al.*, "Design Optimization of Sustainable Off-Grid Power Systems for the Developing World," *ASME Conference Proceedings,* vol. 2011, pp. 1531-1540, 2011.
[85] A. Fragaki and T. Markvart, "Stand-alone PV system design: Results using a new sizing approach," *Renewable Energy,* vol. 33, pp. 162-167, 2008.
[86] T. Markvart*, et al.*, "PV system sizing using observed time series of solar radiation," *Solar Energy,* vol. 80, pp. 46-50, 2006.
[87] M. Egido and E. Lorenzo, "The sizing of stand alone PV-system: A review and a proposed new method," *Solar Energy Materials and Solar Cells,* vol. 26, pp. 51-69, 1992.
[88] A. Balouktsis*, et al.*, "Sizing stand-alone photovoltaic systems," *International Journal of Photoenergy,* vol. 2006, 2006.
[89] G. Giannakoudis*, et al.*, "Optimum design and operation under uncertainty of power systems using renewable energy sources and hydrogen storage," *International Journal of Hydrogen Energy,* vol. 35, pp. 872-891, 2010.
[90] P. Arun*, et al.*, "Optimum sizing of photovoltaic battery systems incorporating uncertainty through design space approach," *Solar Energy,* vol. 83, pp. 1013-1025, 2009.
[91] F. Domínguez-Muñoz*, et al.*, "Design of solar thermal systems under uncertainty," *Energy and Buildings,* vol. 47, pp. 474-484, 2012.

[92] A. Roy, *et al.*, "Physical design space for isolated wind-battery system incorporating resource uncertainty," *Proceedings of the Institution of Mechanical Engineers, Part A: Journal of Power and Energy,* vol. 225, pp. 421-442, June 1, 2011 2011.
[93] A. M. Helal, *et al.*, "Economic feasibility of alternative designs of a PV-RO desalination unit for remote areas in the United Arab Emirates," *Desalination,* vol. 221, pp. 1-16, 2008.
[94] H. M. Ettouney, *et al.*, "Evaluating the economics of desalination," *Chemical Engineering Progress,* vol. 12, pp. 32-38, 2002.
[95] T. Jackson and M. Oliver, "The viability of solar photovoltaics," *Energy Policy,* vol. 28, pp. 983-988, 2000.
[96] National Oceanographic Data Center (U.S.). World Ocean Atlas 2005 [Online]. Available: http://www.nodc.noaa.gov/OC5/WOA05/pr_woa05.html
[97] United Nations World Water Assessment Programme, "The 2nd United Nations World Water Development Report - Water: A Shared Responsibility," UNESCO, Paris, France, 2006.
[98] I. C. Karagiannis and P. G. Soldatos, "Current status of water desalination in the Aegean Islands," *Desalination,* vol. 203, pp. 56-61, 2007.
[99] Dow Filmtec Membrane Systems. Filmtec Membranes – System design: System performance projection [Online]. Available: http://www.dow.com/PublishedLiterature/dh_0036/0901b803800362e9.pdf
[100] M. Q. Wang, "GREET 1.5 - transportation fuel-cycle model - Vol. 1 : methodology, development, use, and results," AH200130, 1999.
[101] O. Barron, "Desalination options and their possible implementation in Western Australia: Potential role for CSIRO Land and Water," CSIRO: Water for a Healthy Country National Research Flagship, Canberra, Australia, 2006.
[102] A. Hafez and S. El-Manharawy, "Economics of seawater RO desalination in the Red Sea region, Egypt. Part 1. A case study," *Desalination,* vol. 153, pp. 335-347, 2003.
[103] R. Wiser, *et al.*, "Letting the sun shine on solar costs: An empirical investigation of photovoltaic cost trends in California," Berkeley, California, LBNL-59282, 2006.
[104] M. Muselli, *et al.*, "Design of Hybrid-Photovoltaic Power Generator with Optimization of Energy Management," *Solar Energy,* vol. 65, pp. 143-157, 1999.
[105] Solarbuzz. (2012, July 19, 2012). *Inverter Prices*. Available: http://www.solarbuzz.com/facts-and-figures/retail-price-environment/inverter-prices
[106] United States Energy Information Administration. (2009). *Annual U.S. No. 2 diesel retail sales by all sellers, Dec. 1, 2009*. Available: http://tonto.eia.doe.gov/dnav/pet/hist/d220600002m.htm
[107] T. G. Eschenbach, "Engineering Economy - Applying Theory to Practice (2nd Edition)," Oxford University Press, 2003.
[108] Reuters, "France sets carbon tax at 17 Euros a ton," in *The New York Times*. New York City, NY, 2009.
[109] J. K. Kaldellis, *et al.*, "Renewable energy desalination plants for the Greek islands—technical and economic considerations," *Desalination,* vol. 170, pp. 187-203, 2004.
[110] C. Burroughs. (2009, April 3, 2009). *Desalination of saline and brackish water becoming more affordable*. Available: https://share.sandia.gov/news/resources/news_releases/desalination-of-saline-and-brackish-water/

[111] S. M. Habali and I. A. Saleh, "Design of stand-alone brackish water desalination wind energy system for Jordan," *Solar Energy,* vol. 52, pp. 525-532, 1994.
[112] S. J. Lewis*, et al.*, "Assessment of groundwater resources in the Broken Hill region," Geoscience Australia Professional Opinion, 2008.
[113] R. Trabelsi*, et al.*, "Groundwater salinization of the Sfax superficial aquifer, Tunisia," *Hydrogeology Journal,* vol. 15, pp. 1341-1355, 2007.
[114] Y. Effendi, "Three years experiences for PVRO-desalination," in *Photovoltaic Specialists Conference, 1988., Conference Record of the Twentieth IEEE*, 1988, pp. 1194-1199 vol.2.
[115] P. C. M. de Carvalho*, et al.*, "The Brazilian experience with a photovoltaic powered reverse osmosis plant," *Progress in Photovoltaics: Research and Applications,* vol. 12, pp. 373-385, 2004.
[116] S. Bouguecha*, et al.*, "Small scale desalination pilots powered by renewable energy sources: case studies," *Desalination,* vol. 183, pp. 151-165, 2005.
[117] A. Al Malki*, et al.*, "Experimental study of using renewable energy in the rural areas of Oman," *Renewable Energy,* vol. 14, pp. 319-324, 1998.
[118] J. H. Holland, *Adaptation in Natural and Artificial Systems*: The University of Michigan Press, Ann Arbor, 1975.
[119] NASA/WMAP Science Team. (2011, July 12, 2012). *WMAP: What is the Universe Made of?* Available: http://map.gsfc.nasa.gov/universe/uni_matter.html
[120] L. F. Greenlee*, et al.*, "Reverse osmosis desalination: Water sources, technology, and today's challenges," *Water Research,* vol. 43, pp. 2317-2348, 2009.
[121] United States Department of Energy. (2012). *New Plug-in Hybrids*. Available: http://www.fueleconomy.gov/feg/phevsbs.shtml
[122] E. Lorenzo, "Energy Collected and Delivered by PV Modules," in *Handbook of Photovoltaic Science and Engineering*, A. Luque and S. Hegedus, Eds., ed: John Wiley & Sons, Ltd, 2005, pp. 905-970.
[123] L. L. Kazmerski, "Photovoltaics: A review of cell and module technologies," *Renewable and Sustainable Energy Reviews,* vol. 1, pp. 71-170, 1997.
[124] S.R. Wenham*, et al.*, *Applied Photovoltaics*. London, U.K.: Earthscan, 2007.
[125] ASTM, "D4516-00 Standard Practice for Standardizing Reverse Osmosis Performance Data," ASTM Interational, 2010.
[126] L. Kelley, "The design and control of a thermal management system for a photovoltaic reverse osmosis system," M.S., Mechanical Engineering, Massachusetts Insistute of Technology, Cambridge, MA, 2011.
[127] A. M. Bilton*, et al.*, "MIT Lavare PVRO Experimental System," Field and Space Robotics Laboratory, 2010.
[128] F. J. Millero*, et al.*, "The composition of Standard Seawater and the definition of the Reference-Composition Salinity Scale," *Deep Sea Research Part I: Oceanographic Research Papers,* vol. 55, pp. 50-72, 2008.
[129] Miguel Angel Sanz and R. L. Stover, "Low Energy Consumption in the Perth Seawater Desalination Plant," presented at the IDA World Congress, Gran Canaria, Spain, 2007.
[130] World Health Organization, *Guidelines for Drinking-water Quality - Fourth Edition*: World Health Organization, 2011.
[131] SolarPanelsOnlne.org. (2011, Nov. 17, 2011). *Solar Panel Center*. Available: http://solarpanelsonline.org

[132] Array Technologies. (2010, November 17, 2011). *Wattsun Solar Tracker Retail Price Sheet*. Available: http://www.wattsun.com/prices/Wattsun_Tracker_Prices.pdf
[133] Wateranywhere.com. (2011). *Reverse Osmosis Membranes*. Available: http://www.wateranywhere.com/Water_Filtration_Products/index.php?cPath=22
[134] Leeson Motors. (2011, July 17, 2011). *Leeson Electric Motors, Gearmotors and Drives*. Available: http://www.leeson.com/
[135] BigBrandWater.com. (2011, November 17, 2011). *Water Pumps, Well Pumps, Industrial Pumps, Delivery Pumps*. Available: http://www.bigbrandwater.com/waterpumps.html
[136] Atlantic RO. (2012). *Atlantic RO Price List*. Available: http://www.atlanticro.com/Code.pdf
[137] G. Barbose, "Tracking the Sun III; The Installed Cost of Photovoltaics in the United States from 1998-2009," 2011.
[138] J. Worm and T. van Hattum, *Rainwater harvesting for domestic use*. Wageningen, The Netherlands: Agromisa Foundation and CTA, 2006.
[139] S. A. Klein and W. A. Beckman, "Loss-of-load probabilities for stand-alone photovoltaic systems," *Solar Energy,* vol. 39, pp. 499-512, 1987.
[140] C. W. Richardson, "Stochastic simulation of daily precipitation, temperature, and solar radiation," *Water Resour. Res.,* vol. 17, pp. 182-190, 1981.
[141] S. L. Zhou*, et al.*, "Forecasting operational demand for an urban water supply zone," *Journal of Hydrology,* vol. 259, pp. 189-202, 2002.
[142] G. M. Jenkins and D. G. Watts, *Spectral analysis and its applications*: Holden-Day, 1969.
[143] P. A. MacMahon, *Collected Papers - Volume 1: Combinatorics,*. Boston, MA: MIT Press, 1978.

APPENDIX

A

ENUMERATION OF PVRO DESIGN SPACE

A.1 Rules of Combinatorics

The enumeration of the total number of system configurations for a given inventory of PV and RO components rely on basic rules of combinatorics, which are outlined here.

Product Rule

If event A can occur in α ways and event B can occur in β ways and the events are independent, then the total number of ways that A and B can simultaneously occur is αβ ways.

Sum Rule

If event A can occur in α ways and event B can occur in β ways and the two events cannot occur at that same time, then the total number of ways that A and B can occur is α + β ways.

Permutations

A permutation is an ordered arrangement of the elements of a set. The number of permutations with *r* elements that can be formed from a set with *n* distinct elements is given by:

$$P(n,r) = n(n-1)(n-2)\cdots(n-r+1) = \frac{n!}{n-r!} \tag{A.1}$$

Combinations

A combination is an unordered arrangement of the elements of a set. The number of combinations with *r* elements that can be formed from a set with *n* distinct elements is given by:

$$C(n,r) = \binom{n}{r} = \frac{n!}{(n-r)!r!} \tag{A.2}$$

Combinations and Permutations of Multi-Sets

A multi-set is a set which contains multiple elements that are not unique. An example of a multi-set with 8 elements and 3 objects is S={a,a,b,b,c,c,c,c}.

Infinite repetition number

If there is an infinite number of each type of object in the set, the objects are said to have an infinite repetition number. In this special case the number of r-permutations of the set is:

$$P(n,r) = k^r \tag{A.3}$$

where n is the total number of objects and k is the number of distinct objects. When there are finite numbers of objects, this expression is also true if $n_k \leq r$ for all k, where n_k is the number of object k available in the inventory.

For cases with infinite repetition number, the number of r-combinations of the multi-set is:

$$C(n,r) = \left\langle \begin{matrix} n \\ r \end{matrix} \right\rangle = \begin{pmatrix} n+r-1 \\ r \end{pmatrix} = \begin{pmatrix} n+r-1 \\ n-1 \end{pmatrix} \tag{A.4}$$

Again, this expression is also valid for finite repetition number sets where $n_k < r$ for all k.

Finite Repetition Number

If there are finite numbers of each type of object in the set, the objects are said to have a finite repetition number. In this case the number of permutations of the set is:

$$P(n) = \frac{n!}{n_1!n_2!\cdots n_k!} \tag{A.5}$$

where n_i is the total number of type i objects.

The number of r-combinations of a multi-set is as follows [143]:

$$C(r;n_1,n_2,\ldots,n_k) = \sum_{p=0}^{k} (-1)^p \sum_{1 \leq i_1 \leq i_2 \leq \cdots \leq i_p \leq k} \begin{pmatrix} k+r-\sum_{j=1}^{p} n_{i_j} - p - 1 \\ k-1 \end{pmatrix} \tag{A.6}$$

where the sum is taken for all terms where $k + r - \sum_{j=1}^{p} n_{i_j} - p - 1 > 0$.

For example, for simple set, S={a,a,b,b,b}, the 3-combinations are {a,a,b},{a,b,b} and {b,b,b}, and the total number can be calculated as:

$$C(3;n_1,n_2)=\sum_{p=0}^{2}(-1)^p\sum_{1\le i_1\le i_p\le 2}\binom{4-\sum_{j=1}^{p}n_{i_j}-p}{1}=\binom{4}{1}-\left[\binom{4-2-1}{1}+\binom{4-3-1}{1}\right]=3 \quad \text{(A.7)}$$

A.2 Number of Possible Reverse Osmosis Systems

In this section, the number of possible reverse osmosis systems is determined for different inventories. A simple case with all distinct pumps, membranes, and energy recovery devices is considered first. This is followed by a case with all identical components. Finally, a realistic inventory with mixed component types is considered.

A.2.1 Distinct Reverse Osmosis Components

To determine the total number of configurations, the component connection matrix representation is used. A simple connection matrix for a RO system with two pumps, two reverse osmosis membranes and one energy recovery device is shown in Figure A.1. In this connection matrix, the columns represent individual component inputs and the rows represent the individual component outputs. An entry of 1 within the matrix indicates that the components are connected. Using this representation, it can be seen that the total number of system configurations for a selection of distinct components can be written as:

$$n_{config}=2^{n_{inputs}n_{outputs}} \quad \text{(A.8)}$$

where n_{inputs} are the total number of component inputs and $n_{outputs}$ are the total number of component outputs for a given subset of components.

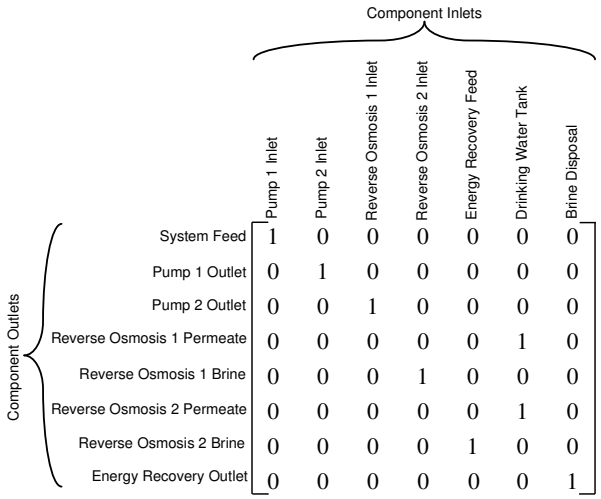

Figure A.1: Pareto plot of lifetime system cost versus loss-of-water probability for direct LOWP calculation approach.

For a simple set of components with n_p distinct pumps in the system, n_{ro} distinct reverse osmosis membranes and n_{er} distinct energy recovery devices or pressure control valves, the total number of component outputs is given by:

$$n_{outputs} = n_p + 2n_{ro} + n_{er} + 1 \tag{A.9}$$

and total number of component inputs is given by:

$$n_{inputs} = n_p + n_{ro} + n_{er} + 2 \tag{A.10}$$

Even with distinct components, not all of the configurations are distinct. If a zero row or column exists in this connection matrix, a component is not connected. Taking this into account, the number of matrices that do not result in a fully connected system can be written as:

$$n_{discon} = n_{zr} + n_{zc} - n_{zrzc} \tag{A.11}$$

where n_{zr} represents the number of connection matrices with zero rows, n_{zc} represents the number of connection matrices with zero columns, and n_{zrzc} represent the number of connection matrices with zero rows and zero columns.

The number of connection matrices that have zero rows is found using the following methodology. The number of cases that have $n_{outputs}$ zero rows (all zero rows) is 1. The number of configurations with $n_{outputs}$-1 zero rows is given by:

$$n_{zr,n_{outputs}-1} = n_{outputs} 2^{n_{inputs}} - n_{zr,n_{outputs}} \tag{A.12}$$

Next, considering the number of configurations with $n_{outputs}$-2 zero rows,

$$n_{zr,n_{outputs}-2} = \binom{n_{outputs}}{n_{outputs}-2} 2^{(n_{outputs}-2)n_{inputs}} - n_{zr,n_{outputs}-1} \tag{A.13}$$

This trend continues and total number of connection matrices with zero rows is given by:

$$n_{zr} = \sum_{i=1}^{n_{outputs}} \binom{n_{outputs}}{i} 2^{(n_{outputs}-i)n_{inputs}} (-1)^{i+1} \tag{A.14}$$

Similarly, the number of connection matrices that have zero columns is given by:

$$n_{zc} = \sum_{i=1}^{n_{inputs}} \binom{n_{inputs}}{i} 2^{(n_{inputs}-i)n_{outputs}} (-1)^{i+1} \tag{A.15}$$

The same methodology can be followed to determine the number of cases that contain a zero row and zero column:

$$n_{zrzc} = \sum_{i=1}^{n_{outputs}} \sum_{j=1}^{n_{inputs}} \binom{n_{outputs}}{i} \binom{n_{inputs}}{j} 2^{(n_{outputs}-i)(n_{inputs}-j)} (-1)^{(i+j)} \tag{A.16}$$

Using equations (A.8)-(A.11) and equations (A.14)-(A.16), the total number of configurations for a given selection of components when all components in the inventory are distinct can be written as:

$$\begin{aligned} n_{config,exact} &= n_{conmatrix} - n_{discon} \\ &= 2^{n_{inputs}n_{outputs}} + \sum_{i=1}^{n_{outputs}} \sum_{j=1}^{n_{inputs}} \left[\binom{n_{outputs}}{i} \binom{n_{inputs}}{j} 2^{(n_{outputs}-i)(n_{inputs}-j)} (-1)^{(i+j)} \right. \\ &\quad \left. + \binom{n_{outputs}}{i} 2^{(n_{outputs}-i)n_{inputs}} (-1)^{i} + \binom{n_{inputs}}{j} 2^{(n_{inputs}-j)n_{outputs}} (-1)^{j} \right] \end{aligned} \tag{A.17}$$

Taking into account the number of different ways to select the components, the total number of configurations when all components are distinct is given by

$$n_{config,total} = \sum_{i=1}^{N_p}\sum_{j=1}^{N_{ro}}\sum_{k=1}^{N_{er}}\binom{N_p}{i}\binom{N_{ro}}{j}\binom{N_{er}}{k}\Big[2^{n_{out}(i,j,k)n_{in}(i,j,k)} + \sum_{l=1}^{n_{out}(i,j,k)n_{in}(i,j,k)}\sum_{m=1}^{}\Big[\binom{n_{out}(i,j,k)}{l}\binom{n_{in}(i,j,k)}{m}2^{n_{out}(i,j,k)(n_{in}(i,j,k)-m)}(-1)^{(l+m)} + \binom{n_{out}(i,j,k)}{l}2^{(n_{out}(i,j,k)-l)n_{in}(i,j,k)}(-1)^{l} + \binom{n_{in}(i,j,k)}{m}2^{(n_{in}(i,j,k)-m)(n_{out}(i,j,k)-l)}(-1)^{m}\Big]\Big] \quad \text{(A.18)}$$

where N_p is the total number of pumps in the inventory, N_{ro} is the total number of reverse osmosis membranes in the inventory, and N_{er} is the total number of energy recovery units or pressure control valves in the inventory. The number of component outputs for configuration (i,j,k) is given by:

$$n_{out}(i,j,k) = i + 2j + k + 1 \quad \text{(A.19)}$$

and the number of component inputs for configuration (i,j,k) is given by:

$$n_{in}(i,j,k) = i + j + k + 2 \quad \text{(A.20)}$$

A.2.2 Identical Reverse Osmosis Components

Determining the number of different configurations that can result from an inventory in which all the pumps, reverse osmosis membranes, and energy recovery devices are the same follows a similar methodology. The main difference here is that the order of the rows and columns in the connection matrix associated with individual components does not matter, and different connection matrices result in the same system configuration. As a result, the number of configurations for a given selection of components becomes:

$$n_{config,exact} = \frac{1}{n_p!\,n_{ro}!\,n_{er}!}\Big[2^{n_{inputs}n_{outputs}} + \sum_{i=1}^{n_{outputs}}\sum_{j=1}^{n_{inputs}}\Big[\binom{n_{outputs}}{i}\binom{n_{inputs}}{j}2^{(n_{outputs}-i)(n_{inputs}-j)}(-1)^{(i+j)} + \binom{n_{outputs}}{i}2^{(n_{outputs}-i)n_{inputs}}(-1)^{i} + \binom{n_{inputs}}{j}2^{(n_{inputs}-j)n_{outputs}}(-1)^{j}\Big]\Big] \quad \text{(A.21)}$$

Using the sum rule, the total number of configurations that result when accounting for the number of different ways to select components is:

$$n_{config,total} = \sum_{i=1}^{N_p}\sum_{j=1}^{N_{pv}}\sum_{k=1}^{N_{er}} \frac{1}{i!\,j!\,k!}\Bigg[2^{n_{out}(i,j,k)n_{in}(i,j,k)} + \sum_{l=1}^{n_{out}(i,j,k)n_{in}(i,j,k)}\sum_{m=1}^{}\Bigg[\binom{n_{out}(i,j,k)}{l}\binom{n_{in}(i,j,k)}{m}2^{(n_{out}(i,j,k)-l)(n_{in}(i,j,k)-m)}(-1)^{(l+m)} + \binom{n_{out}(i,j,k)}{l}2^{(n_{out}(i,j,k)-l)n_{in}(i,j,k)}(-1)^{l} + \binom{n_{in}(i,j,k)}{m}2^{(n_{in}(i,j,k)-m)(n_{out}(i,j,k)-l)}(-1)^{m}\Bigg]\Bigg] \tag{A.22}$$

A.2.3 Full Reverse Osmosis Component Inventory

A realistic inventory for an RO system consists of different types of pumps, membranes and energy recovery devices. The inventory will likely consist of more than one of each type of component. This example is a combination of the cases presented above. For this case, the number of system configurations for a given selection of components is given by:

$$n_{config,exact} = \frac{1}{\prod_{i=1}^{N_p}(n_{p,i}!)\prod_{i=1}^{N_{PV}}(n_{ro,i}!)\prod_{i=1}^{N_{ER}}(n_{er,i}!)}\times\Bigg[2^{(n_{outputs})(n_{inputs})} + \sum_{l=1}^{n_{outputs}}\sum_{m=1}^{n_{inputs}}\Bigg[\binom{n_{outputs}}{l}\binom{n_{inputs}}{m}2^{(n_{outputs}-l)(n_{inputs}-m)}(-1)^{(l+m)} + \binom{n_{outputs}}{l}2^{(n_{outputs}-l)(n_{inputs}-m)}(-1)^{l} + \binom{n_{inputs}}{m}2^{(n_{outputs}-l)(n_{inputs}-m)}(-1)^{m}\Bigg]\Bigg] \tag{A.23}$$

where $n_{p,i}$ is the number of pumps of type i, $n_{ro,i}$ is the number of RO membranes of type i in the configuration, $n_{er,i}$ is the number of energy recovery devices or pressure control valves of type i in the configuration, N_p is the total number of different types of pumps, N_{ro} is the number of different types of reverse osmosis membranes, and N_{er} is the number of different types of energy recovery devices. The number of component outputs will be given by:

$$n_{outputs} = \sum_{i=1}^{N_p} n_{p,i} + 2\sum_{i=1}^{N_{ro}} n_{ro,i} + \sum_{i=1}^{N_{er}} n_{er,i} + 1 \tag{A.24}$$

and the total number of component inputs is given by:

$$n_{inputs} = \sum_{i=1}^{N_p} n_{p,i} + \sum_{i=1}^{N_{ro}} n_{ro,i} + \sum_{i=1}^{N_{er}} n_{er,i} + 2 \tag{A.25}$$

Using the sum rule, the total number of system configurations for the mixed reverse osmosis system component inventory is:

$$n_{config,total} = \sum_{n_{p,1}=0}^{N_{p,1}} \cdots \sum_{n_{p,N_p}=\max(1-\sum_{i=1}^{N_p-1} n_{p,i},0)}^{N_{p,N_p}} \sum_{n_{ro,1}=0}^{N_{ro,1}} \cdots \sum_{n_{ro,N_{ro}}=\max(1-\sum_{i=1}^{N_{ro}-1} n_{ro,i},0)}^{N_{ro,N_{ro}}} \sum_{n_{er,1}=0}^{N_{er,1}} \cdots \sum_{n_{er,N_{er}}=\max(1-\sum_{i=1}^{N_{er}-1} n_{er,i},0)}^{N_{er,N_{er}}} \frac{1}{\prod_{i=1}^{N_p}(n_{p,i}!)\prod_{i=1}^{N_{PV}}(n_{ro,i}!)\prod_{i=1}^{N_{ER}}(n_{er,i}!)}$$
$$\times\left[2^{(n_{outputs})(n_{inputs})} + \sum_{l=1}^{n_{outputs}}\sum_{m=1}^{n_{inputs}}\left[\binom{n_{outputs}}{l}\binom{n_{inputs}}{m}2^{(n_{outputs}-l)(n_{inputs}-m)}(-1)^{(l+m)} + \binom{n_{outputs}}{l}2^{(n_{outputs}-l)(n_{inputs}-m)}(-1)^{l} + \binom{n_{inputs}}{m}2^{(n_{outputs}-l)(n_{inputs}-m)}(-1)^{m}\right]\right] \quad \text{(A.26)}$$

where $N_{p,i}$ is the total number of pumps of type i in the inventory, $N_{ro,i}$ is the total number of RO membranes in the inventory of type i and $N_{er,i}$ is the total number of energy recovery devices of type i in the inventory. Using this relationship, the total number of distinct configurations can be derived for any reverse osmosis component inventory.

A.3 Number of Possible Photovoltaic Power Systems

This section determines the number of possible configurations for a PV system. A PV array consists of multiple PV panels in combinations of series and parallel connections. The layout of the array will affect the voltage and current output. The overall power will not be impacted as long as the modules connected in an individual sub array are matched in power/current output and configured in a way that is compatible with the control electronics.

Since the configuration of panels does not impact the performance, the design choice for the PV subsystem is the number of panels to include in the system. For an inventory containing multiple types of PV panels, the number of configurations can be determined using the following methodology. For a given number of panels, the number of distinct configurations is given directly from the rules for combinations of multi-sets given in equation (A.6) as follows:

$$n_{pv,exact} = C(r;n_{pv,1},n_{pv,2},\ldots,n_{pv,N_{pv,type}}) = \sum_{p=0}^{N_{pv,type}}(-1)^p \sum_{1\le i_1\le i_2\le\cdots\le i_p\le N_{pv,type}} \binom{N_{pv,type}+r-\sum_{j=1}^{p} n_{pv,i_j}-p-1}{N_{pv,type}-1} \quad \text{(A.27)}$$

where $n_{pv,j}$ is the number of PV panels of type j in the inventory, $N_{pv,type}$ is the number of different types of PV panels, and r is the number of PV panels selected for the configuration.

Fortunately, when considering the total number of panels in the inventory, the calculation becomes much simpler. Since there are $(n_{pv,i} + 1)$ ways to choose the number of PV panel type i

to include in the system, the number of different PV system configurations can be written using the product rule:

$$N_{PV} = \prod_{i=1}^{N_{pv,type}} \left(n_{pv,i} + 1\right) - 1 \tag{A.28}$$